FEASIBILITY OF THE MARINE CONTROLLED SOURCE ELECTROMAGNETIC METHOD FOR HYDROCARBON EXPLORATION; WESTERN AUSTRALIA

Report No.: GPH 2/07

By Sean Phillips

BSc. (Geophysics) Curtin

This report is presented as part of the requirement for the units
Geophysics Honours Dissertation 494 Part A & B, units totaling 50 credit points in the
BSc (Geophysics) Honours from Curtin University of Technology. The work
is the result of supervised research; however, the report has been prepared
by the student who is solely responsible for its contents.

DEPARTMENT OF EXPLORATION GEOPHYSICS

Curtin University of Technology

November 2007

ABSTRACT

Recently in the petroleum exploration industry there has been a surge of interest in the marine controlled-source electromagnetic (CSEM) method. This exploration method can detect the presence of deep thin hydrocarbon reservoirs and other electrically resistive structures such as salt bodies and gas hydrates below the seabed. Electrical properties derived from a marine CSEM survey have a more direct relationship with reservoir fluids than seismic methods. CSEM measurements respond directly to increases in hydrocarbon saturation and reservoir thickness. Commercial application of the marine CSEM method was first seen in about 2002 and until recently no offshore surveys had been completed in Western Australia. There is potential for widespread application of the marine CSEM in the Northwest Shelf; however the feasibility of the method must firstly be evaluated to determine if it is an appropriate exploration tool.

Critical geological factors and survey parameters should be considered prior to design of a marine CSEM survey. Geological factors include water depth, bathymetry, target depth, saturation and thickness, host formation resistivity and the effect of shallow resistive formations. Survey parameters investigated in this research include: (a) transmission frequency and harmonic content, (b) required offsets and (c) the components of the electromagnetic field that need to be measured. Target reservoir detect-ability is determined through the use a forward modelling code capable of numerically simulating the response from a 3D resistive body embedded in a layered earth. Layered earth (1D) modelling helps to develop an intuitive feel for how controlled-source electromagnetic fields interact with the sub seafloor and can ultimately

determine if a target is detectable or not. 1D sensitivity analysis provides good approximations to the frequencies and offsets required for a given target. The results of modelling can then be used for survey design to ensure the optimal response from the target reservoir.

For areas of the Northwest Shelf including Scarborough gas field and Browse Basin; 1D models were built from geophysical bore-hole logs and seismic data. Scarborough gas field is deep; however it is a laterally extensive deposit in a deep water setting. Forward modelling results indicate that this commercial scale deposit is detectable. In Browse Basin the issue is water depth which is seen as the main problem with the CSEM method. Reservoirs located at North Scott Reef, Walkley and Caswell appear to have sufficient water depth to be detectable with current CSEM technology. However closer to the shore, on the Yampi Shelf, the water is too shallow relative to target reservoir depth and it is highly unlikely that current typical CSEM technology would be an effective exploration method in this setting.

The marine CSEM method works best in areas where: (a) the large scale resistivity of the background sediments is relatively uniform, (b) high reservoir resistivities, (c) there exists well defined field edges, and (d) there is a smooth seafloor. The method is not well suited to areas: (a) where the reservoir is in close proximity to crystalline basement, (b) below salt structures, (c) in very shallow water or (d) at a depth much greater than the water depth. Vertical electric field sensors may provide the additional information required to move exploration into shallower water. In general, all components of the electromagnetic field should be acquired along with MT data to move the marine CSEM method into area currently considered unsuitable.

ACKOWLEDGMENTS

Firstly I would like to thank my family, Janet, Donald and Sophie for supporting me in all my decisions and always being there for me. I acknowledge my supervisor Dr. Brett Harris, not only for taking me on as his student but for his guidance and deep knowledge in the area. I feel deeply indebted to fellow student Andrew Pethick for his adeptness in various programming languages. Andrew worked with me for countless hours with programming; if it wasn't for his skills and generosity I would not have been able to produce the results I have here, or done what I wanted to do with this project.

CONTENTS

LIST OF FIGURES

1 INTRODUCTION

The marine controlled-source electromagnetic (CSEM) method has seen a recent surge of interest within the petroleum exploration industry. Early proposals to use the method for petroleum exploration (e.g., Chave et al., 1991) concentrated on relatively shallow water and exploration targets. The CSEM method was originally developed for deepwater studies of the oceanic lithosphere (Cox, 1981) and with the first experimental surveys completed in 1979 (Spiess et al., 1980). Over the last two decades various university researchers (Scripps Institute of Oceanography, University of Toronto, Cambridge, and later Southampton University) have used both natural electromagnetic fields and active EM sources to image the conductivity structure beneath the seafloor. Academic applications of this method have seen the study of the oceanic lithosphere (Constable and Cox, 1996) and mid-ocean-ridges (MacGregor et al., 2001).

With the migration of hydrocarbon exploration into the deeper waters of the continental shelves the marine CSEM method recently has become an important exploration tool for the hydrocarbon industry (e.g., Ellingsrud et al., 2002; Eidsmo et al., 2002; Johansen et al., 2005). The marine CSEM method aims to recover the large scale electrical resistivity distribution below the seabed and is designed to detect the presence of thin resistive layers. Marine CSEM methods have the potential to detect petroleum, natural gas, gas hydrates and other resistive zones in an otherwise conductive background. Until recently no offshore CSEM surveys had been completed in Western Australia. The CSEM method has great potential for widespread application in the Northwest Shelf, since there is extensive sediment cover even in deep water, suitable for hydrocarbon plays.

However there remain many questions and concerns over the application of the marine CSEM method. One key issue is water depth. Survey design is critical for success; the geo-electrical structure must be evaluated through feasibility analysis. Some studies used forward modelling to provide understanding of the CSEM responses from typical geology. Flosadottir and Constable (1996) also used forward modelling for experiment design.

This dissertation contains an overview of electromagnetic exploration on the seafloor in terms of the underlying physics and instrumentation, a description of the forward modelling algorithm used, a general overview of the effects of various geological and survey parameters and a feasibility study of selected areas within the Northwest Shelf, Western Australia.

1.1 Project Background

Two exploration tools exist that can be used to determine the properties of fluid in the sub seafloor, reflection seismic and electromagnetic methods. Direct hydrocarbon indicators (DHI) from seismic can relate to reservoir potential however after ~10% saturation there is little variation in seismic amplitude; further AVO techniques must be used. In contrast electrical resistivity increases in a predictable way with increasing oil or gas saturation. CSEM measurements respond directly to this increase as shown in Figure 1.1. Reflection seismic relies on the contrast of acoustic properties, and as such is very reliable for determining structure, but fails to readily distinguish between fluids with similar acoustic properties such as water and oil.

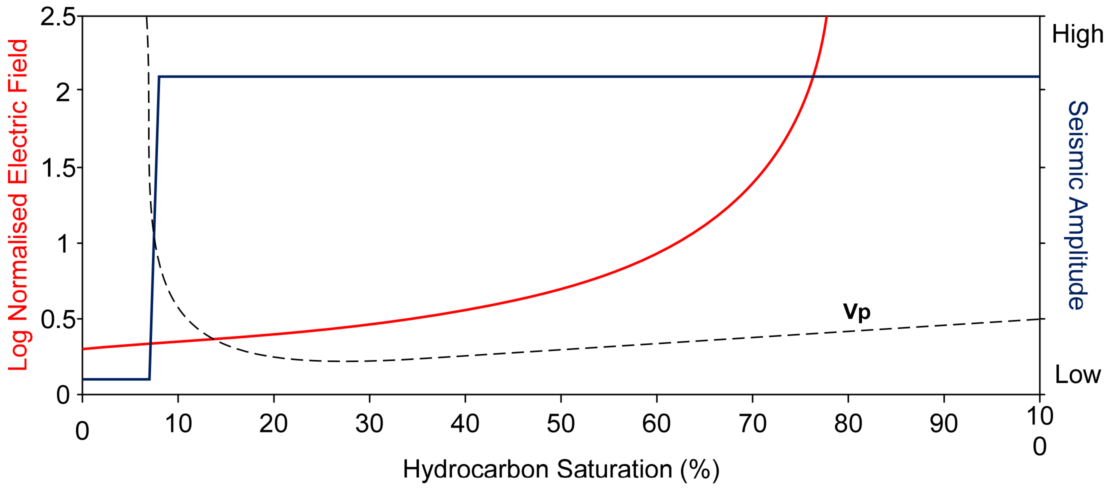

Figure 1.1 Electrical (CSEM) and seismic amplitude response of an arbitrary reservoir for increasing hydrocarbon saturation. Seismic methods fail to distinguish between 10-100% hydrocarbon saturation whereas CSEM measurements respond directly to the increasing hydrocarbon saturation (Modified from MacGregor, 2006).

There are also various types of geology where seismic methods fail such as low velocity zones (e.g. magma chambers) or high velocity layers (e.g. sub-basalt or sub-salt). Electromagnetic methods are not yet ready for sub-salt imaging but are ideally more suited to fluid dominated geology than seismic methods. CSEM methods work well in deep water turbidites, deep water deltas, stacked reservoir sequences and under shallow gas hydrates. With recent technological innovations CSEM methods are now feasible for reservoirs at the flanks of salt diapirs, in carbonates and in shallow water (MacGregor, 2006).

CSEM methods have been used since 1979 (Spiess et al., 1980) and there now exists several strong reasons for the recent surge of interest within the petroleum exploration industry. Frontier exploration into deeper waters is where marine CSEM methods work best. Drilling to test seismic prospects is very expensive and there are a high percentage of dry wells, many prospects go untested due to this expense and low success rate. Many appraisal wells are also drilled to determine field edges, which CSEM methods can achieve remotely.

However as mentioned, like also exploration tools, CSEM methods must be applied under suitable geological conditions and hydrocarbon plays. Commercial projects always begin with a feasibility study that evaluates the electromagnetic response of the marine lithology and reservoir, giving an indication of whether the target reservoir will be detectable or not. A plane-layer (1D) modelling algorithm is normally used during the initial phase. Modelling is fast and provides sensitivity analysis of subsurface parameters, including vertical anisotropy (layering). Not only is there an indication of the expected responses but the frequency content and offsets that will be required to resolve the given targets can be estimated. At this stage a decision can be made on whether or not the target reservoir is detectable and if CSEM is a suitable exploration tool capable of quantifying the prospective hydrocarbon play. From here an optimum survey can be designed based on the forward modelling results. As of now, no feasibility studies of the Northwest Shelf, Western Australia have been published.

1.2 The Controlled Source Electromagnetic Method

The marine CSEM method uses a high power (1000 A) horizontal electric dipole (HED) source that is towed within 50 m above the seafloor over an array of seafloor receivers (Figure 1.2). The transmitter produces a long period square wave current; the electromagnetic fields that arise diffuse into the water column and the seabed. The response of the earth is measured by highly sensitive electromagnetic seafloor receivers and from the attenuation and phase of the transmitted signal at the receiver location, the electrical structure of the seabed through which the source signal interacted with can be obtained. A marine CSEM survey involves many source and receiver locations and geometries and current receivers are capable of measured all Cartesian vectors of the electromagnetic field. In deep water marine areas the saturated, inter-bedded, shales, mudstones and sandstones are dominate the lithology and have low electrical resistivity, A hydrocarbon reservoir can have a resistivity or 1 or 2 orders or magnitude greater. This acts as a high impedance electrical structure, analogous to a high rigidity mechanical structure that guides energy for many kilometres with low attenuation. The increase in electrical field due to the reservoir can measured at the seafloor at offsets roughly double the depth of the reservoir below the seabed.

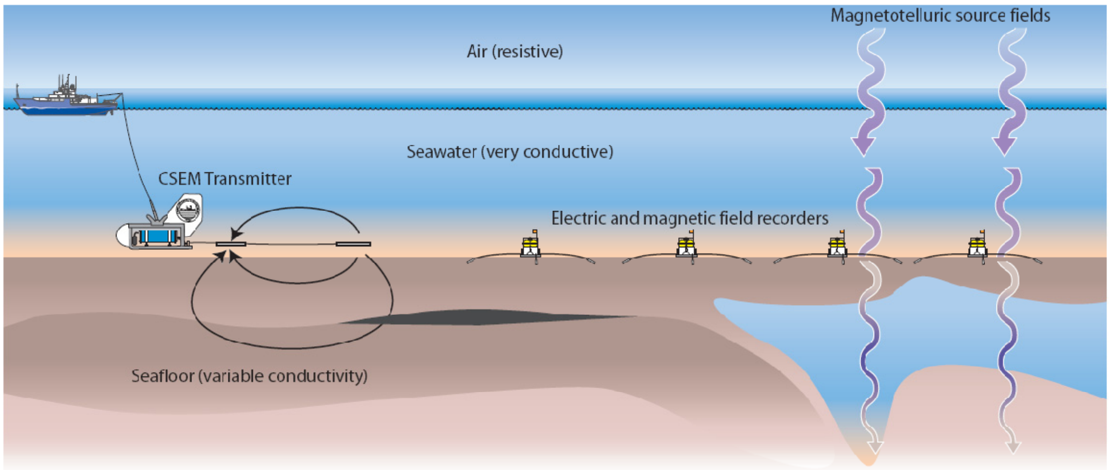

Figure 1.2 Schematics of a typical marine CSEM survey showing an array of seafloor receivers over a reservoir with the transmitter towed with along the axis of the structure (Reproduced from Constable, 2006).

2 ELECTROMAGNETIC EXPLORATION ON THE SEAFLOOR

In this chapter the practical and theoretical aspects of controlled source electromagnetic (CSEM) exploration on the seafloor are presented. This includes a review of the instrumentation, a description of the physics of diffusive electromagnetic energy and an overview of the common ways to display and interpret CSEM data.

2.1 Detecting the Distribution of a Petrophysical Parameter: Resistivity

Every geological system can be characterised at least in terms of elastic, electric, magnetic and electromagnetic parameters. Electrical resistivity is one of the most widely varying petrophysical parameters. While seismic attributes and density typically vary by a factor of 2 and at most by an order of magnitude, electrical resistivity can vary by orders of magnitude (Keys, 2003). These large variations, primarily controlled by the fluid phase, make electrical resistivity methods a very useful tool for geophysicists interested in exploring the fluid distribution of the subsurface.

Resistivity variations in sediments are controlled by variations in porosity, permeability, pore connectivity geometry and the fluids contained within the pores. Minerals that comprise the rock framework of a reservoir are highly resistive (10^{11} - 10^{14} Ωm) whereas the pore fluids including low resistivity saline water (0.04 - 0.19 Ωm) and or infinitely resistive hydrocarbons ultimately determine the formations resistivity. These fluids give rise to the variation of the orders of magnitude of electrical resistivity over the range of saturation (Johansen et al., 2005). There are few methods that we can use to readily explore the resistivity distribution in marine environments. In the petroleum industry, resistivity has been almost exclusively measured by wire-line logging of wells (Eidesmo et al., 2002a). Another well established technique for measuring and imaging electrical resistivity structure is the Magnetotelluric (MT) method. Marine MT methods are useful for characterising the overall background resistivity structure, whereas CSEM methods are effective at detecting thin layers of high resistivity, such as hydrocarbon reservoirs. This makes the marine CSEM method an excellent exploration tool for geophysicists in the application of remotely detecting hydrocarbon reservoirs.

In deep water settings geological strata mainly consist of shale or mudrock with rather low resistivity. A hydrocarbon reservoir can have a resistivity of up to 2 orders of magnitude greater (Eidesmo et al., 2002b). Marine sediments saturated with saline water have low resistivities (1 - 5 Ωm); by displacing the saline water with hydrocarbons the bulk resistivity of the reservoir will significantly increase (10 - 500 Ωm). The marine CSEM method exploits this dramatic change in electrical resistivity to potentially delineate water-bearing formations from those containing hydrocarbons (Hoversten et al., 2006).

The presence of a thin hydrocarbon saturated layer essentially acts as a high impedance electrical structure preventing the diffusion of the controlled source energy, and guiding this energy across the hydrocarbon saturated layer for many kilometres with low attenuation. The electric field of a horizontal electric dipole is shown for a typical deep ocean basin in Figure 2.1; for the same setting the presence of a thin hydrocarbon saturated layer (1500 m below the seabed) is shown in Figure 2.2, to demonstrate the increase in the electric field at the high impedance reservoir which guides the energy laterally across the structure.

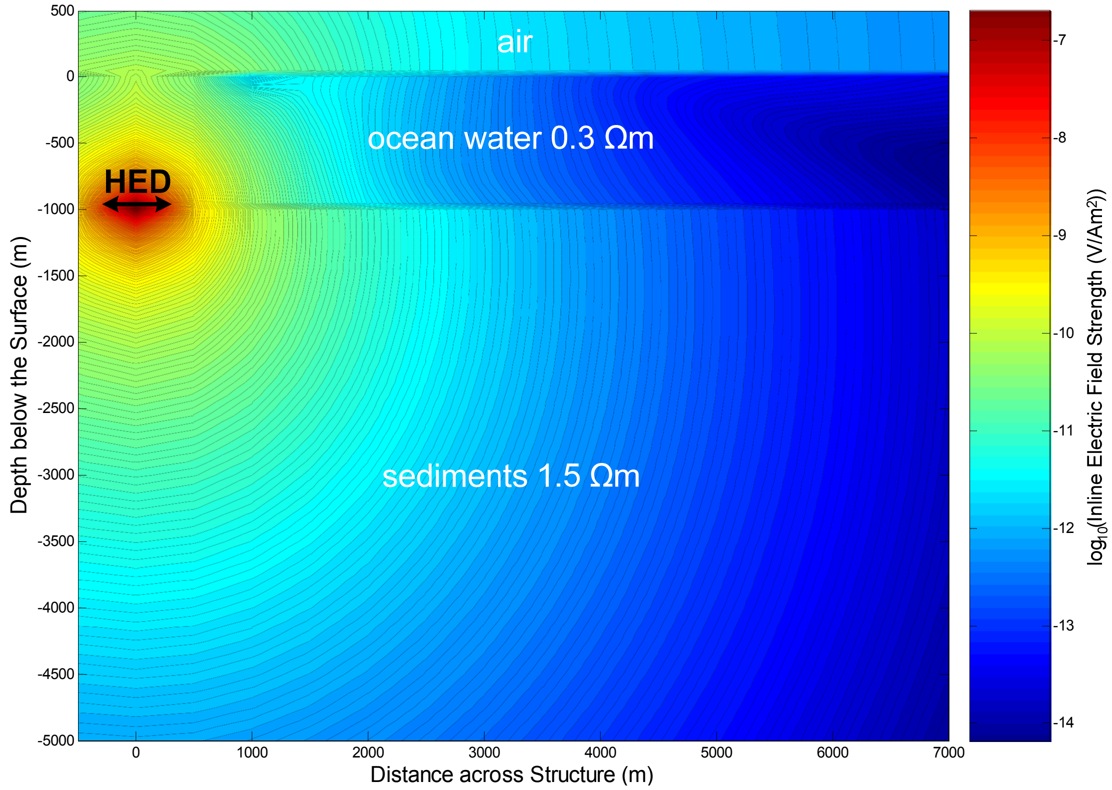

Figure 2.1 Electric field strength of a horizontal electric dipole source in a typical deep ocean basin.

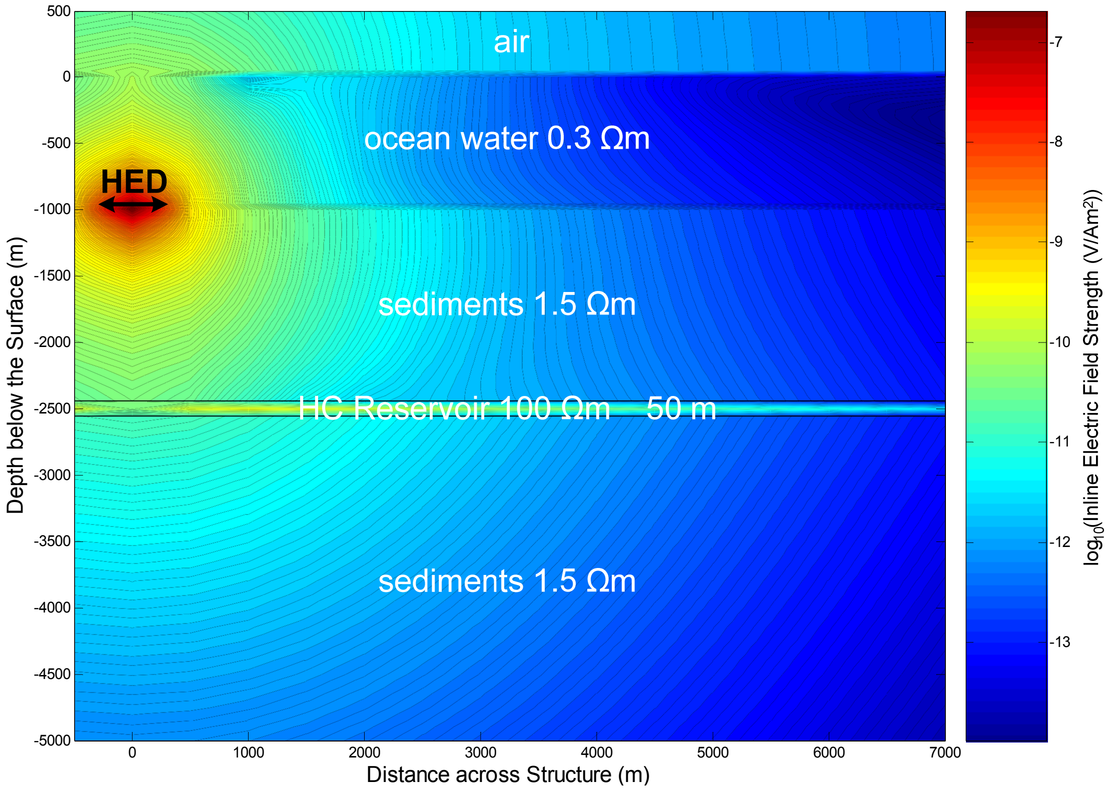

Figure 2.2 Electric field strength of a horizontal electric dipole source in the presence of a thin hydrocarbon saturated layer.

2.2 Marine CSEM Instruments

Recent developments in technology have seen the introduction of highly sensitive seafloor receivers and a new powerful horizontal electric dipole (HED) source which has made improved acquisition of marine CSEM data possible.

2.2.1 Multi-component seafloor receivers

Marine Magnetotelluric (MT) instrumentation underwent a major advancement during the late 1990's with the introduction the Scripps Institution of Oceanography broadband marine MT instrument (Constable et al., 1998). Most commercial contractors use receivers modelled on the Scripps Mark III design as shown in Figure 2.3. These receivers record time series data, stored onboard on an internal device. For receivers to be accurately positioned on the seafloor, they must be designed to descend at a fast rate. Once they are deployed, the receivers are tracked acoustically using onboard acoustic units. A digital magnetic compass/tilt-meter records the instrument orientation on the seafloor (WesternGeco, 2007). The operating depth range of the seafloor EM receiver is up to 6 km (OHM, 2007).

The seabed-logging receivers must be capable of measuring field strengths that vary greatly in magnitude, from weak, naturally occurring MT signals to strong direct signals from the controlled source. Measuring the EM phase with respect to the source requires precise measurement of the timing of the signal. Most receivers have four electric and two magnetic channels that record vertical and horizontal field components. Data loggers have 24-bit A-D converters and AGC, which enables high resolution data to be recorded at all source-receiver offsets without signal saturation.

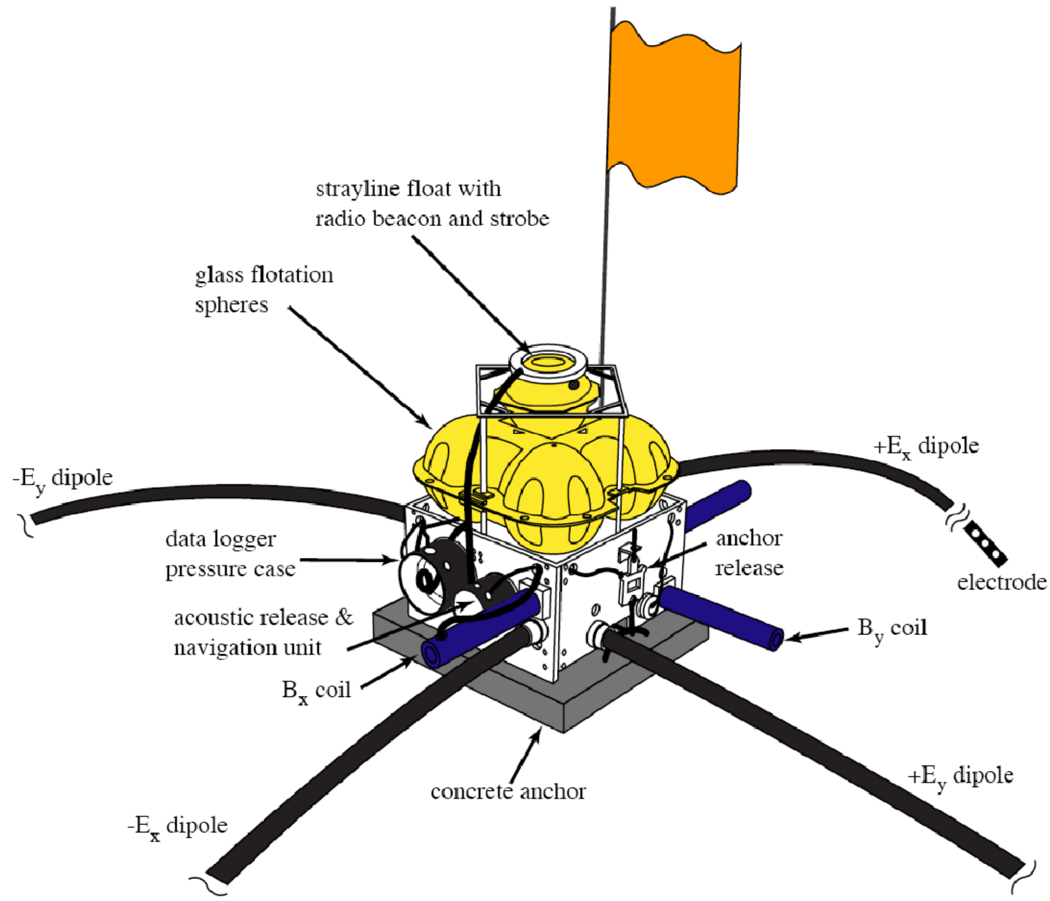

Figure 2.3 Diagram of the Scripps Institute of Oceanography Mark III design (Constable et al., 1998; reproduced from Keys, 2003).

A system of low noise and low impedance silver-silver chloride electrodes measures the horizontal electric field at the ends of ~10 m long dipole arms. A stiff vertical arm can also be added to record vertical electric fields. Horizontal magnetic fields are measured using highly sensitive, light weight and low power induction coil magnetometers (Keys, 2003).

Different measures of noise can be considered when assessing the signal level that can be expected to be measurable. The noise floor of the seafloor receivers must be assessed when considering the use of marine CSEM methods in the application of detecting hydrocarbons. Detectability of a target reservoir will depend on whether or not the measured signal is above or below the noise floor at the offsets at which the reservoir response is dominant. Assuming optimum survey geometry and parameters; for the offsets at which the reservoir response is dominant the measured signal must be above the level of both the ambient noise and the instrument noise for the reservoir to be detectable. There are two types of electromagnetic noise for seafloor measurements. One is the ambient electromagnetic noise which is temporal and varies with location. In deep water ambient noise is greatly attenuated by the conductive ocean water. The other component of noise is the detection threshold of the instruments, which is predominantly controlled by amplifier noise (Constable and Weiss, 2007), and the electrodes (Hoversten et al., 2006). Commercial contractors consider an electric field noise floor of 3×10^{-16} V/Am^2 at 1 Hz for receivers currently deployed (WesternGeco, 2007).

Amplifier noise e_n is inversely proportional to the root of the recording bandwidth. A noise level of $1\ \mathrm{nV}/\sqrt{\mathrm{Hz}}$ is achieved for the amplifiers used in the application of the marine CSEM method (OHM, 2007). The total noise is given by $v_n^2 = e_n^2.\Delta f$. If the average recording period is 10 s, Δf is 0.1 Hz; then v_n is 3×10^{-10} V *RMS*. The electric field noise is given by $\frac{v_n}{d}$. Commercial EM receivers currently deployed operate with ~8 m electric dipoles. The electric field noise is 4×10^{-11} V/m for 8 m dipoles.

For commercial operations the transmitter current is 1000 A at peak output. The transmitter moment is I.l where l is transmitter length of 100 - 300 m. The noise floor η, for a 200 m long transmitter operating at 500 A is 4×10^{-16} V/Am^2 at 0.1 Hz as given by equation (1). This is close to the noise floor of receivers used in commercial application.

$$\eta = \frac{v_n}{I.l.d} = \frac{\sqrt{e_n^2.\Delta f}}{I.l.d} \quad (1)$$

Such noise levels (10^{-16} V/Am^2) can be approached in very deep water. For water depths typical of continental shelf exploration, water motion and MT signals lift the noise floor to about an order of magnitude worse than this (Constable and Weiss, 2006). Therefore a noise floor of 10^{-15} V/Am^2 at all frequencies will be considered for modelling.

2.2.2 Transmitter

The marine CSEM method uses a horizontal electric dipole that is towed at approximately 50 m above the seabed at a tow speed of 1.5 to 2.0 knots. A powerful source is required to illuminate deep targets. Commercial transmitters have a peak output of ~1000 A. Survey success requires the use of a source waveform that can be controlled to enable the strongest response from the reservoir. Fundamental transmission frequencies vary from 0.05 to 10 Hz.

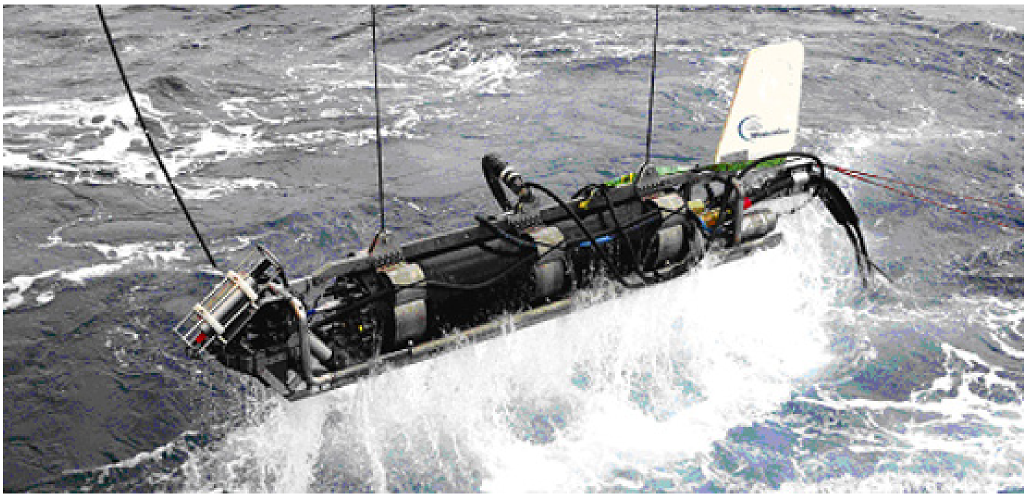

Figure 2.4 Picture of a commercial transmitter (Reproduced form WesternGeco, 2007).

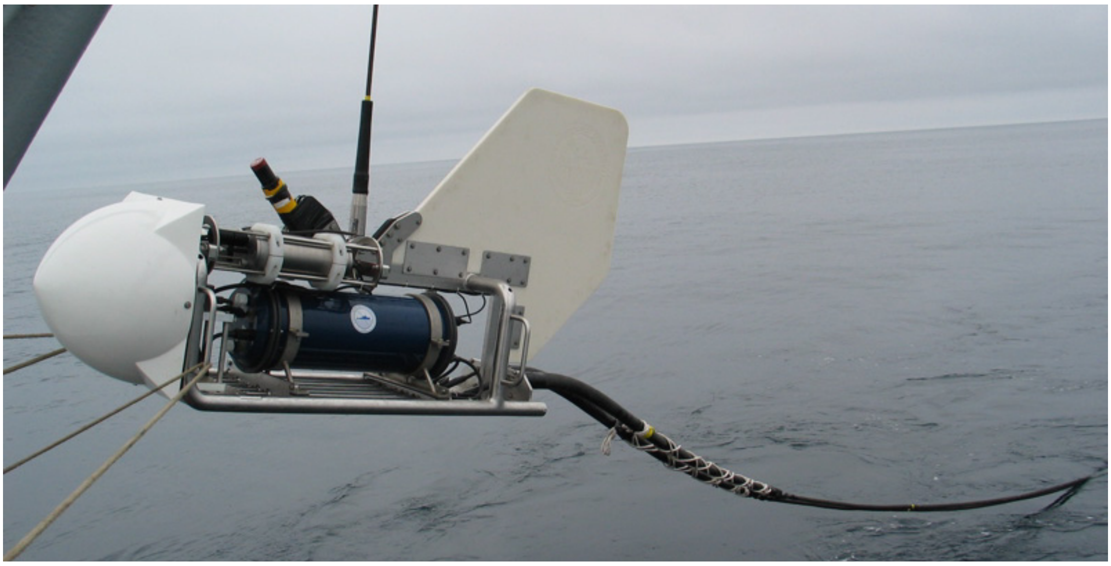

Figure 2.5 Picture of the Scripps Institute of Oceanography SUESI, a horizontal electric dipole source (Reproduced from Scripps Institute of Oceanography, 2004).

Harmonics of this fundamental frequency are derived through a FFT of the current waveform. High frequencies and can be used to constrain shallow formations, and the entire range of useable frequencies can be used in inversions of the survey data. Using the largest range of frequencies will provide the best inversion results. In reality the current waveform is a square wave; this is simulated in the modelling code by a sinusoidal wave of a chosen fundamental frequency.

Transmission parameters are controlled from the survey vessel in real time, and the transmission characteristics are logged throughout a survey allowing real-time QC of the current waveform. For processing of seabed-logging data, the location of the source must be accurately known and the timing of the received EM fields must be synchronized with the source signature (WesternGeco, 2007). Typical tow speeds for marine CSEM operations are close to 1 m/s (1.5 to 2.0 knots). At a fundamental transmission frequency of 0.25 Hz a receiver records 25 transmitter cycles for every 100 m the boat travels. 100 m is a typical averaging window over which data is stacked, for a tow speed of 1 m/s data is recorded for a period of 100 s. Stacking over this time period reduces the noise by a factor of 5 ($1/\sqrt{N}$, N = 25), inversely proportional to the root of the number of transmitter cycles recorded (Hoversten et al., 2006).

2.3 Working in the Conductive Ocean

Both source and receivers are coupled directly to the seawater. At typical ocean floor temperatures, seawater resistivity is about 0.3 Ωm and reaches a minimum of 0.04 Ωm at

350 °C. Seawater resistivity varies with temperature and salinity as shown in the following equation

$$\sigma = 3 + \frac{T}{10}$$

where

σ is the conductivity of the seawater (S/m)

T is the temperature of the seawater (°C)

Higher seawater conductivities result in more rapid attenuation of the electromagnetic fields, yielding lower received field strengths away from the source.

2.3.1 The Filtering effect of seawater

The conductive seawater in the ocean has an attenuating effect on the incident MT source fields (Constable et al., 1998) and acts like a low-pass filter. Fields with skin depths much less than the ocean depth will experience severe attenuation. Signals as low as 1 Hz, will be almost completely attenuated in just a few hundred metres of water. This filtering effect practically eliminates EM noise sources including cultural noise. Measurements of the electric field on the seafloor have determined that background noise is of the order of 1 pV/m at 1 Hz. Background noise includes the effects of sea motion in the earth's magnetic field, swell and wind (Mehta et al., 2005). Despite this rapid attenuation electromagnetic fields that propagate in the underlying sediments from a controlled source are still measureable at the order of 10 km away from the source. The practical implication of this is that the signals measured by seafloor receivers have mainly interacted with the subsurface, which is what we require for the marine CSEM method.

2.4 Water Depth

Water depth is a key issue in the application of marine CSEM. In deep water where the water depth is comparable with the depth of the target reservoir below the seabed the depth to which CSEM methods are sensitive to the target increases to a maximum at source-receiver offsets that are approximately double the target depth. In shallow water the sensitivity depth is greatly reduced (MacGregor et al., 2006). This reduction in shallow water reduces the ability of the marine CSEM method to detect resistive structures such as hydrocarbon reservoirs. The reduced sensitivity in shallow water is demonstrated in the Figure 2.6. With decreasing water depth, the onset of the air-wave occurs as shorter source-receiver offsets due to the source being closer to the air. Essentially the source needs to be closer to the target than air. The effect of the air-wave for different water depths is shown in Figure 2.7.

In deep water the effect of a hydrocarbon saturated reservoir is to increase the measured electric field strength at the seafloor, at far offsets by more than a factor of four and advance of the phase of the measured signal compared to the background, water-saturated case as demonstrated in Figures 2.8 and 2.9. In contrast a shallow water setting; the effect of the air/water interface has a dramatic effect on the measured response resulting in an overall increase in the measured field strength and an advance in the phase at all offsets as demonstrated in Figures 2.11 and 2.12 (MacGregor et al., 2006).

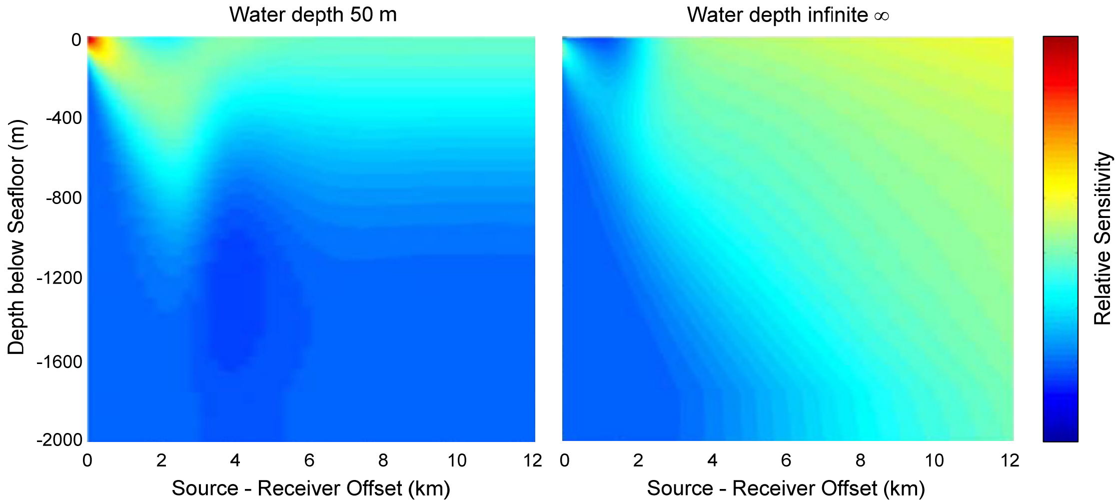

Figure 2.6 Sensitivity of the electric fields to seabed resistivity with depth as a function of source-receiver offset. The transmission frequency is 0.25 Hz. Sensitivity of the response is quantified by the derivative of the inline electric field with respect to the resistivity of the structure, a 1 Ωm halfspace (Reproduced from MacGregor et al., 2006).

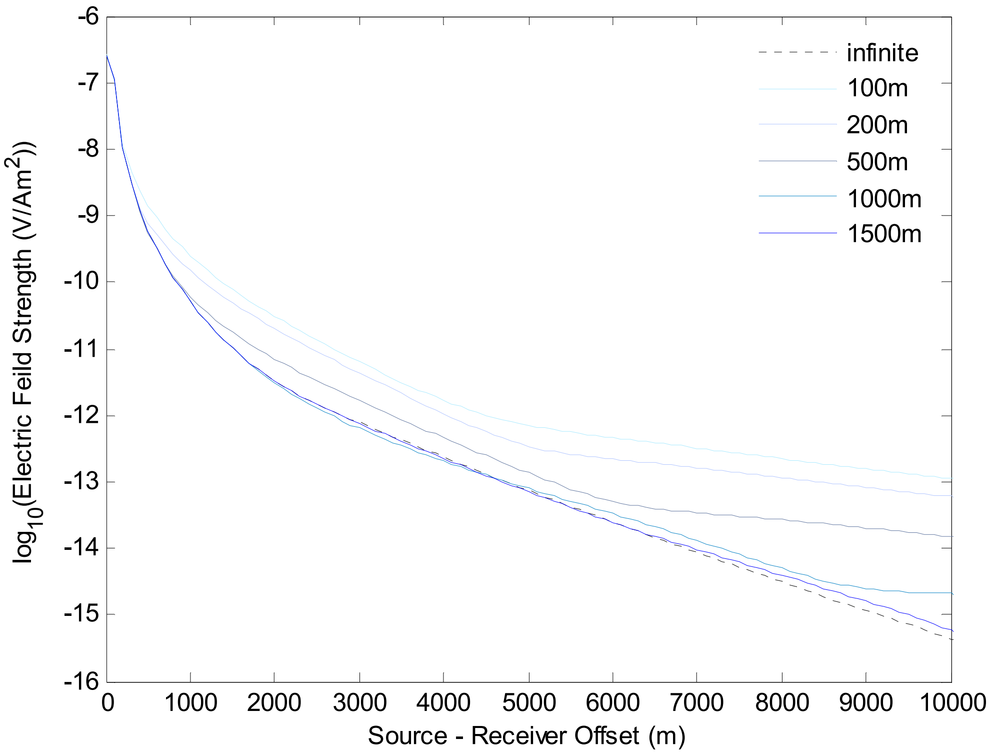

Figure 2.7 Effect of water depth as compared to an infinite water column for a halfspace resistivity of 1.5 Ωm at 0.3 Hz. The onset of the air-wave can be seen as a break in slope. For a water depth of 1500 m the air-wave does not interfere with measurements even at 10 km as the response is almost identical to an infinite water column.

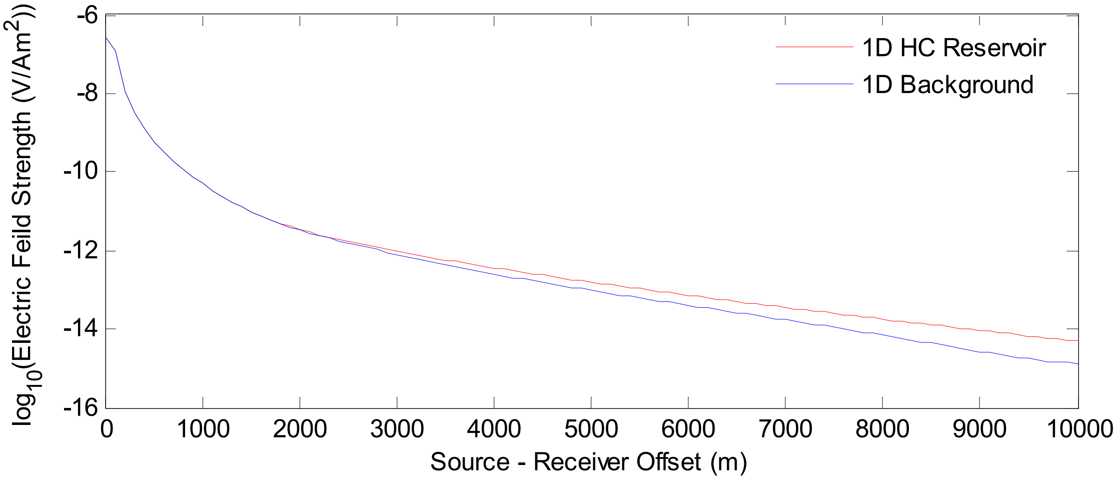

Figure 2.8 Inline electric field strength for 1D background (blue) and reservoir (red) models at 0.3 Hz.

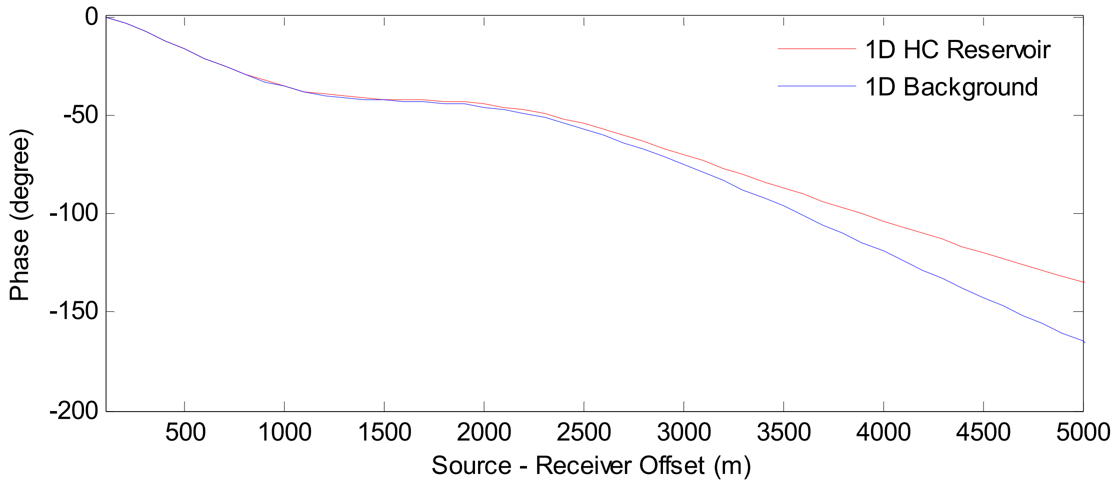

Figure 2.9 Inline electric field phase for 1D background (blue) and reservoir (red) models at 0.3 Hz.

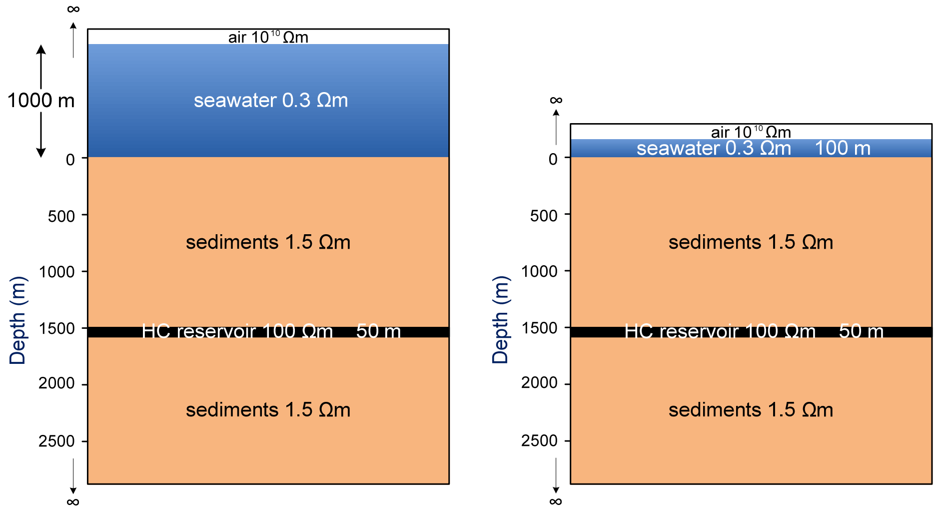

Figure 2.10 Four layer 1D reservoir models for deep (1000 m) and shallow (100 m) water.

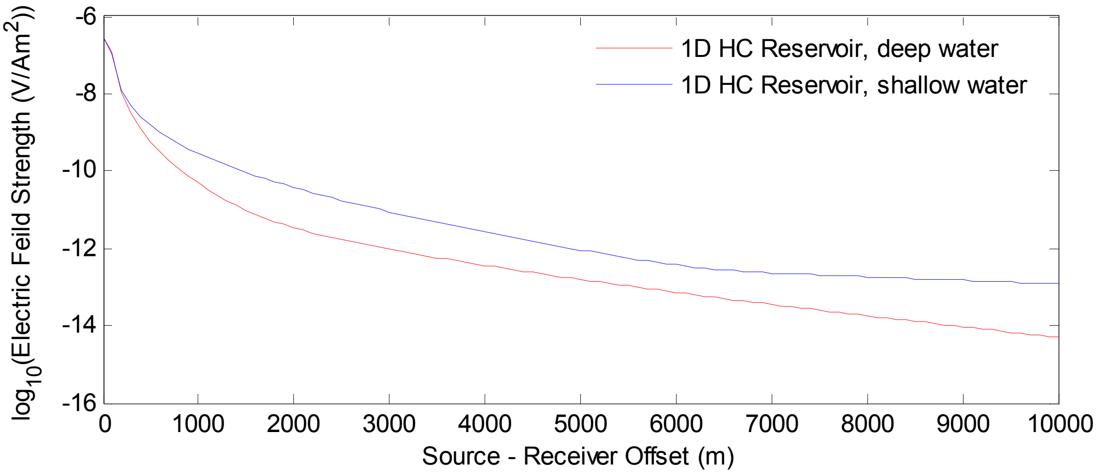

Figure 2.11 Inline electric field strength for shallow reservoir model (red) and deep reservoir model (blue) at 0.3 Hz.

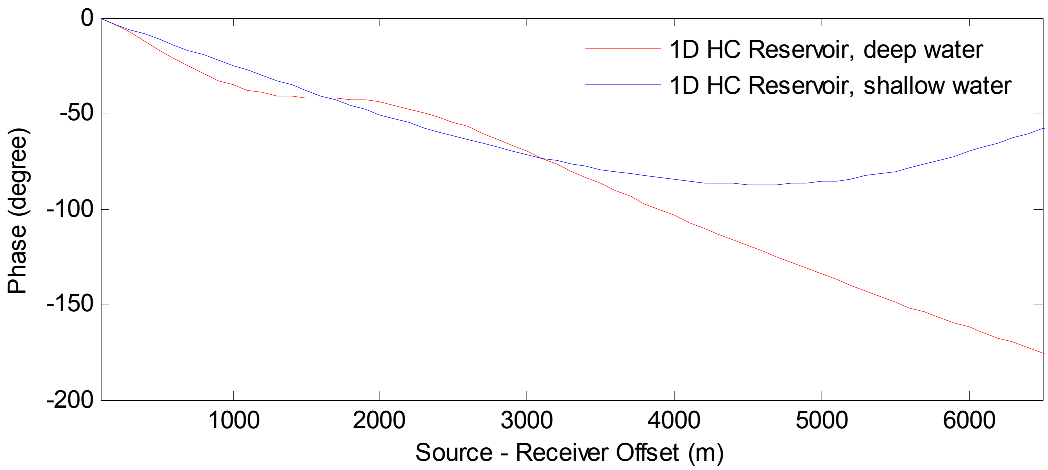

Figure 2.12 Inline electric field phase for shallow reservoir model (red) and deep reservoir model (blue) at 0.3 Hz.

2.5 Underlying Physics of the Marine CSEM Method

At the very low frequencies used in the marine CSEM method (0.1 - 10Hz) and for the high conductivities of the sea water (0.3 Ωm) and marine sediments (1 - 5 Ωm), the behaviour of electromagnetic energy is considered to be diffusive. Starting with Maxwell's equations the diffusion equation for the electric and magnetic fields is derived. The solution for the electric and magnetic fields at a distance away from the source is given in terms of the skin depth.

2.5.1 Behaviour of electric and magnetic fields

All currently known aspects of electromagnetic phenomena can be described by the empirical Maxwell's equations. These equations describe the interrelationship between the electric field, magnetic field, electric charge, and electric current. Following the approach of Ward and Hohmann (1988), the equations that describe the underlying physics of the CSEM method can be derived by starting from Maxwell's equations

$$\nabla \times \boldsymbol{E} = -\frac{\partial \boldsymbol{B}}{\partial t} \tag{1}$$

$$\nabla \times \boldsymbol{H} = \mathbf{J} + \frac{\partial \boldsymbol{D}}{\partial t} \tag{2}$$

where

$\boldsymbol{E}$ is the electric field intensity (V/m)

$\mathbf{J}$ is the electric current density (Am^2)

$\boldsymbol{H}$ is the magnetic field intensity (A/m)

$\boldsymbol{B}$ is the magnetic flux density (Tesla)

$\boldsymbol{D}$ is the dielectric displacement (C/m^2)

In a homogenous isotropic medium the following scalar constitutive relations apply

$$\boldsymbol{D} = \varepsilon \boldsymbol{E}$$

$$\boldsymbol{B} = \mu \boldsymbol{H}$$

$$\mathbf{J} = \sigma \boldsymbol{E}$$

where

ε is the electrical permittivity (F/m)

μ is the magnetic permeability (H/m)

σ is the electrical conductivity (S/m)

When substituted into the Maxwell's equations, the constitutive relations quantify the electromagnetic properties of matter, permittivity, permeability and conductivity. Taking the curl of equation (1) and substituting in the constitutive relation for magnetic flux density $\boldsymbol{B}$ yields

$$\boldsymbol{\nabla} \times (\boldsymbol{\nabla} \times \boldsymbol{E}) = -\mu \left(\boldsymbol{\nabla} \times \frac{\partial \boldsymbol{H}}{\partial t} \right)$$

we can now apply the follow vector identity

$$\boldsymbol{\nabla} \times \boldsymbol{\nabla} \times \boldsymbol{A} \equiv -\boldsymbol{\nabla}^2 \boldsymbol{A} + \boldsymbol{\nabla}(\boldsymbol{\nabla} \cdot \boldsymbol{A})$$

Considering the equation for the divergence of the electric field in a charge free region ($\boldsymbol{\nabla} \cdot \boldsymbol{E} = 0$), and substituting for $\mathbf{J}$ and $\boldsymbol{D}$ yields the wave equation

$$\boldsymbol{\nabla}^2 \boldsymbol{E} = \mu\sigma \frac{\partial \boldsymbol{E}}{\partial t} + \mu\varepsilon \frac{\partial^2 \boldsymbol{H}}{\partial t^2} \tag{3}$$

Fourier transformation yields the Helmholtz equations

$$(\boldsymbol{\nabla}^2 \boldsymbol{E} + k^2 \boldsymbol{E}) = 0 \tag{4}$$

$$(\boldsymbol{\nabla}^2 \boldsymbol{H} + k^2 \boldsymbol{H}) = 0 \tag{5}$$

where k is the propagation constant or complex wave number in the medium

$$k^2 = \mu\varepsilon\omega^2 - i\mu\sigma\omega$$

where ω is the angular frequency and $e^{i\omega t}$ is the time dependence for $\boldsymbol{E}$ and $\boldsymbol{H}$

The very low frequencies used in marine CSEM method and the high conductivities of the ocean water and saturated sediments result in $\mu\varepsilon\omega^2 \ll \mu\sigma\omega$ (known as the quasi-static assumption which is valid for earth materials at frequencies less than 10^5 Hz). At these frequencies displacement currents are much smaller than conduction currents.

At the low frequencies the propagation constant k becomes

$$k \cong \sqrt{(-i\sigma\mu\omega)} = \sqrt{\left(\frac{\sigma\mu\omega}{2}\right)} - i\sqrt{\left(\frac{\sigma\mu\omega}{2}\right)} = \sqrt{(\sigma\mu\omega)}e^{-i\frac{\pi}{4}}$$

The quasi-static assumption allows the second term of the wave equation to be neglected, yielding the diffusion equations

$$\boldsymbol{\nabla}^2\boldsymbol{E} = \mu\sigma\frac{\partial\boldsymbol{E}}{\partial t} \tag{6}$$

$$\boldsymbol{\nabla}^2\boldsymbol{H} = \mu\sigma\frac{\partial\boldsymbol{H}}{\partial t} \tag{7}$$

Equations (6) and (7) represent diffusion equations. These equations describe the behaviour of electric and magnetic fields at the frequencies used in marine CSEM. The inherent lack of resolution of the CSEM method is related to the diffusion of EM energy. The effective resolution of the CSEM method falls between that of exploration methods governed by the wave equation and methods that can be described by Laplace's equation (Keys, 2003).

High frequency wave propagation, wave equation (e.g. seismic and radar)

$$\boldsymbol{\nabla}^2\boldsymbol{u} = \frac{1}{c^2}\frac{\partial^2\boldsymbol{u}}{\partial t^2}$$

Low frequency EM diffusion equation (e.g. **CSEM** and MT)

$$\boldsymbol{\nabla}^2\boldsymbol{E} = \mu\sigma\frac{\partial\boldsymbol{E}}{\partial t}$$

Zero frequency potential field (e.g. gravity, magnetics, DC resistivity methods)

$$\boldsymbol{\nabla}^2\boldsymbol{V} = 0$$

Fourier transformation gives the frequency domain harmonic time representations of equations (6) and (7), for a halfspace, where $e^{i\omega t}$ is the time dependence for $\boldsymbol{E}$ and $\boldsymbol{H}$

$$\frac{\partial^2\boldsymbol{E}}{\partial z^2} = i\mu\sigma\omega\boldsymbol{E} \tag{8}$$

$$\frac{\partial^2\boldsymbol{H}}{\partial z^2} = i\mu\sigma\omega\boldsymbol{H} \tag{9}$$

2.5.2 Monochromatic plane wave solution to the diffusive wave equation

The simplest solution to the diffusive EM wave equation is a monochromatic plane wave that describes the electric and magnetic field intensity with depth z

$$\boldsymbol{E}(z) = \boldsymbol{E}_0 e^{-\beta z} e^{-i\alpha z}\, e^{i\omega t} \tag{10}$$

$$\boldsymbol{H}(z) = \boldsymbol{H}_0 e^{-\beta z} e^{-i\alpha z}\, e^{i\omega t} \tag{11}$$

where

$\boldsymbol{E}_0$ and $\boldsymbol{H}_0$ are the values of the field at $z = 0$

When conduction currents dominate over displacement currents as with the marine CSEM method α and β become equal, real quantities where

$$\alpha = \beta = \sqrt{\frac{\omega\sigma\mu}{2}}$$

Equations (10) and (11) show that the fields oscillate sinusoidally with both depth and time due to the $e^{-i\alpha z}$ term and the $e^{i\omega t}$ term. $\boldsymbol{E}_x$ and $\boldsymbol{H}_y$ have constant amplitudes over a plane perpendicular to the z axis, this is uniform plane wave. In any plane $\boldsymbol{E}$ and $\boldsymbol{H}$ will exhibit the same phase. The fields will attenuate with depth due to the $e^{-\beta z}$ term.

2.5.3 Electromagnetic skin depth

The solutions to the diffusive wave equation describe attenuation of the electric and magnetic fields with depth. An electromagnetic wave will be reduced in amplitude by a factor of e^{-1} at a distance within the medium, described by the skin depth δ, where

$$\delta = \frac{1}{\beta} = \sqrt{\frac{2\rho}{\mu\omega}} \approx 503\sqrt{\frac{\rho}{f}} \approx 503\sqrt{\rho T}$$

where ρ is the resistivity (Ωm), f is the frequency (Hz) of the controlled source and T is the period (s) of the current waveform .

Thus equations (10) and (11) can be written in terms of the skin depth δ

$$\boldsymbol{E}(z) = \boldsymbol{E}_0 e^{-\frac{z}{\delta}} e^{i\left(\frac{z}{\delta}-\omega t\right)} \tag{12}$$

$$\boldsymbol{H}(z) = \boldsymbol{H}_0 e^{-\frac{z}{\delta}} e^{i\left(\frac{z}{\delta}-\omega t\right)} \tag{13}$$

The expression for the skin depth is derived only for plane waves; however this gives an indication of the decay depths that we are dealing with when target hydrocarbon reservoirs are below sediments with relatively even resistivity distributions. An overburden with low resistivity attenuates EM fields more rapidly, thus having a smaller skin depth than a higher resistivity overburden. When using a current waveform with a short period (high frequency) the fields skin depth will be shorter than when using a longer period (low frequency) current waveform. The geological factor that determines the maximum depth at which a target reservoir can be detected is primarily controlled by the overburden resistivity. Low resistivity overburdens require lower fundamental transmission frequencies so that sufficient energy reaches the hydrocarbon reservoir producing a measurable response. However using low frequencies ultimately reduces the resolution.

To demonstrate the effect of the overburden resistivity and the current waveform on the skin depth of the arising field, skin depth for a range of halfspace resistivities and current waveform periods is shown in Figure 2.13. The CSEM representation of this is shown in Figures 2.14 and 2.15 illustrating the attenuation of the electric field with source-receiver offset for a range of halfspace resistivities and harmonic frequencies.

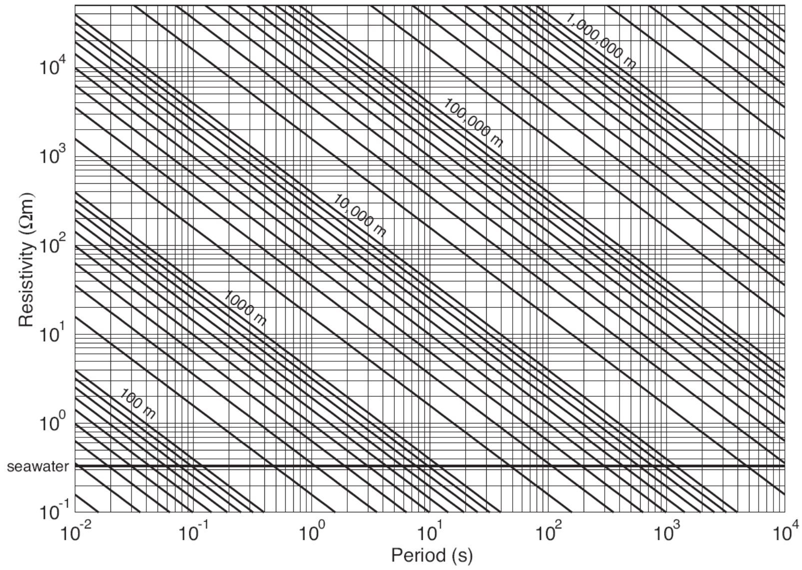

Figure 2.13 Skin depth versus current waveform period for different halfspace resistivities (Reproduced from (Keys, 2003).

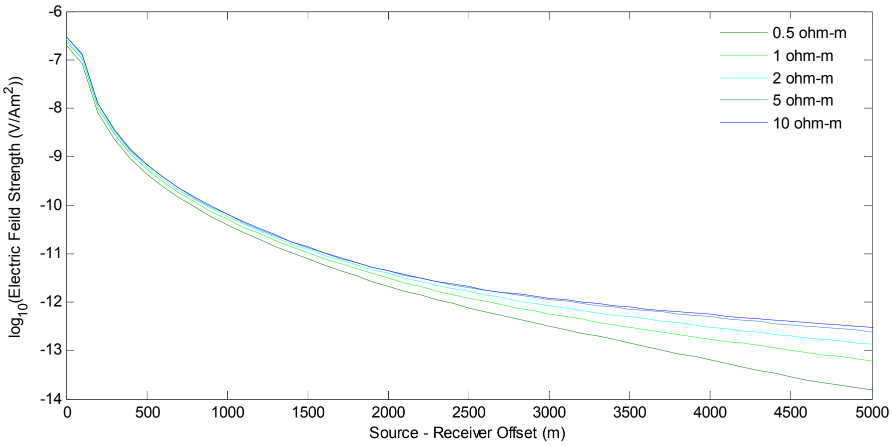

Figure 2.14 Electric field strength versus offset for a water depth of 1000 m over a halfspace of varying resistivity ρ at 0.3 Hz.

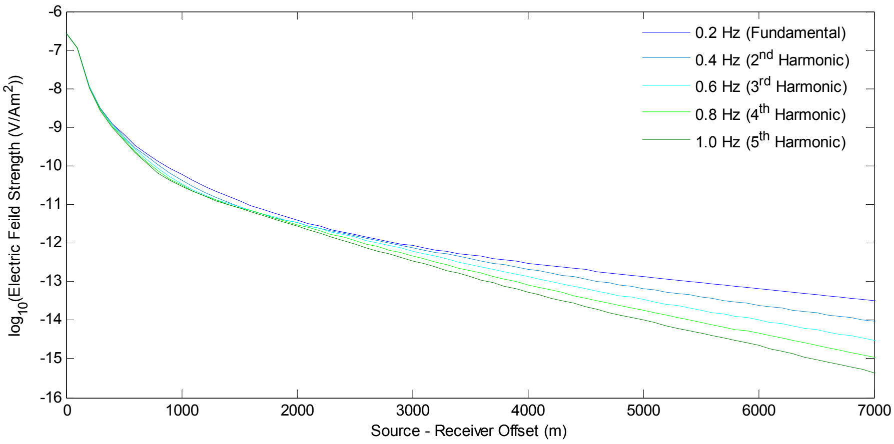

Figure 2.15 Electric field strength versus offset for a water depth of 1000 m over a halfspace of 1.5 Ωm for fundamental frequency of 0.2 Hz up to 1.0 Hz (the 5th Harmonic).

Seawater has a low resistivity of about 0.3 Ωm, and a small skin depth of ~270 m for signals of 1 Hz. On the seafloor of a deep ocean (several skin depths deep) incident magnetotelluric (MT) fields due to natural time variations of Earth's magnetic field, in the period range of about 10^{-3} to 10^{5}s, are almost completely attenuated except for the very longest period signals. Thus the seafloor provides an electromagnetically quiet environment for controlled source EM methods. Onshore CSEM provides a challenge in that the air is around and above the instruments; a large amount of energy is broadcast from the controlled source directly to the receivers through the air, with much less interaction with the subsurface. Onshore environments are also much noisier due to background noise, including cultural and short period MT sources (Interview Srnka, 2007).

2.6 Transverse resistance

Results from 1D modelling illustrate that marine CSEM is affected by the equivalency principle and as such is sensitive, within limits, primarily to the transverse resistance of the target, which is the resistivity thickness product in Ωm^2 (Mehta et al., 2006). Figure 2.17 demonstrates the equivalent response of different deep water 1D reservoir models, each with a transverse resistance of 5000 Ωm^2, it can be seen that each model has an almost identical response. The problem of equivalence is due to that fact that resistivity and thickness are the two contributions to size in the 1D sense, these two parameters are correlated inevitably to some extent (Constable and Weiss, 2006). In application, unlike DC resistivity, marine CSEM should in principle be able to resolve the resistivity and thickness of a target layer individually. Constable and Weiss (2006) showed that marine CSEM is not entirely affect by the equivalence principle. A horizontal electric dipole source excites both galvanically and inductively coupled modes, and the response of a given resistivity structure depends on the interplay between the galvanic and inductive effects, which tend to work in opposition (Eidesmo et al., 2002). Due to the fact that the galvanic component of current flow will be as in DC resistivity, whereas the inductive component of field attenuation will be sensitive to the target resistivity and independent of the thickness both parameters can be individually resolved. The electric field response increases with increasing thickness. Equivalence is observed only for low frequencies; at higher frequencies equivalence was less apparent. Constable and Weiss (2006) suggested that the galvanic response accounts for most of the sensitivity to thin resistive layers, and as the resistivity and skin depth increase, there is an increase in inductive response.

The implication of this for a real world survey is by combining data at different frequencies, the thickness and resistivity of a target reservoir can be estimated separately.

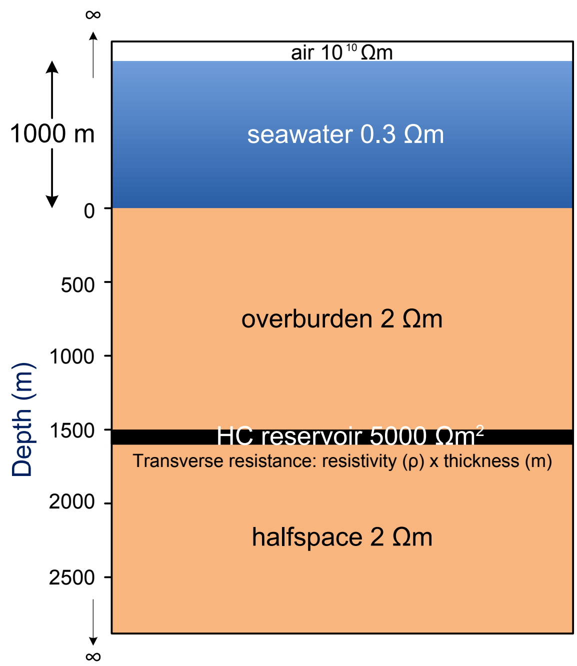

Figure 2.16 Deep water four layer 1D model for a targets with transverse resistivity of 5000 Ωm^2.

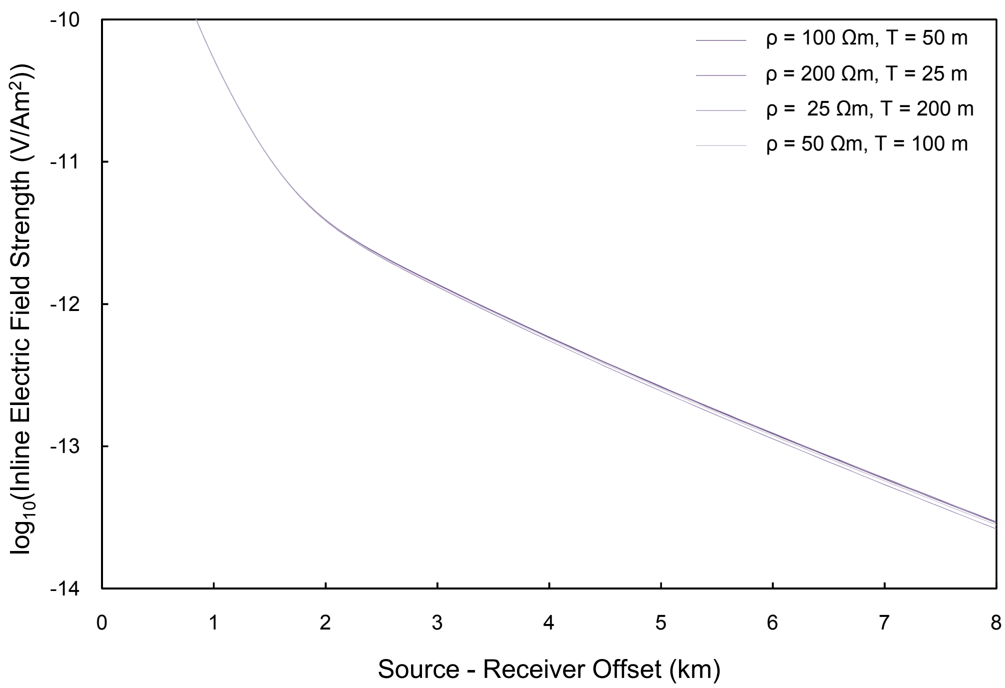

Figure 2.17 Equivalency principle demonstrated for the 1D model shown in Figure 2.16 for four different targets each with a transverse resistance of 5000 Ωm^2. It can be seen that the response for each case is almost identical.

2.6.1 Hydrocarbon saturation and formation resistivity

Potential reservoir formations, when dry, are effectively infinitely resistive. Electrical current will only flow through the interstitial saline water that saturates the pore space. Electrical conductivity is a strong indicator of porosity and pore fluid properties. Electrical properties derived from a marine CSEM survey have a direct relationship with reservoir fluids. CSEM methods remotely characterise these fluids relating electrical resistivity to water saturation. Since hydrocarbons are effectively infinitely resistive, when these buoyant fluids displace water from a formation, increasing the hydrocarbon saturation, they effectively reduce the water saturation. CSEM measurements respond directly to this increase in hydrocarbon saturation. Archie's Law (Archie, 1942) is an empirical formulation that can be used to relate hydrocarbon saturation, pore water resistivity and porosity to true resistivity of a reservoir. This true resistivity is what the CSEM method is sensitive to. Archie's Law is given as

$$R_T = \frac{R_w a}{(1 - S_h)^n \phi^m}$$

where

R_T is the true resistivity of the hydrocarbon bearing formation in (Ωm)

R_w is the resistivity of the pore water in (Ωm)

S_h is the hydrocarbon saturation factor

a is an empirical constant, a value of 0.65 is used for the Northwest Shelf

m is the cementation exponent, a value of 1.8 is used

n is the saturation exponent, a value of 2 is used

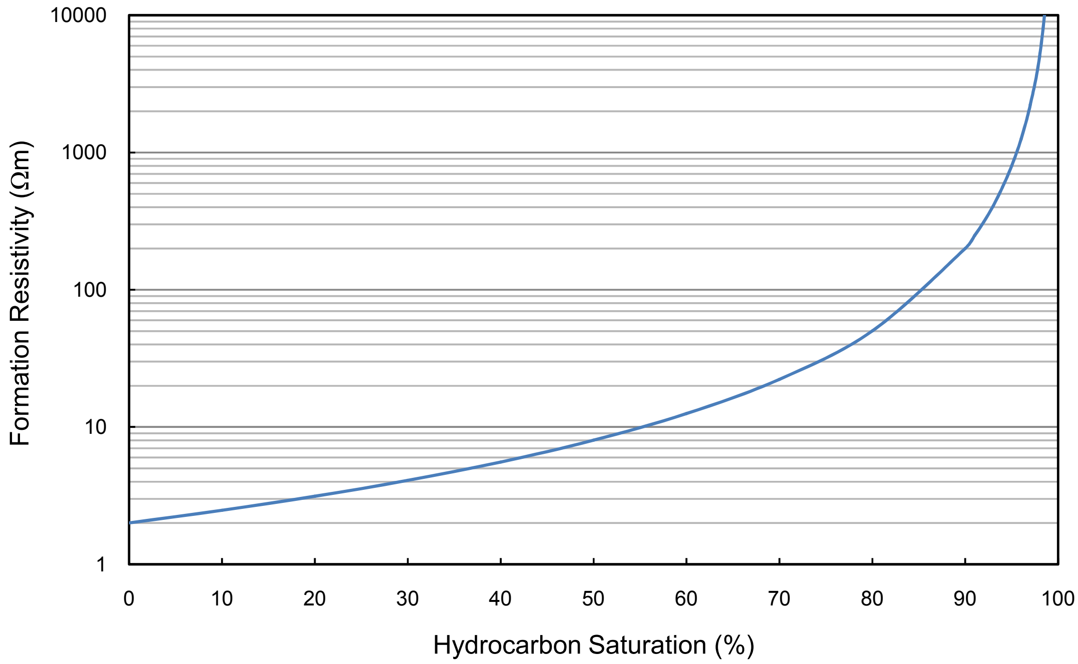

Figure 2.18 Formation resistivity versus hydrocarbon saturation for a typical offshore sandstone reservoir with a pore fluid resistivity of 0.1 Ωm and 15% porosity; a = 0.65, m = 1.8, n = 2. For 100% water saturation, the formation resistivity is 2 Ωm. For hydrocarbon saturations of 50%, 80% and 90% the formation resistivity is 8 Ωm, 50 Ωm and 200 Ωm respectively.

2.7 Component Data Display and Field Measurments

It is important to understand what each CSEM data display represents in terms of the survey geometry in relation to the components of the electromagnetic field that are measured. Most often the inline horizontal component of the electric field is displayed as a function of source-receiver offset. Figure 2.19 shows the geometry of a horizontal electric dipole source. The measured field along the axis of the transmitter (Azimuth of 0°) is considered as the inline field. The measured field perpendicular to the major horizontal direction of the field (Azimuth of 90°) is considered as the broadside field. Usually the source is towed along an array of receivers; electric dipole receiver antennas along this tow direction measure the inline field. The transmitter can also be towed perpendicular to an array of receivers; electric dipole receiver antennas at an azimuth of 90° to the major horizontal direction of the field record the broadside electric field.

To detect the presence of a thin horizontal resistive layer only some components of the electromagnetic field need to be measured. To understand why particular components need to be measured we must understand the direction of the coupled vector field at the hydrocarbon layer and at the air/water interface. Hydrocarbons reservoirs in their most simple geometrical expression are flat thin layers. The thin hydrocarbon saturated layer is a high impedance electrical structure that prevents the vertical diffusion of energy, and guides this energy across the structure for many kilometres with low attenuation. There is some diffusion of energy vertically through the layer, but this is a small component. At the air/water interface with the effective infinite resistance of the air, there is no diffusion of energy past interface and the field becomes totally horizontal, there is no vertical component; vertical receiver antennas are not affected by the air-wave.

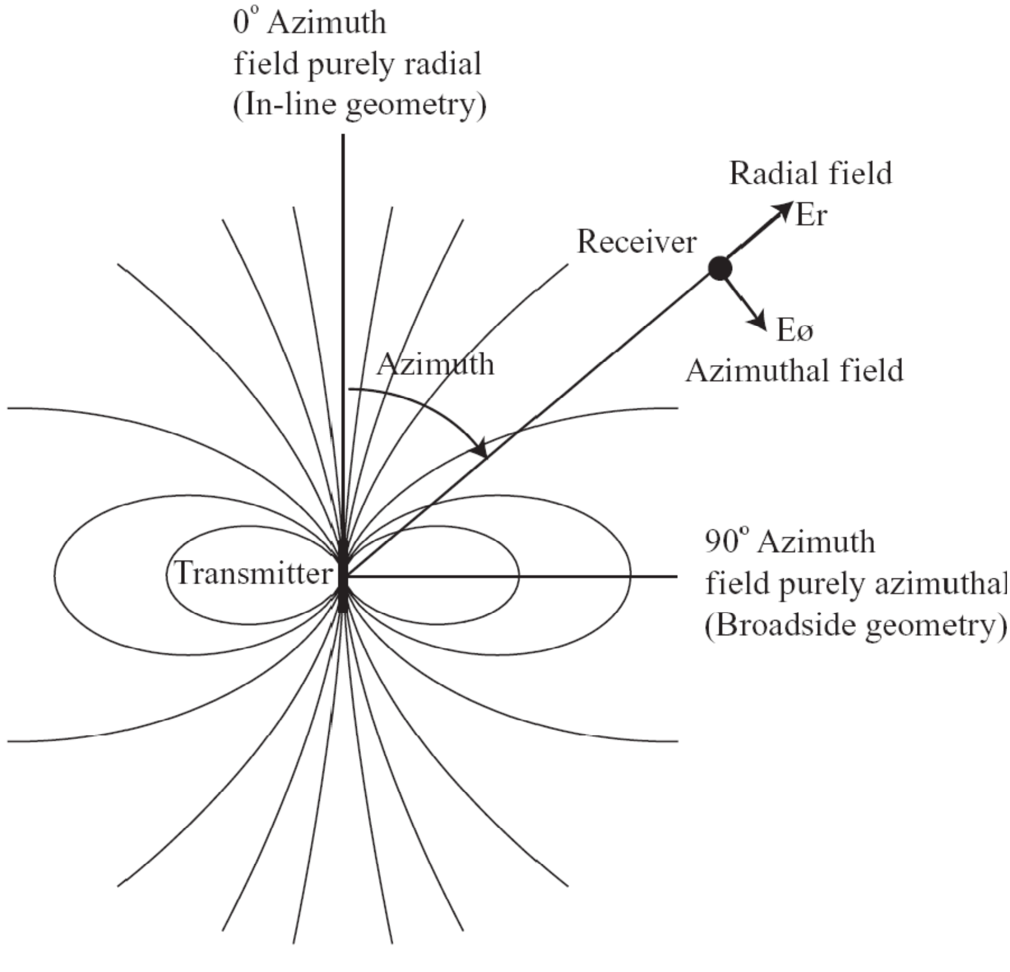

Figure 2.19 The geometry of CSEM dipole fields. The transmitter dipole is shown in red and is towed along this axis, inline receiver array is shown in blue and the broadside receiver array is shown in orange (Modified from Constable and Weiss, 2006).

2.7.1 Normalisation of response with the background structure

Because CSEM field amplitudes vary over such a large range (10^{-6} to 10^{-16} V/Am^2 for the electric field), it is useful to consider the normalised response (Constable and Weiss, 2006). A common data representation is to normalise the observed electric field by a background response (structure without the target reservoir) and plot the results as a function of the source-receiver offset. This effectively shows response due to the target reservoir as a function of the source-receiver offset. The background response chosen for the normalisation can produce significantly different normalised responses (Hoversten et al., 2006). Therefore it is crucial to accurately define the background electrical structure.

Integration of both marine MT and marine CSEM techniques can be used to characterize and constrain the overall background conductivity structure, which is useful for producing accurate normalisation and for CSEM numerical modeling and interpretation (Keys, 2003). MT data can be easily acquired by marine EM receivers when the CSEM source is not operating without any loss of productivity and at no extra logistical cost. The fastest and most common data presentation in early field reports is often the first option, assuming a half-space model. Building models using existing resistivity logs is also an option, although the seabed section is rarely logged and the point measurements that logging involves, misrepresent the large scale electrical structure. Use of either the CSEM data itself (at a location where there is no reservoir response) or the MT data collected while the CSEM transmitter is not operating are the best options (Constable and Weiss, 2006). However using CSEM at a location off the reservoir will not properly characterise the background electrical structure of the location of the reservoir.

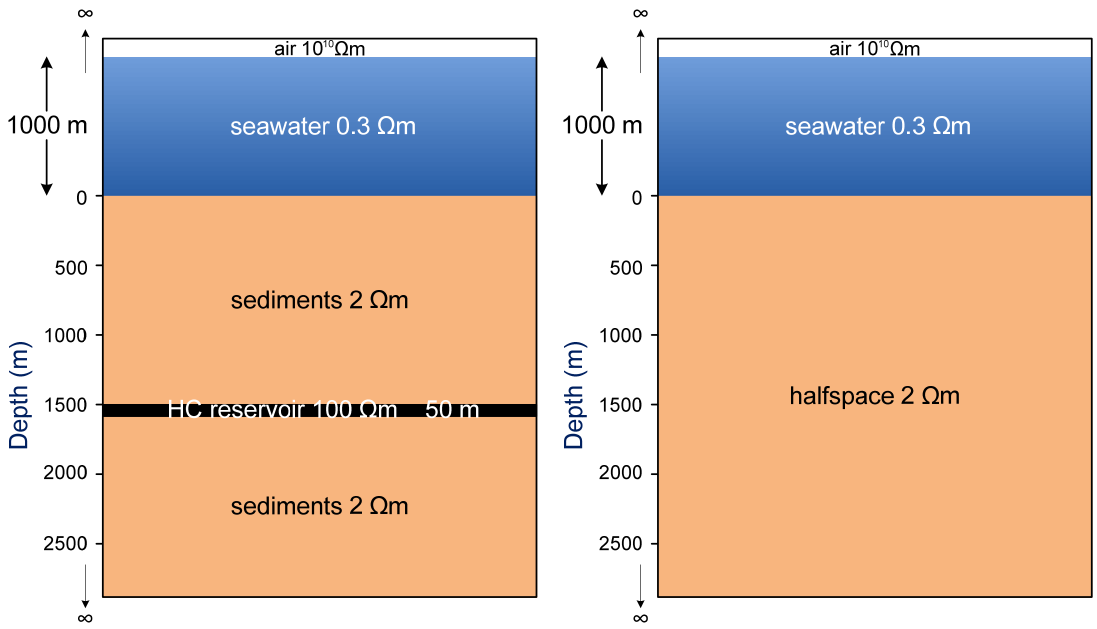

Figure 2.20 Simple four layer reservoir model (left) and background halfspace model (right) used for normalization.

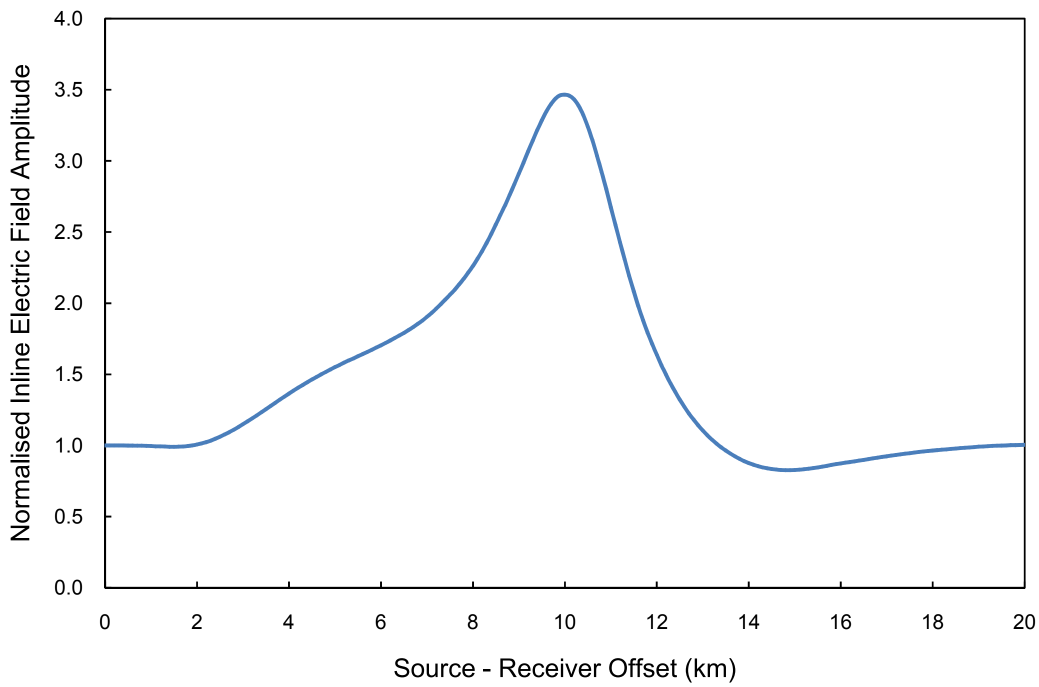

Figure 2.21 Normalised inline electric field response obtained by dividing the response of the reservoir model by the background halfspace response.

3 MODELLING OF THE CSEM RESPONSE

This chapter contains a description of the forward modelling algorithm used to numerically simulate real marine CSEM survey data. A general overview of hydrocarbon reservoir detectability with current technology is then presented. The effects and limitations of geology and survey parameters are shown. These are the critical factors that should be considered when planning a marine CSEM survey.

3.1 Modified Integral Equation Code

Forward modelling solutions for one-dimensional (1D) layered earth models have been available for many years. These solutions consist of Fourier or Bessel integrals which can be easily evaluated numerically. A frequency domain modified integral equation code is used here to numerically simulate real marine CSEM survey data. This code provides efficient evaluation of 1D layered earth models excited by current bipole(s). The coupled vector field can be calculated at any point in space. **Primary** and **secondary** fields are calculated individually. Real and imaginary components of the electric field ($\boldsymbol{E}$) and magnetic field ($\boldsymbol{H}$) are calculated for all Cartesian vectors ($\boldsymbol{E}_x$, $\boldsymbol{E}_y$, $\boldsymbol{E}_z$, $\boldsymbol{H}_x$, $\boldsymbol{H}_y$ and $\boldsymbol{H}_z$) of the coupled vector field from which amplitude and phase can be derived.

The approach of Hohmann (1988) is followed with application to a simple model that consists of; the air/water interface, water column, host sediments, and a target layer (hydrocarbon reservoir) over a halfspace. Due to attenuation in the earth only low frequencies are of interest, so displacement currents can be ignored. Frequency domain equations used by this integral equation code are obtained by performing a Fourier transformation of the time domain equations described below.

If the displacement currents are neglected, the coupled space and time dependence of electric and magnetic fields can be described by Maxwell's equations as functions of position, **r** and time, t:

$$\boldsymbol{\nabla} \times \boldsymbol{E}(\boldsymbol{r},t) = -\mu_0 \frac{\partial \boldsymbol{H}(\boldsymbol{r},t)}{\partial t} - \mu_0 \frac{\partial \boldsymbol{m}_p}{\partial t}(\boldsymbol{r},t) \tag{1}$$

and

$$\boldsymbol{\nabla} \times \boldsymbol{H}(\boldsymbol{r},t) = \sigma \boldsymbol{E}(\boldsymbol{r},t) + \boldsymbol{j}_p(\boldsymbol{r},t) \tag{2}$$

Here $\boldsymbol{m}_p$ is the **primary** magnetic current and $\boldsymbol{j}_p$ is the **primary** electric current. Taking the curl of equation (1) and substituting into equation (2) yields a vector diffusion equation for the electric field:

$$\boldsymbol{\nabla} \times \boldsymbol{\nabla} \times \boldsymbol{E} + \mu_0 \sigma \frac{\partial \boldsymbol{E}}{\partial t} = -\mu_0 \frac{\partial \boldsymbol{j}_p}{\partial t} - \mu_0 \boldsymbol{\nabla} \times \frac{\partial \boldsymbol{m}_p}{\partial t} \tag{3}$$

Taking the curl of equation (2) and substituting equation (1) yields a diffusion equation for the magnetic field:

$$\boldsymbol{\nabla} \times \left(\frac{\boldsymbol{\nabla} \times \boldsymbol{H}}{\sigma}\right) + \mu_0 \frac{\partial \boldsymbol{H}}{\partial t} = \boldsymbol{\nabla} \times \left(\frac{\boldsymbol{j}_p}{\sigma}\right) - \mu_0 \frac{\partial \boldsymbol{m}_p}{\partial t} \tag{4}$$

Equations (3) and (4) demonstrate the fact that due to attenuation in the earth, CSEM frequencies must be so low such that we deal with a diffusion of EM energy rather than the propagation of a wave. Hence the low resolution of the resistivity distribution within the earth than can be obtained from the marine CSEM method.

We can now apply the vector identity

$$\boldsymbol{\nabla} \times \boldsymbol{\nabla} \times \boldsymbol{A} \equiv -\boldsymbol{\nabla}^2 \boldsymbol{A} + \boldsymbol{\nabla}(\boldsymbol{\nabla} \cdot \boldsymbol{A})$$

Equation (3) becomes

$$-\boldsymbol{\nabla}^2\boldsymbol{E} + \boldsymbol{\nabla}(\boldsymbol{\nabla}\cdot\boldsymbol{E}) + \mu_0\frac{\partial\boldsymbol{E}}{\partial t} = -\mu_0\frac{\partial\boldsymbol{j}_p}{\partial t} - \mu_0\boldsymbol{\nabla}\times\frac{\partial\boldsymbol{m}_p}{\partial t} \tag{5}$$

Taking the divergence of equation (2) gives

$$\boldsymbol{\nabla}\cdot(\sigma\boldsymbol{E}) = \sigma\boldsymbol{\nabla}\cdot\boldsymbol{E} + \boldsymbol{\nabla}\sigma\cdot\boldsymbol{E} = -\boldsymbol{\nabla}\cdot\boldsymbol{j_p}$$

Substituting for $\boldsymbol{\nabla}\cdot\boldsymbol{E}$ into equation (5) gives

$$\boldsymbol{\nabla}^2\boldsymbol{E} + \boldsymbol{\nabla}\left(\boldsymbol{E}\cdot\frac{\boldsymbol{\nabla}\sigma}{\sigma}\right) - \mu_\sigma\sigma\frac{\partial\boldsymbol{E}}{\partial t} = \mu_0\frac{\partial\boldsymbol{j}_p}{\partial t} - \rho\boldsymbol{\nabla}(\boldsymbol{\nabla}\cdot\boldsymbol{j}_p) + \mu_0\boldsymbol{\nabla}\times\frac{\partial\boldsymbol{m}_p}{\partial t} \tag{6}$$

Assuming that the source is in a region of homogenous conductivity the following identity can be used:

$$\boldsymbol{\nabla}\times\phi\boldsymbol{A} = \phi\boldsymbol{\nabla}\times\boldsymbol{A} - \boldsymbol{A}\times\boldsymbol{\nabla}\phi$$

Equation (4) can be written as

$$-\boldsymbol{\nabla}^2\boldsymbol{H} + \boldsymbol{\nabla}(\boldsymbol{\nabla}\cdot\boldsymbol{H}) - \sigma(\boldsymbol{\nabla}\times\boldsymbol{H})\times\boldsymbol{\nabla}\rho + \mu_0\sigma\frac{\partial\boldsymbol{H}}{\partial t} = \boldsymbol{\nabla}\times\boldsymbol{j}_p - \mu_0\sigma\frac{\partial\boldsymbol{m}_p}{\partial t}$$

The divergence of the magnetic field is non-zero only at a magnetic source; taking the divergence of equation (1) shows that:

$$\boldsymbol{\nabla}\cdot\boldsymbol{H} = -\boldsymbol{\nabla}\cdot\boldsymbol{m}_p$$

Giving

$$\boldsymbol{\nabla}^2\boldsymbol{H} + \sigma(\boldsymbol{\nabla}\times\boldsymbol{H})\times\boldsymbol{\nabla}\rho - \mu_0\sigma\frac{\partial\boldsymbol{H}}{\partial t} = \mu_0\sigma\frac{\partial\boldsymbol{m}_p}{\partial t} - \boldsymbol{\nabla}(\boldsymbol{\nabla}\cdot\boldsymbol{m}_p) - \boldsymbol{\nabla}\times\boldsymbol{j}_p \tag{7}$$

Equations (6) and (7) are the general equations for the **total** electric and magnetic fields valid at any point in space. Either equation can be solved numerically by time stepping, and then the other field can be calculated from equations (1) and (2). The **primary** fields which apply at any point in a layered earth if there is no body present satisfy the following two equations:

$$\boldsymbol{\nabla} \times \boldsymbol{E}_p = -\mu_0 \frac{\partial \boldsymbol{H}_p}{\partial t} - \mu_0 \frac{\partial \boldsymbol{m}_p}{\partial t} \tag{8}$$

$$\boldsymbol{\nabla} \times \boldsymbol{H}_p = \sigma_{layering} \boldsymbol{E}_p + \boldsymbol{j}_p \tag{9}$$

Where $\sigma_{layering}$ is the normal layered earth conductivity with no body present. These **primary fields** are in the form of integrals that can be evaluated numerically. To obtain equations in the frequency domain, a Fourier transformation is performed on time domain equations (6) and (7) using the following integrals, assuming $e^{i\omega t}$ time dependence:

$$\boldsymbol{F}(\boldsymbol{r}, \omega) = \int_{-\infty}^{\infty} \boldsymbol{f}(\boldsymbol{r}, t) e^{-i\omega t} dt$$

$$\boldsymbol{f}(\boldsymbol{r}, t) = \frac{1}{2\pi} \int_{-\infty}^{\infty} \boldsymbol{F}(\boldsymbol{r}, \omega) e^{i\omega t} d\omega$$

Equation (6) then becomes

$$\boldsymbol{\nabla}^2 \boldsymbol{E} + \boldsymbol{\nabla}\left(\boldsymbol{E} \cdot \frac{\boldsymbol{\nabla}\sigma}{\sigma}\right) + k^2 \boldsymbol{E} = i\omega\mu_0 \mathbf{J}_p - \rho \boldsymbol{\nabla}\left(\boldsymbol{\nabla} \cdot \mathbf{J}_p\right) + i\omega\mu_o \boldsymbol{\nabla} \times \boldsymbol{M}_p \tag{10}$$

Equation (7) then becomes

$$\boldsymbol{\nabla}^2 \boldsymbol{H} + \sigma(\boldsymbol{\nabla} \times \boldsymbol{H}) \times \boldsymbol{\nabla}\rho + k^2 \boldsymbol{H} = i\omega\mu_0 \boldsymbol{M}_p - \boldsymbol{\nabla}\left(\boldsymbol{\nabla} \cdot \boldsymbol{M}_p\right) - \boldsymbol{\nabla} \times \mathbf{J}_p \tag{11}$$

Equations (10) and (11) are the general frequency domain equations for the **total** electric and magnetic fields valid for every point for a layered earth, i.e. in the absence of any bodies embedded in the layered earth. For the **total field**, away from the source, either equation can be solved numerically, where the other component can be found using the frequency domain versions of equations (1) and (2).

3.1.1 Modelling 3D bodies in a layered earth using integral equations

For a 3D body embedded in a layered earth we must consider the **total field** as the summation of the **primary field** as the response of the layered earth, plus the **secondary field** as the scattering response of a body embedded within the layered earth.

Subtracting (8) from equation (1) and equation (9) from equation (2) gives the time domain equations for the **secondary field** due to the body:

$$\nabla \times \boldsymbol{E}_s = -\mu_0 \frac{\partial \boldsymbol{H}_s}{\partial t} \tag{12}$$

and

$$\nabla \times \boldsymbol{H}_s = \sigma \boldsymbol{E}_s + \sigma_{body} \boldsymbol{E}_p$$

or

$$\nabla \times \boldsymbol{H}_s = \sigma_{layering} \boldsymbol{E}_s + \boldsymbol{j}_s \tag{13}$$

where

$$\boldsymbol{j}_s = \sigma_{body} \boldsymbol{E}$$

Note $\sigma_{body} = \sigma - \sigma_{layering}$ is the point conductivity of the 3D body. The quantity $\boldsymbol{j}_s$ is the scattering current of the body and is the source of the **secondary field**.

The equation for $\boldsymbol{E}_s$ is the same as that for $\boldsymbol{E}$ in equation (6), without the magnetic source terms and with $\boldsymbol{j}_s$ replaced by $\sigma_{body}\boldsymbol{E}_p$

$$\boldsymbol{\nabla}^2\boldsymbol{E}_s + \boldsymbol{\nabla}\left(\boldsymbol{E}_s \cdot \frac{\boldsymbol{\nabla}\sigma}{\sigma}\right) - \mu_\sigma\sigma\frac{\partial \boldsymbol{E}_s}{\partial t} = \mu_0\sigma_{body}\frac{\partial \boldsymbol{E}_p}{\partial t} - \boldsymbol{\nabla}\left(\boldsymbol{E}_p \cdot \frac{\boldsymbol{\nabla}\sigma_{body}}{\sigma}\right) \quad (14)$$

Since $\boldsymbol{\nabla} \cdot \boldsymbol{E}_p$ is zero in the body, which is the only place where σ_{body} is not zero, the secondary magnetic field can be derived by modifying equation (7) in a similar way to which we modified equation (6)

$$\boldsymbol{\nabla}^2\boldsymbol{H}_s + \boldsymbol{\nabla} \times \boldsymbol{H_s} \times \boldsymbol{\nabla}\rho - \mu_0\sigma\frac{\partial \boldsymbol{H}_s}{\partial t} = \mu_0\sigma_{body}\frac{\partial \boldsymbol{H}_p}{\partial t} - \sigma\boldsymbol{\nabla}\left(\frac{\sigma_{body}}{\sigma}\right) \times \boldsymbol{E}_p \quad (15)$$

The reasons for solving equations (14) and (15) rather than the equations for the **total field** are that the **secondary fields** require fine discretization which involves dividing the 3D body into a number of cells and treating each cell as a source. The code used here uses the principle of symmetry for the body and reciprocity to reduce computation time.

To obtain equations in the frequency domain, a Fourier transformation is performed on time domain equations (14) and (15) assuming $e^{i\omega t}$ time dependence:

Equation (14) then becomes

$$\boldsymbol{\nabla}^2\boldsymbol{E}_s + \boldsymbol{\nabla}\left(\boldsymbol{E}_s \cdot \frac{\boldsymbol{\nabla}\sigma}{\sigma}\right) + k^2\boldsymbol{E}_s = -{k_a}^2\boldsymbol{E}_s - \boldsymbol{\nabla}\left(\boldsymbol{E}_p \cdot \frac{\boldsymbol{\nabla}\sigma_{body}}{\sigma}\right) \quad (16)$$

Equation (15) then becomes

$$\boldsymbol{\nabla}^2\boldsymbol{H_s} + \sigma(\boldsymbol{\nabla} \times \boldsymbol{H_s}) \times \boldsymbol{\nabla}\rho + k^2\boldsymbol{H_s} = -{k_a}^2\boldsymbol{H_s} - \sigma\boldsymbol{\nabla}\left(\frac{\sigma_{body}}{\sigma}\right) \quad (17)$$

For the **secondary field** solutions the other component can be calculated using the frequency domain versions of equations (12) and (13):

$$\nabla \times \boldsymbol{E}_s = -i\omega\mu_0 \boldsymbol{H}_s \tag{18}$$

$$\nabla \times \boldsymbol{H}_s = \sigma_{layering} \boldsymbol{E}_s + \mathbf{J}_s \tag{19}$$

In order to formulate an integral equation we need to treat $\mathbf{J}_s$ as a source current. In a wholespace the secondary electric field is given by

$$\boldsymbol{E}_s = -i\omega\mu_0 \boldsymbol{A}_s - \nabla V_s \tag{20}$$

where $\boldsymbol{A}_s$ and V_s are the secondary vector and scalar potentials for the Lorentz gauge given by

$$\boldsymbol{A}_s(\boldsymbol{r}) = \int_v \mathbf{J}_s(\boldsymbol{r}')G(\boldsymbol{r},\boldsymbol{r}')dv'$$

and

$$V_s(\boldsymbol{r}) = -\rho_{layering} \int_v \mathbf{J}_s(\boldsymbol{r}')G(\boldsymbol{r},\boldsymbol{r}')dv'$$

where G is the scalar EM Green's function:

$$G(\boldsymbol{r},\boldsymbol{r}') = \frac{e^{-ik_{layering}|\boldsymbol{r}-\boldsymbol{r}'|}}{4\pi|\boldsymbol{r}-\boldsymbol{r}'|}$$

For a body in a halfspace, an additional term given by Hohmann (1975) for a homogenous earth and in Wannamaker, et al. (1984) for a layered earth, must be added to expression (20) to account for the layering response.

Adding the **primary field** to the **secondary field** of expression (20) we get a singular Fredholm integral equation for the **total electric field** which is written as

$$\boldsymbol{E}(\boldsymbol{r}) = \boldsymbol{E}_p(\boldsymbol{r}) + \int_v \widetilde{\boldsymbol{G}}(\boldsymbol{r},\boldsymbol{r}') \cdot \sigma_{body}(\boldsymbol{r}')\boldsymbol{E}(\boldsymbol{r}')dv' \qquad (21)$$

where $\widetilde{\boldsymbol{G}}$ is a tensor Green's function

Effectively the 3D body has been replaced by a volume of scattering current. Equation (21) is limited to a 3D body within a layered earth (1D) and as such forms the basis of the modified integral equation code used here to forward model real hydrocarbon deposits as 3D bodies within a layered earth model that consists of the air/water interface, water column, host sediments, and a 3D target body (hydrocarbon reservoir).

3.2 Effect of Water Depth

As discussed in chapter 2, water depth is a key issue in the application of the marine CSEM method. Shallow water dramatically reduces the sensitivity and limits the range of source-receiver offsets over which the target is detectable, as shown in Figure 3.4. For HED sources, used exclusively in commercial application; the air-wave is always present. The amplitude of the air-wave reduces with increasing water depth, and becomes insignificant if the depth if great enough as shown in Figure 2.8. CSEM with an AC source is normally restricted to water depths exceeding 300 m (Ziolkowski et al., 2006), also demonstrated in Figure 3.4. In shallow water the amplitude of the air-wave can be between 1 and 2 orders of magnitude larger than the amplitude of the response from the reservoir as shown in Figure 3.2. With such a large background signals, a thin low resistivity reservoir may be undetectable with the application of current technology.

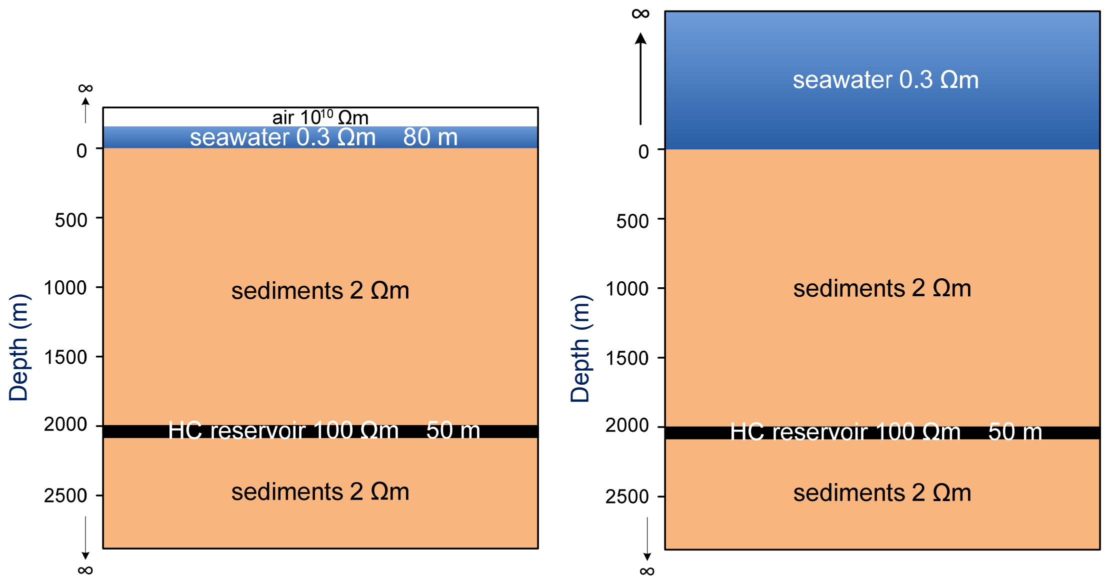

Figure 3.1 Shallow water (80 m) model (left) with reservoir at 2000 m depth. Infinite water column model (right) used for normalisation to derive air-wave component.

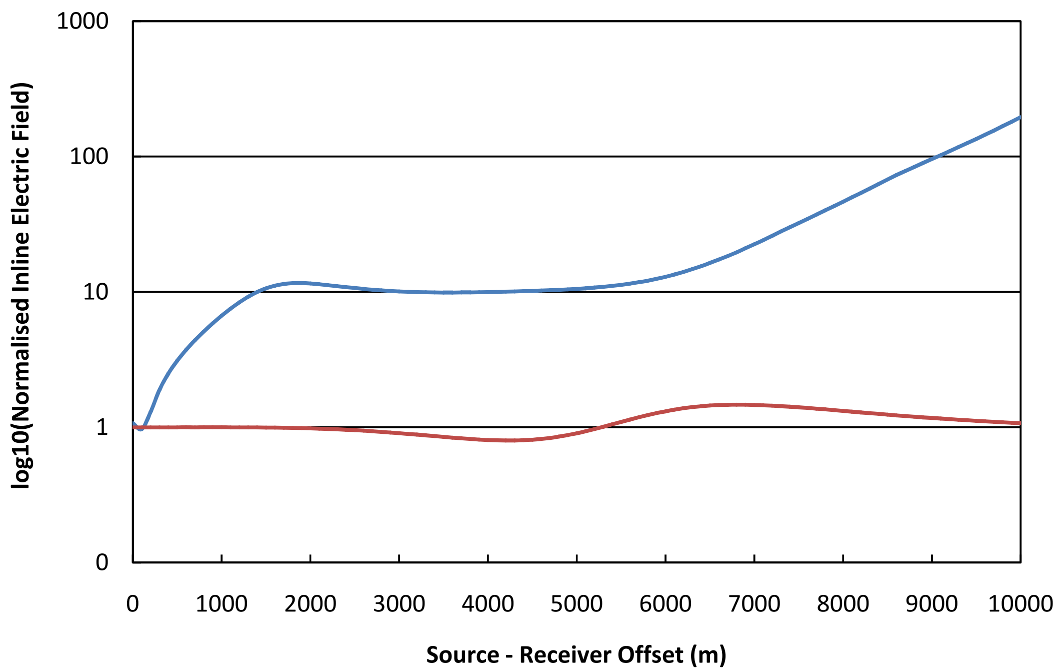

Figure 3.2 Log of the normalised inline electric field. The air-wave component (blue) is derived by normalisation of the shallow water model with the infinite water column shown in Figure 3.1. The reservoir component (red) is derived by normalisation of the shallow water model with a 2 Ωm halfspace. For source - receiver offsets of 1.5 - 5 km the air-wave is 1 order of magnitude stronger than the background response. At offsets of 5.5 - 9.5 km where the response from the reservoir is the greatest, the airwave is between 1 and 2 orders of magnitude greater than the reservoir response, in amplitude.

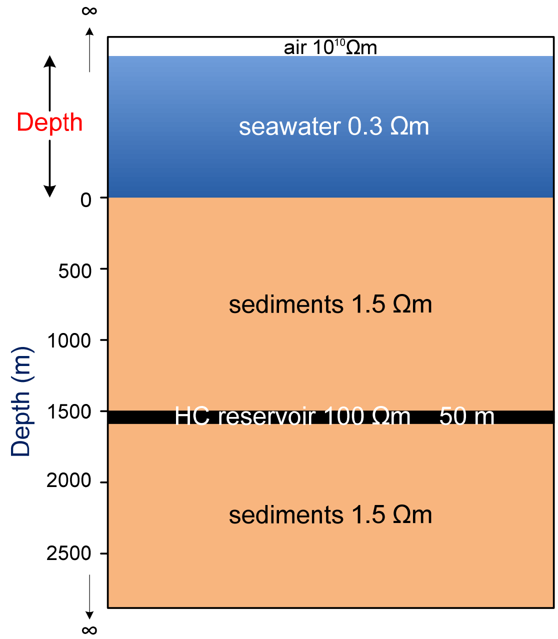

Figure 3.3 Model with reservoir at 1500 m depth for varying water depths of 100 - 1500 m.

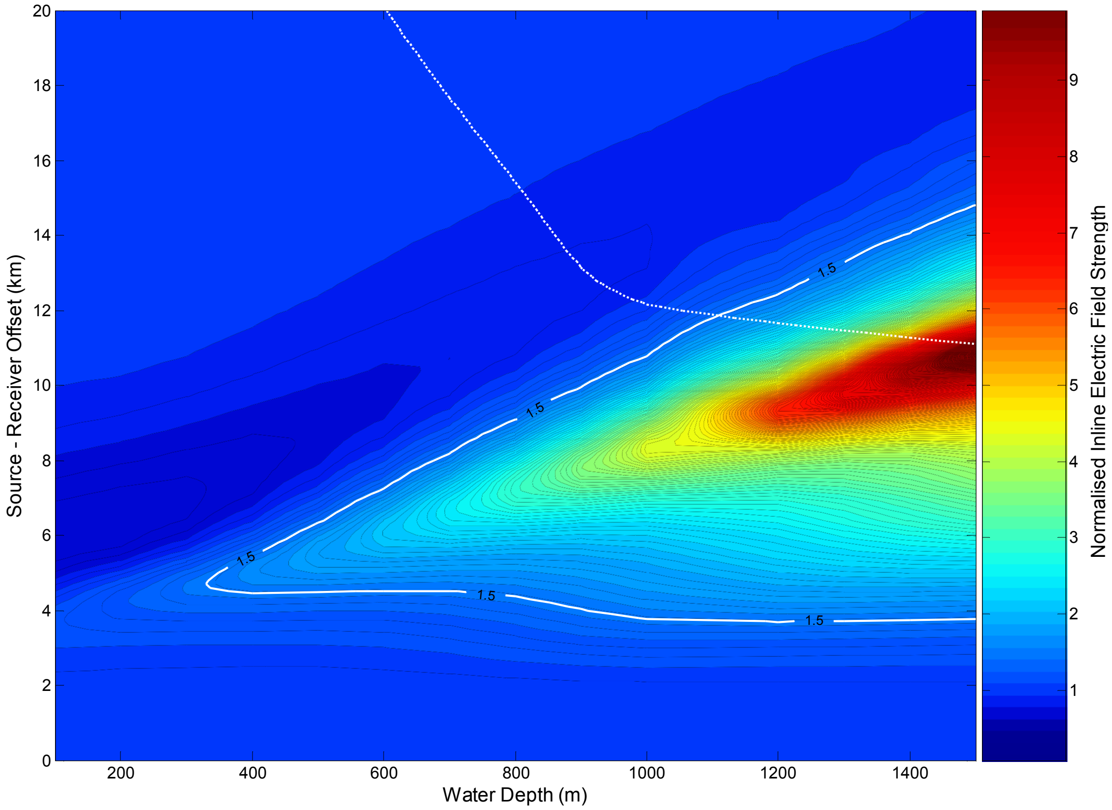

Figure 3.4 Contoured normalised inline electric field response for water depths 100 - 1500 m. Solid contours indicate 150% anomaly due to the reservoir response normalised with the background response for the model shown Figure 3.3. The dotted line indicates the noise floor of the inline electric field for the reservoir model. The minimum water depth for which the target reservoir is detectable against the background signal is ~300 m as indicated by the vertical yellow line. The range of source-receiver offsets over which the target is detectable, increases with increasing water depth.

3.3 Effect of Bathymetry

The marine CSEM method is strongly affected by variations in the seafloor bathymetry. This is due to the resistivity contrast between the seawater and the seabed. Bathymetry effects depend upon transmission frequency, seabed conductivity, ocean depth, transmitter-receiver geometry, and rugosity of the seafloor topography (Li and Constable, 2007). In the marine CSEM method, receivers are placed on the seafloor and must conform to the local slope such that they measure the electromagnetic fields along that slope (Li and Constable, 2007). This must be corrected for and in practice the slope fields can be trigonometrically transformed to the horizontal and vertical fields by using the tilt recorded by the receiver instruments. Modelling bathymetry requires 2D code; the results obtained by Li and Constable (2007) have been used to demonstrate the effect of sloping bathymetry, shown in Figure 3.8, for upward and downward bathymetry slope. The model with the upward slope produces the smallest normalised response. This is because the seafloor receivers on the model with the upward slope topography are further from the reservoir body. Similarly, the receivers on the model with downward slope are closer to the reservoir than those with flat seafloor topography, thus the larger normalised response.

In real world application of the marine CSEM method, the transmitter can be towed at a constant height by following the bathymetry, if it is smooth. This will minimize the effects of bathymetry. If the seafloor is too rugose (valleys and rises) for the transmitter to follow, then the bathymetry must be taken into account during processing. A seafloor rise can produce the same response as a reservoir, however a quantitative interpretation such as inversion may distinguish between these two scenarios (Mehta et al., 2006).

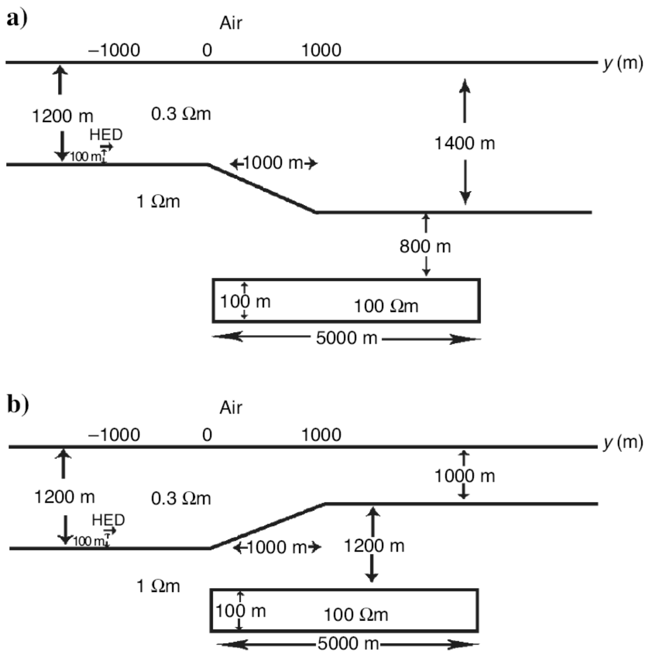

Figure 3.5 Sketch of the 2D resistive reservoir model with bathymetry topography (a) with downward slope (b) with upward slope (Reproduced from (Li and Constable, 2007).

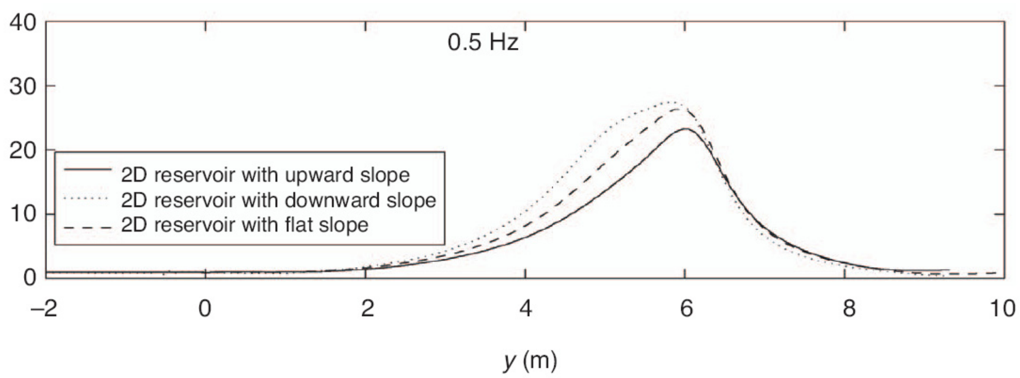

Figure 3.6 Normalised inline electric field response of the 2D reservoir model shown in Figure 351 (Li and Constable, 2007). The model with the upward slope produces the smallest normalised response. The model with the downward slope produces the largest normalised response.

3.4 Transmission Frequency versus Offset

Transmission frequency is critical to survey success and should be optimised to increase the response from the target reservoir. If the frequency is too low the survey will be insensitive to thin targets and resolution will be decreased. Thus there is a trade-off between depth penetration, controlled by the skin depth, which reduces with increasing frequency, and resolution which increases with increasing frequency. Normalised fields depend on the frequency and are larger for higher frequencies; however at high frequencies the signal falls below the instrument noise floor (10^{-15} V/Am^2). A strategy for designing a survey is to contour the normalised fields versus source-receiver offset for a range of transmission frequencies as shown in Figure 3.8. This is an easy way to assess the optimum fundamental frequency needed. By overlaying the contour of the noise threshold for the instrument system, the frequencies and offsets that fall below the noise floor can be identified. Constable and Weiss (2006) suggest a strategy; to make the normalised field as large as possible for the shortest possible offsets. Using the lowest possible frequency where the normalised fields are large enough, at the shortest offsets, allows for a larger range of harmonic frequency content. High frequencies can be used to constrain shallow formations as they are insensitive to deep targets. Using the largest range of frequencies will also provide the best inversion results. In Figure 3.8 the optimum frequency for the reservoir model (Figure 3.7) is considered to be 0.2 Hz for offsets of 5 km where the normalised fields are 150 %. We can see that the reservoir is seen over a limited range of frequencies and offsets; frequencies below 0.2 Hz require long offsets and do not produce large effects. For the optimum frequency range (0.2 - 1.0 Hz) we can see that the target is too deep to be seen at offsets below ~3.5 km and at offsets larger than ~12 km the sensitivity to the target is removed due to the air-wave.

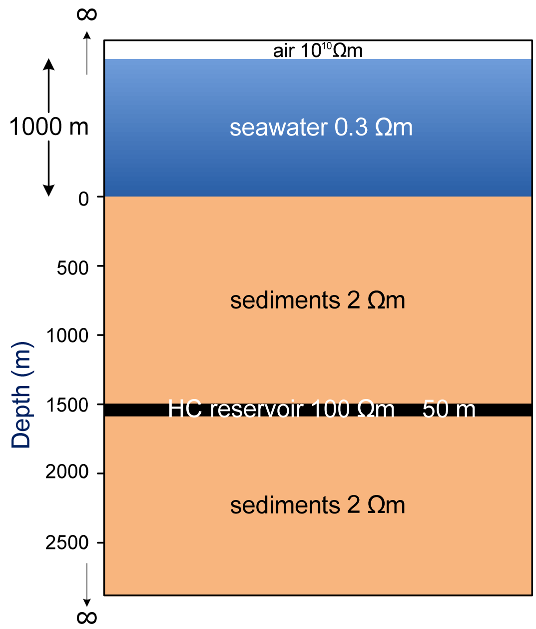

Figure 3.7 1D reservoir model used for optimum frequency analysis with target at 1500 m depth.

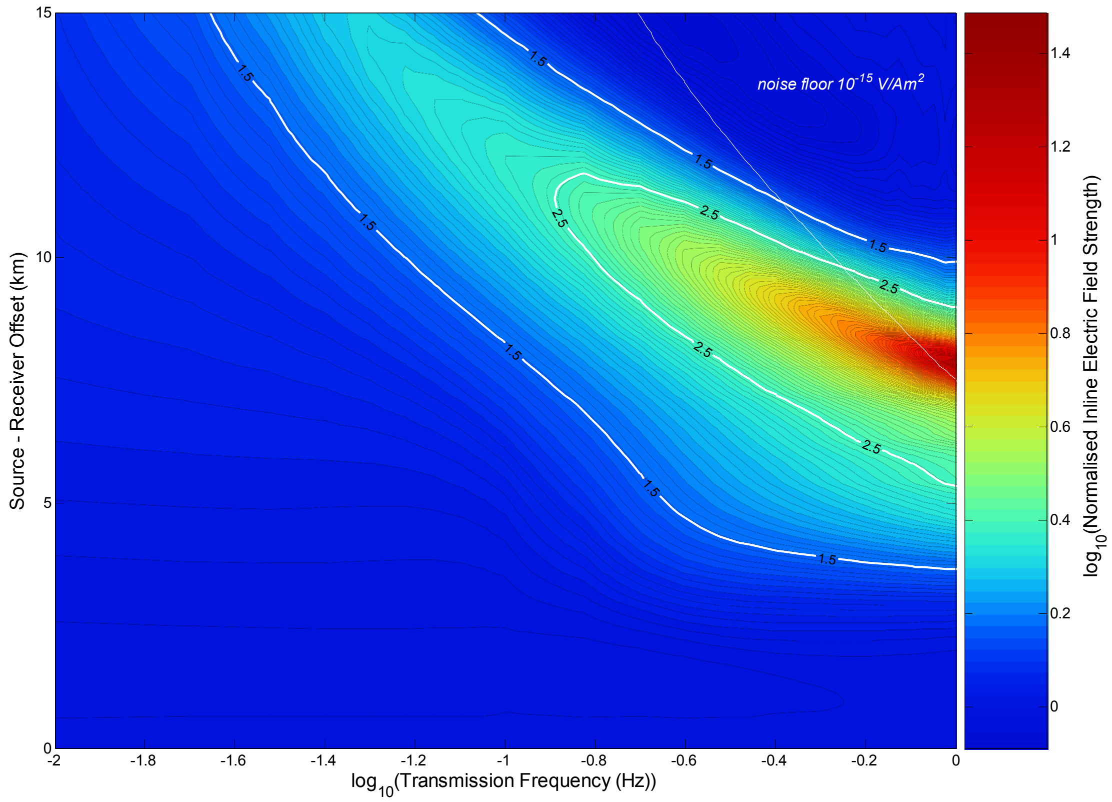

Figure 3.8 Contoured normalised inline electric field for 0.01 - 1.0 Hz transmission frequency. Solid contours indicate 150 % and 250 % anomaly due to the reservoir response normalised with the background response for the model shown figure 3.7. Dotted line indicates the noise floor of the inline electric field for the reservoir model. The optimum fundamental frequency for this geo-electrical structure is indicated by the solid yellow line. This frequency is ~0.2 Hz. Higher harmonic frequencies (0.4, 0.6, 0.8, and 1.0 Hz) are indicated by the dashed white lines and can be derived through FFT of the fundamental current waveform.

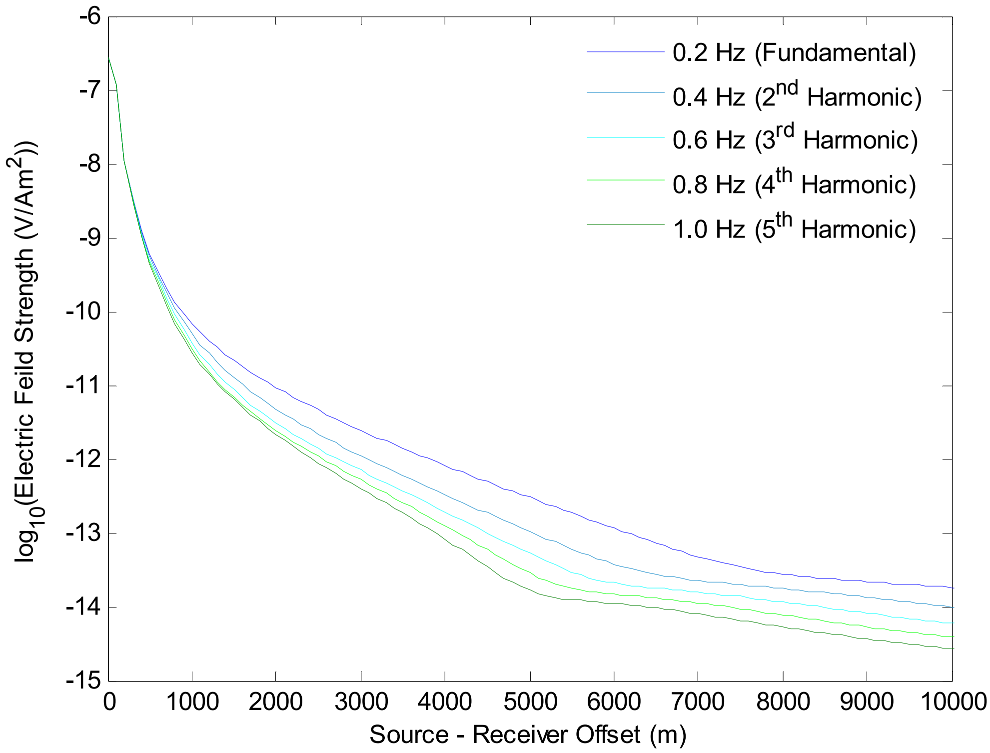

Figure 3.9 Inline electric field strength for a water depth of 500m over a halfspace of 2 Ωm, for a fundamental frequency of 0.2 Hz up to the 5th harmonic frequency of 1.0 Hz. It can be seen that with increasing frequency the onset of the air-wave, as seen by a break in the slope, comes in at shorter offsets. At 0.2 Hz the onset of the air-wave is ~8 km, at 1.0 Hz the onset of the air-wave is at ~5km.

3.5 Sensitivity of the CSEM Response to Target Resistivity/Thickness

As described in the previous chapter, the 1D marine CSEM response it sensitive to the targets transverse resistivity. Archie's Law empirically describes the relationship between hydrocarbon saturation and formation resistivity and can be used to assess the hydrocarbon saturation of a target. Electrical resistivity increases in a predictable way with increasing oil or gas saturation. CSEM measurements respond directly to this increase. CSEM measurements also respond directly to the increase in reservoir thickness.

Once an optimum transmission frequency has been determined a strategy for assessing the minimum transverse resistance detectable over a prospective area, is to contour the normalised fields with source-receiver offset for a range of target transverse resistances as shown in Figure 3.11. For a hydrocarbon reservoir at a depth of 1500 m as shown in Figure 3.10, the minimum transverse resistance detectable is ~500 Ωm^2 (i.e. shown as ~$10^{2.7}$ Ωm^2). Assuming this reservoir is sandstone with the properties described in Chapter 2; the parameters of the minimum detectable target reservoir could be 10 m in thickness with a resistivity of 50 Ωm which would relate to a hydrocarbon saturation of 80 %, or a thickness of 50m with a resistivity of 10 Ωm which would relate to a hydrocarbon saturation of 55 %.

Thus is it important to be able to resolve the resistivity and thickness parameters of a target individually so that the targets hydrocarbon saturation and economic value can be more readily determined.

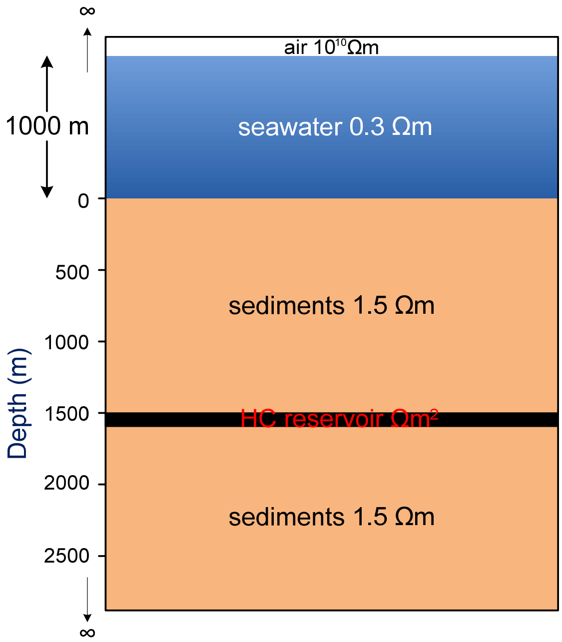

Figure 3.10 1D reservoir model used for varying target transverse resistance with target at 1500 m depth.

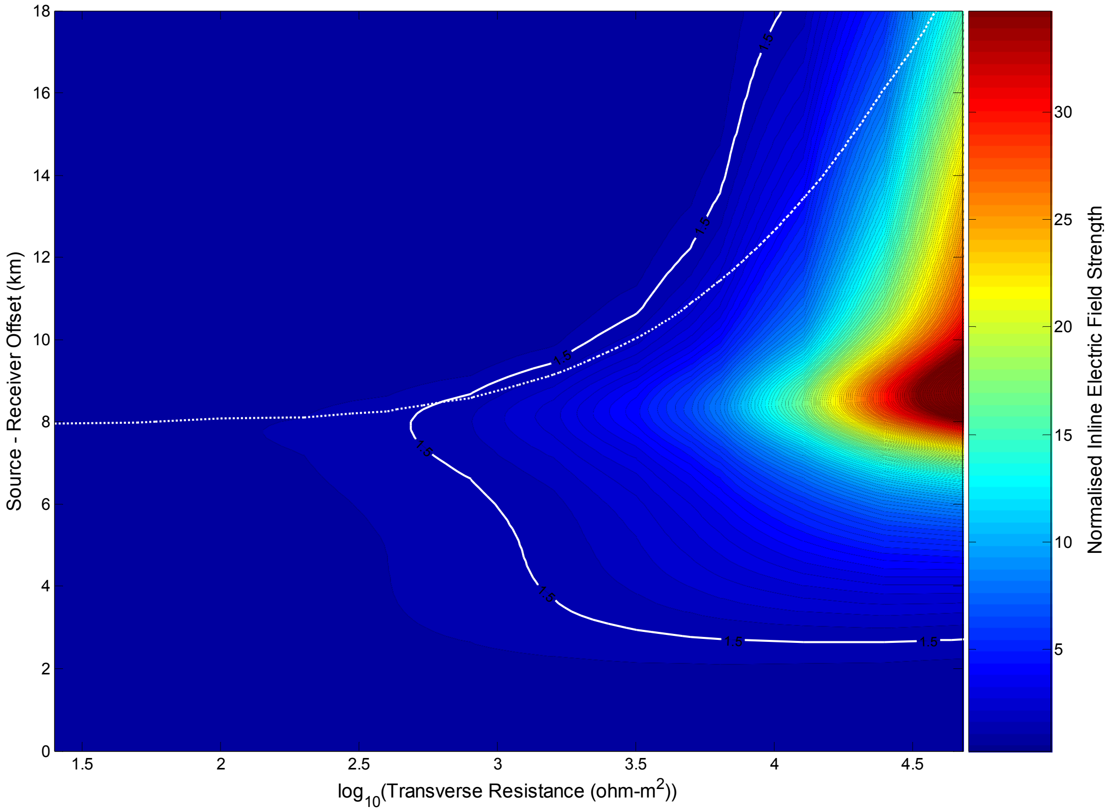

Figure 3.11 Contoured normalised inline electric field for a target transverse resistance of 25 - 50000 Ωm^2, for transmission frequency of 0.3 Hz. Solid contour line indicates 150 % anomaly due to the target. Dotted line indicates the noise floor of the inline electric field for the reservoir model. The minimum transverse resistance detectable is ~500 Ωm^2 (i.e. shown as ~$10^{2.7}$ Ωm^2) as indicated by the vertical yellow line. This target reservoir could be 10 m thick and have a resistivity of 50 Ωm or a thickness of 50m and a resistivity of 10 Ωm. This would relate to a hydrocarbon saturations of ~80 % and ~50 % respectively.

3.6 Effect of Target Depth

Target depth is another key issue when planning a CSEM survey. Target depth ultimately determines the offsets and the frequencies required to resolve the target. Shallow targets have a great effect on the measured response for near offsets and are detectable with high frequencies. Deeper targets have a greater effect at far offsets and are detectable with lower frequencies. Ideally the target depth should be comparable with the water depth so that the signal is not saturated by the air-wave at the offsets at which the response from the target is the greatest. In deep water, where the water depth is comparable with the depth of the target reservoir below the seabed, the depth to which CSEM methods are sensitive to the target increases to a maximum at source-receiver offsets that are approximately double the target depth. There exists a detectability trade-off between target depth and target resistivity as shown in Figure 1.14. However the overburden resistivity is the geological factor that ultimately determines the penetration of marine CSEM systems.

To determine the deepest target below the seafloor that is detectable when designing a CSEM survey, a strategy similar to that in the previous section can be used. The normalised fields with source-receiver offset are contoured for a range of target depths as in Figure 3.13. The depth detection limit is defined as the depth for a given target resistivity, at which the normalised field at the noise floor falls below 150 %. For the model shown in Figure 3.12 the maximum depth below the seafloor at which the target is detectable is ~3000 m for source-receiver offsets of ~8 km. An accurate background electrical structure must define, either through wire-line logging or MT data, so a deep that target reservoirs are distinguishable.

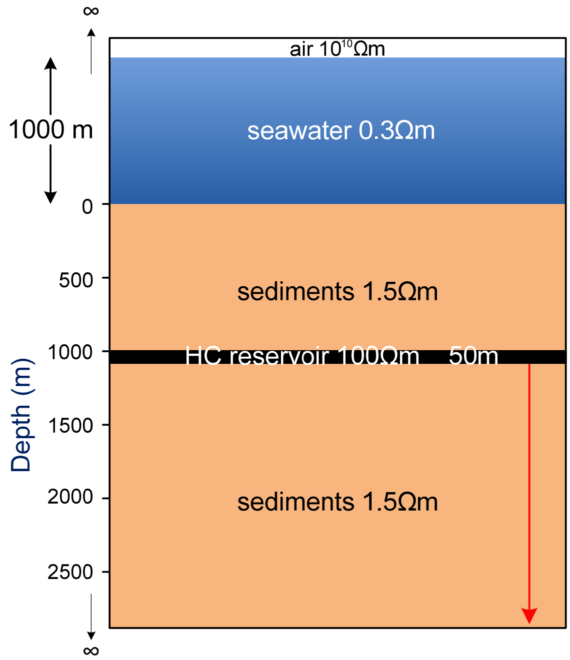

Figure 3.12 1D model with water depth 1000 m used for varying the target depth between 1000 - 5000 m.

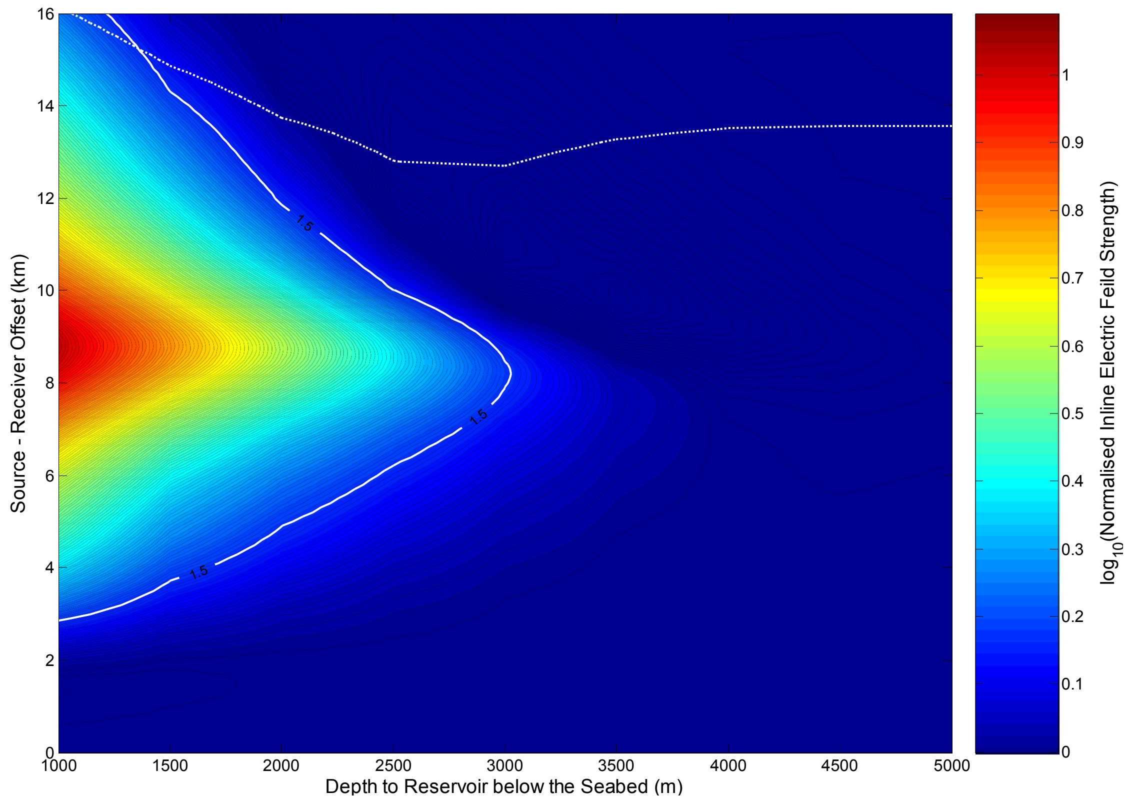

Figure 3.13 Contoured normalised inline electric field for target depths of 1000 - 5000 m, for transmission frequency of 0.3 Hz. Solid contour line indicates 150 % anomaly due to the target. Dotted line indicates the noise floor of the inline electric field for the reservoir model. The maximum depth below the seafloor at which the target is detectable is ~3000 m at an offset of ~ 8km, indicated by the vertical yellow line.

3.7 Effect of Host Formation Resistivity

As previously mentioned the maximum depth of sensitivity is primarily controlled by the overburden resistivity. Field attenuation can be quantified by the skin depth which is a function of overburden resistivity and frequency. A low resistivity overburden will rapidly attenuate fields, and requires a lower fundamental transmission frequency for detection of deep targets. The marine CSEM is sensitive to thin resistive layers and as such a target layer must have a high electrical impedance contrast with the host sediments. The resistivity of marine sediments ranges between 1 - 5 Ωm; the resistivity of reservoirs containing of hydrocarbons ranges between 10 - 500 Ωm. The resistivity contrast can be low for tight formations such as carbonates, and in areas with carbonate strata an accurate background electrical structure must be obtained to improve the accuracy of CSEM data interpretation. However reservoirs containing economic quantities of hydrocarbons will have a sufficient resistivity contrast with the host formation.

3.7.1 Depth detection limit

The depth detection limit of a target is the depth at which the normalised field at the systems noise floor (10^{-15} V/Am^2) falls below a level where the target is no longer distinguishable from the background. MacGregor (2006) considers a normalised field of 150 % for this level. Figure 1.14 shows that the depth detection limit increases with increasing target transverse resistance and skin depth to level at which the field attenuation is too great that high resistivity targets will are not any more detectable. This is primarily controlled by the field skin depth.

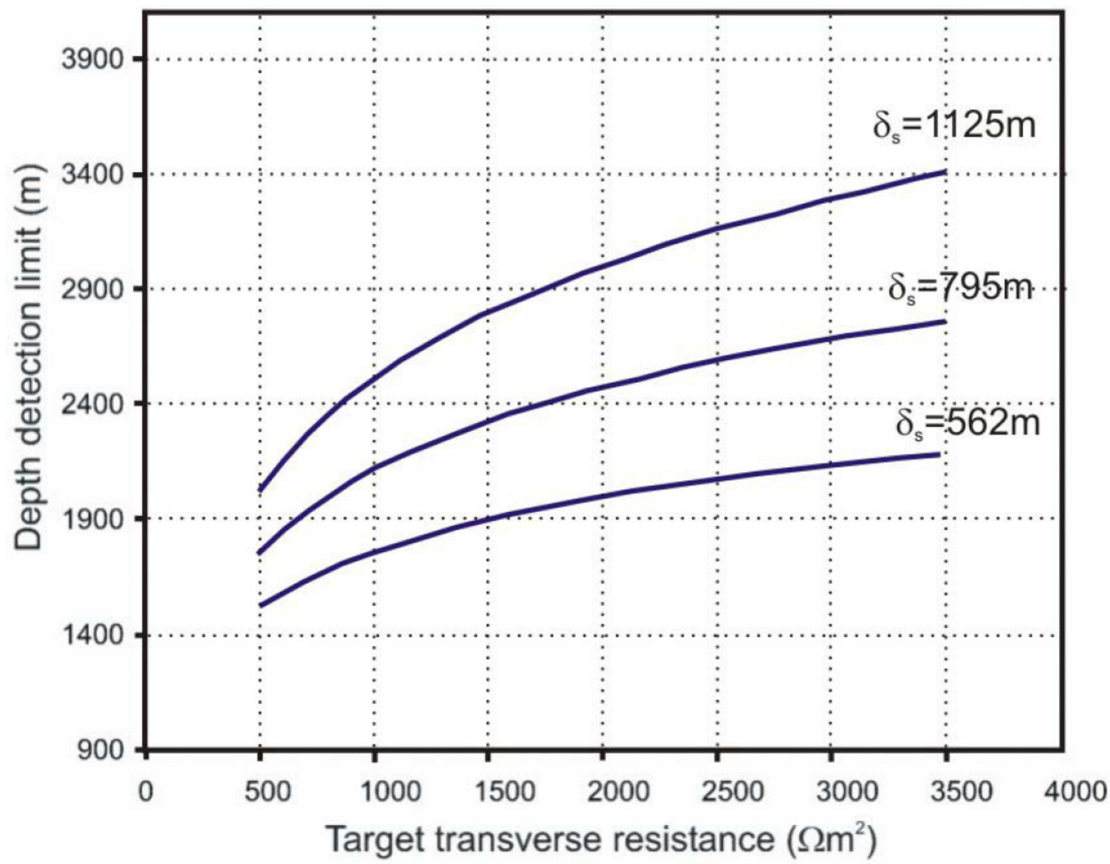

Figure 3.14 Depth detection limit a of target reservoir for different skin depths at frequency of 0.5 Hz. The depth detection limit increases with increasing transverse resistance and skin depth. Skin depths of 1125, 795, and 562 m, relate to overburden resistivities of 2.5, 1.25 and 0.6 Ωm respectively (Reproduced from MacGregor, 2005).

3.8 Effect of Resistive Shallow Formations

Shallow resistive formations such as tight sandstones, carbonates or gas hydrates can potentially mask the response of a reservoir at depth. Shallow resistive layers cause an increase in amplitude and an advance in the phase, which is the same as the response of a target reservoir. In the presence of a shallow resistive formation the amplitude can be almost doubled (Figure 3.20) which could lead to over estimating the resistivity (hydrocarbon saturation) of the target reservoir. The 1D model shown in Figure 3.15 represents a typical stratigraphic sequence of a continental shelf area with shallow carbonate formations. In this deep water (1000 m) model, a shallow (100 m) resistive (3.5 Ωm) carbonate formation is present with a hydrocarbon reservoir at depth (1500 m). At the fundamental transmission frequency of 0.3 Hz, the amplitude response is the combined effect of the carbonates and reservoir (Figures 3.16 and 3.20), however the shallow formation dominates the phase response (Figure 3.17).

To deal with the effects of a shallow resistive formation harmonic frequencies can be used. The 3rd harmonic (0.9 Hz) is used here to constrain the shallow resistive formation. At this higher frequency the sensitivity to the target is minimal due to the reduced skin depth. Figures 3.18 and 3.19 show that the shallow formation has the greatest effect at high frequency. The normalised fields show that the marine CSEM method is sensitive to shallow formations at high frequency and near offsets (Figure 3.21), and sensitive to deep targets at low frequencies and far offsets (Figure 3.20). Effectively the electrical structure within the carbonate formation can be independently constrained at 0.9 Hz. In practice all useable harmonic frequencies should be used to enhance the constraint of the electrical structure with depth.

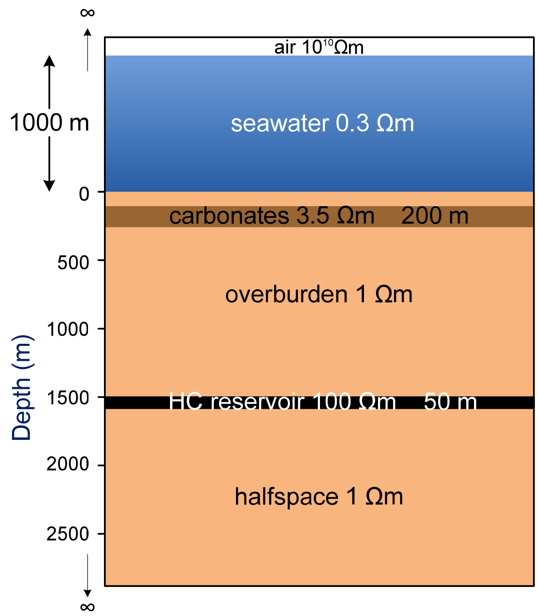

Figure 3.15 Deep water 1D model with a shallow resistive carbonate formation and reservoir at depth.

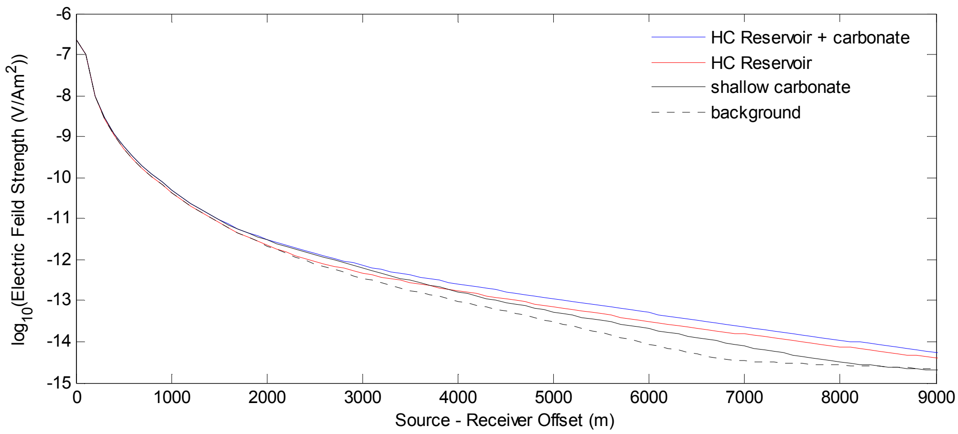

Figure 3.16 Inline electric field strength at 0.3 Hz

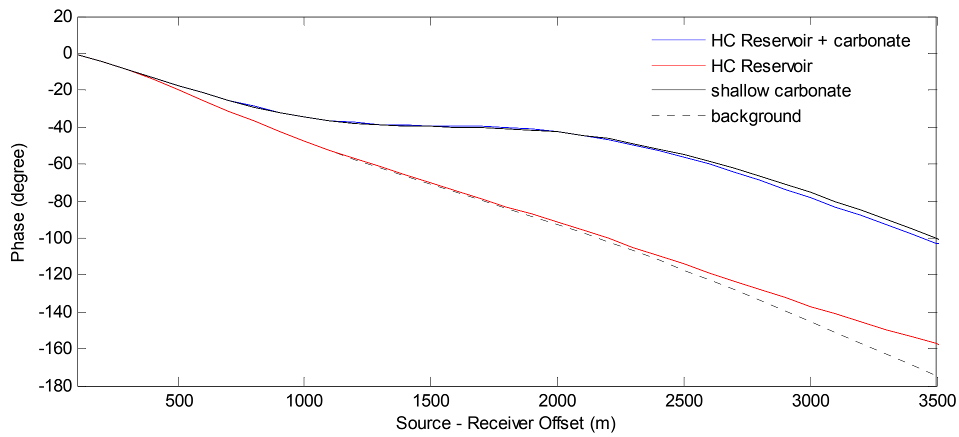

Figure 3.17 Inline electric field phase response at 0.3 Hz.

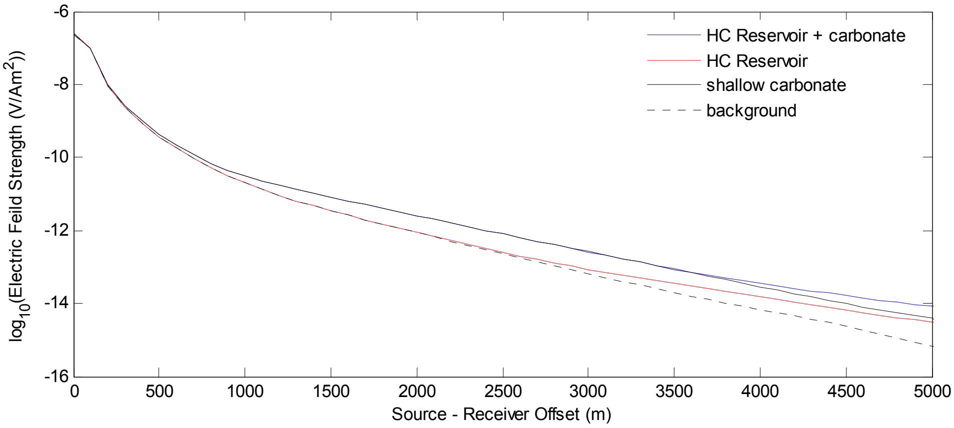

Figure 3.18 Inline electric field strength at the 3rd harmonic frequency (0.9 Hz).

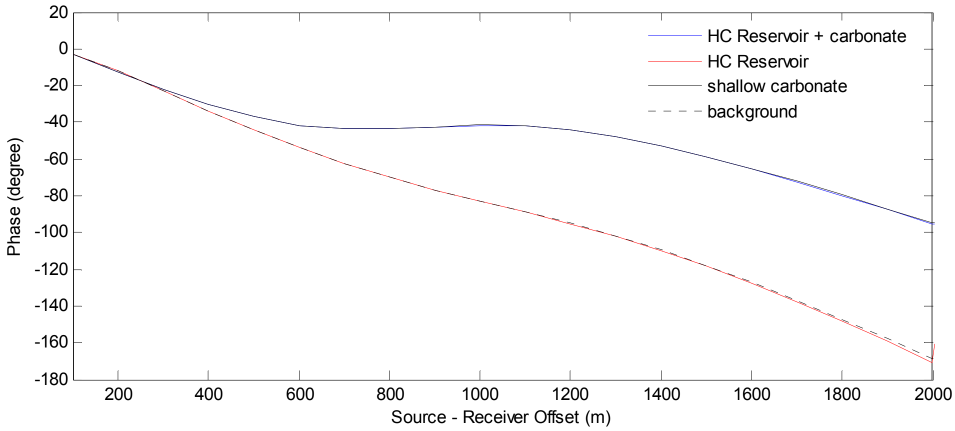

Figure 3.19 Inline electric field phase response at the 3rd harmonic frequecny (0.9 Hz).

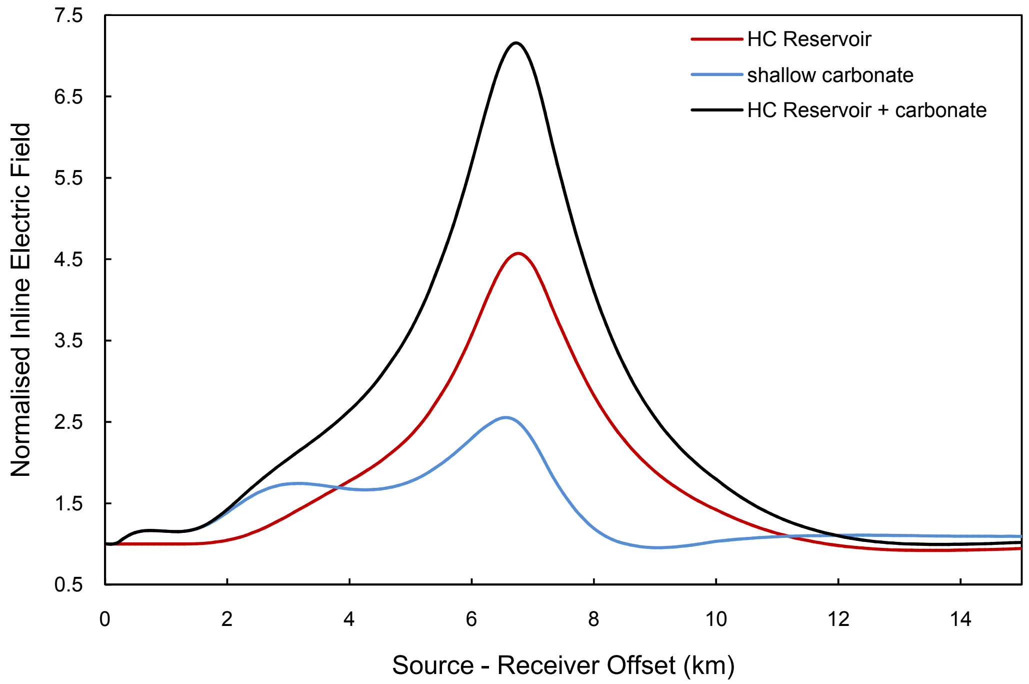

Figure 3.20 Normalised fields at 0.3 Hz. The presence of the shallow formation almost doubles the normalised field strength. At far offsets (6 - 8 km) the reservoir response is dominant. At all offsets the normalised field is the combined effect of the shallow carbonates and the deep reservoir.

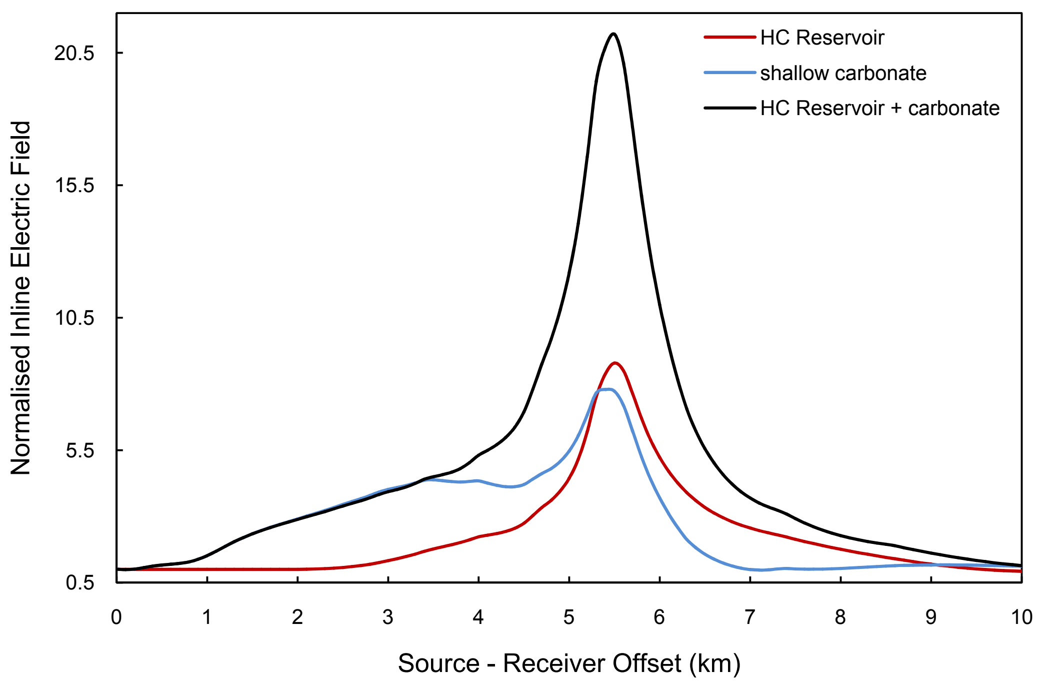

Figure 3.21 Normalised fields at the 3rd harmonic frequency (0.9 Hz). At this frequency the normalised fields are greater in amplitude. The normalised field at near offsets (upto ~3.5km) is only sensitive to the shallow carbonate formation and practically insensitive to the deep reservoir.

3.9 Sub-salt Imaging

Sub-salt imaging poses a severe problem for marine CSEM surveys as salt it is highly resistive (30 Ωm). A salt sill which is a horizontal layer of salt will impede the diffusion of electromagnetic energy and also give the same response as a reservoir. A shallow salt layer causes a problem similar to the air-wave; a break in slope at near offsets. To demonstrate the practicalities of detecting a reservoir below a shallow salt sill, a deep water model (Figure 3.22) was designed with a salt sill at 250 m depth and 250 m thick, and a reservoir at 1500 m depth. Due to high impedance of the shallow salt sill, the diffusive energy is guided along the sill and insignificant energy penetrates to the depth of the reservoir. Figure 3.23 shows that the response of a salt sill with a reservoir at depth is almost indistinguishable from the response of just the salt sill and no reservoir. Normalised field show a maximum of 101 % at offsets of 12 - 14 km, which means a reservoir below a salt sill will not be detectable with the marine CSEM method.

3.10 Shallow Basement

Crystalline basements resistivities can reach 10,000 Ωm. This poses a severe problem if the target reservoir is in close proximity to the crystalline basement. Figure 3.25 shows a model with a basement resistivity of 5000 Ωm with a reservoir just 250 m above the top of the basement. The marine CSEM method is insensitive to reservoirs in this geological setting as shown in Figure 3.27; normalised fields are effectively 100 %. Thus if the target is known to be in close proximity to the basement, the CSEM method cannot be used to detect its presence.

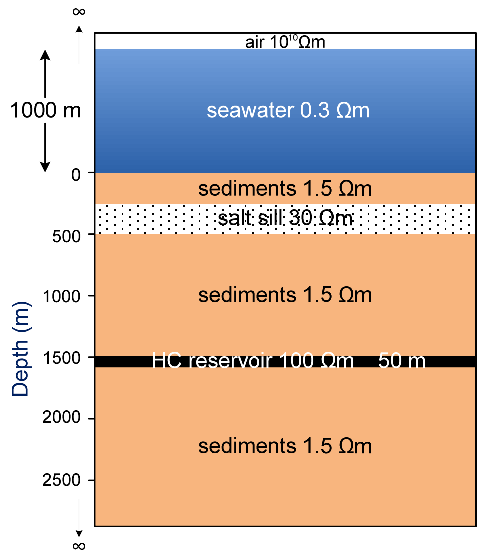

Figure 3.22 Model of shallow salt sill at 250 m depth with a reservoir at 1500 m depth.

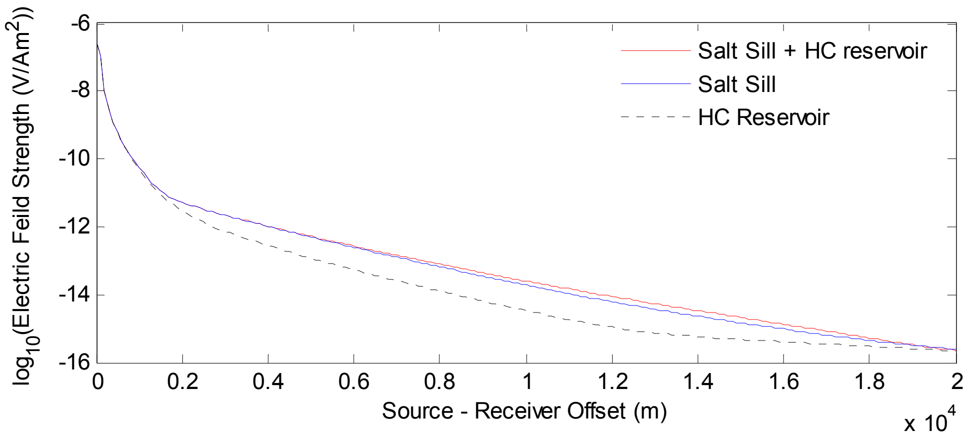

Figure 3.23 Inline electric field strength for the salt sill model in Figure 3.22.

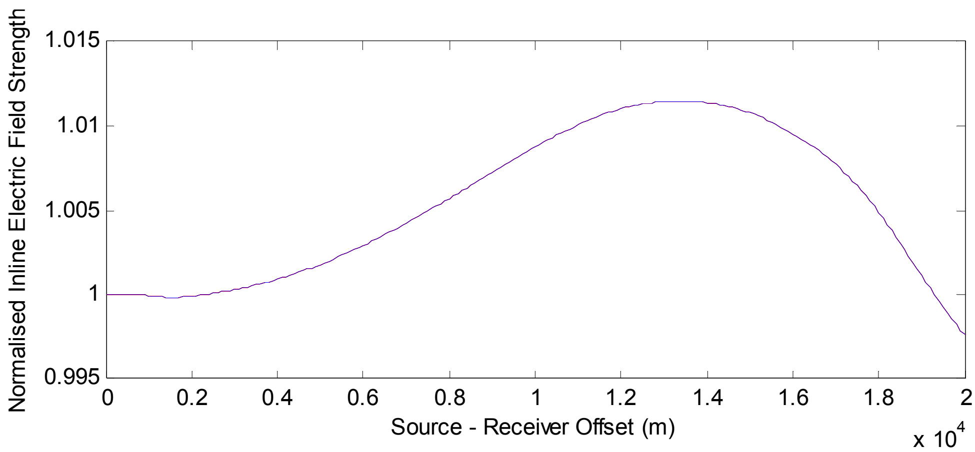

Figure 3.24 Salt sill plus reservoir response normalised by the salt sill response; normalised fields reach a maximum of 101 % at an offset of 12 -14 km. This would be undetectable.

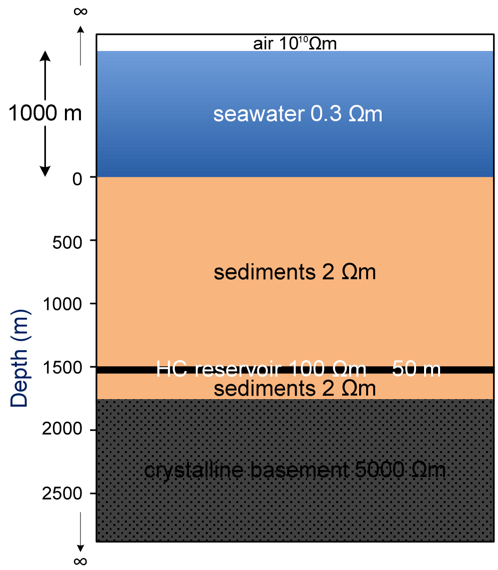

Figure 3.25 Model of shallow basement (5000 Ωm) with a reservoir just 250 m above the top of the basement.

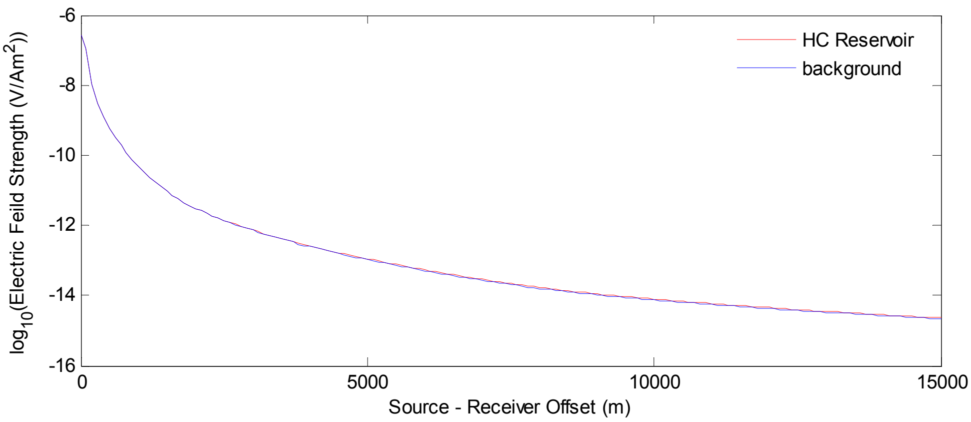

Figure 3.26 Inline electric field strength for the shallow basement model in Figure 3.25.

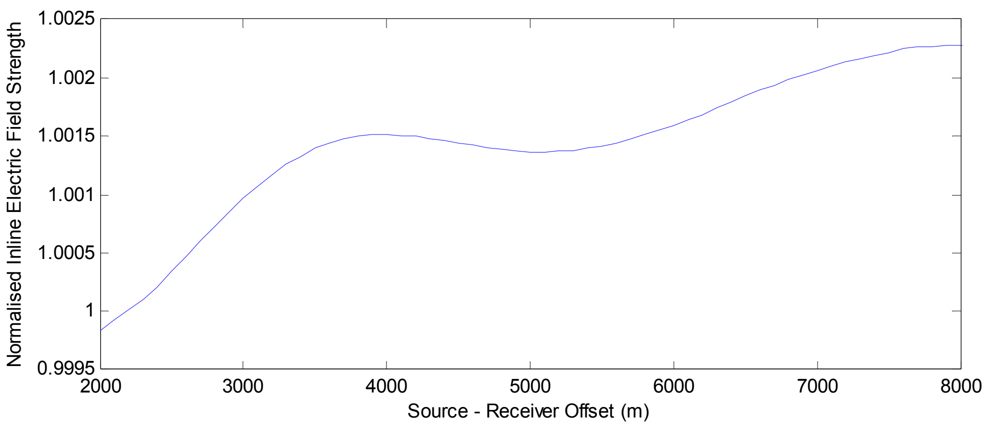

Figure 3.27 Shallow basement reservoir response normalised by a 2 Ωm overburden response. Normalised fields show that marine CSEM methods cannot detect reservoirs in this setting.

3.11 Vertical electric field: a solution to the airwave problem

ID modelling can also numerically simulate the vertical electric field and its role in the marine CSEM method. There are two major reasons for measuring the vertical electric field; there is no vertical field component at the air/water interface and the vertical field increases significantly at reservoir edges. At the air/water interface the electromagnetic field becomes totally horizontal due to the effectively infinite resistivity of the air; at the reservoir edge the field becomes more vertical as the electromagnetic energy diffuses over the structures edge, suggesting the potential to illuminate reservoir edges. Although it has not been modelled, Constable and Weiss (2006) suggest that due to reciprocity the same effects can be achieved using a vertical electric dipole transmitter and horizontal field receivers.

Vertical electric field measurements may allow CSEM methods to be applied in shallow marine settings since this measurement is not affected by the air-wave as shown in Figures 3.28 and 3.29. The response for the vertical component for a shallow water (100 m) reservoir model shown in Figure 3.30 demonstrates that the air-wave is not present and the response increases with increasing reservoir resistivity.

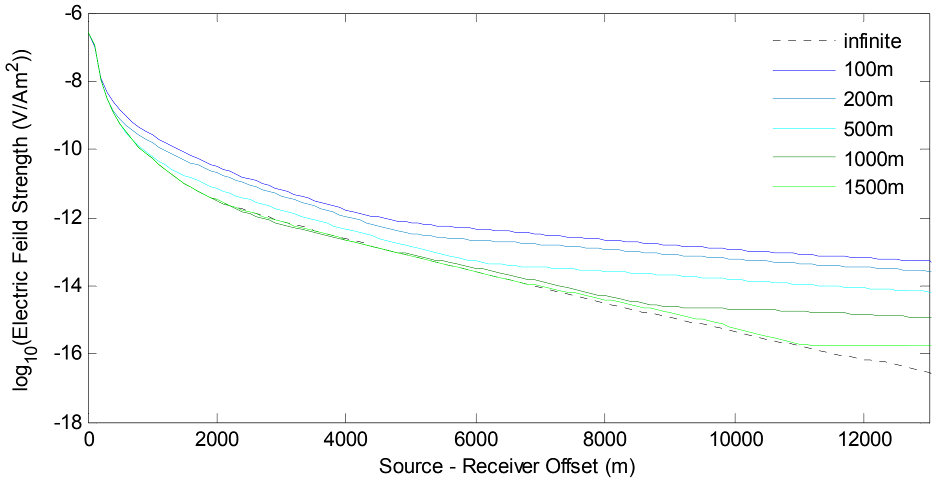

Figure 3.28 Inline electric field response for the E_x component of the electric field for varying water depths.

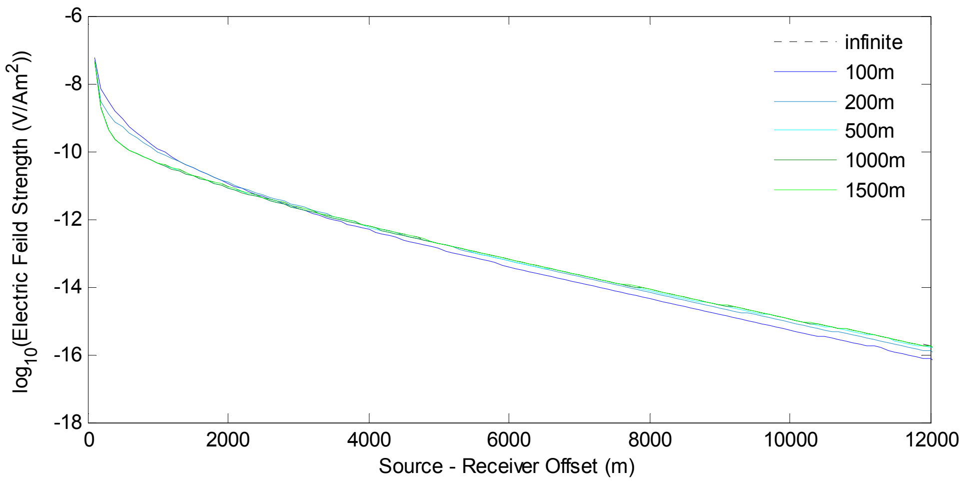

Figure 3.29 Inline electric field response for the E_z component of the electric field for varying water depths.

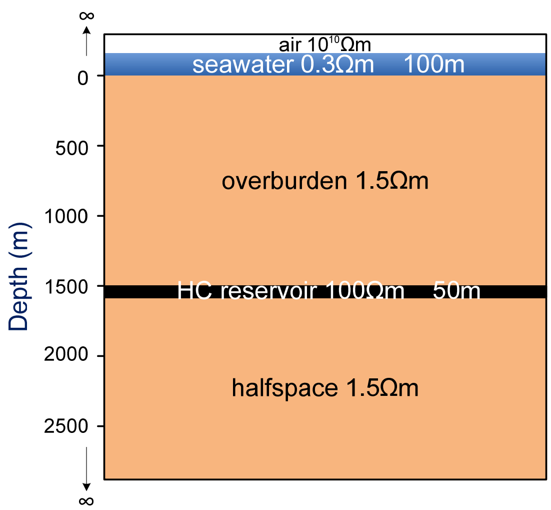

Figure 3.30 Simple shallow water (100 m) reservoir model.

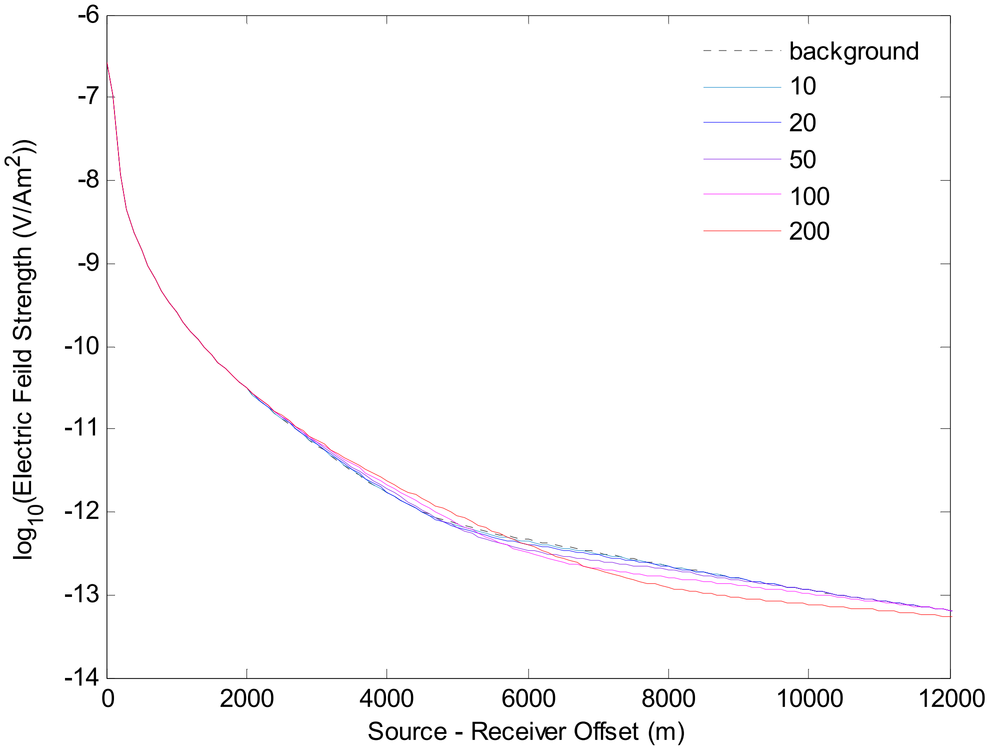

Figure 3.31 Response for the E_x component for the shallow water reservoir model shown in Figure 3.30; the air-wave masks the response from the reservoir.

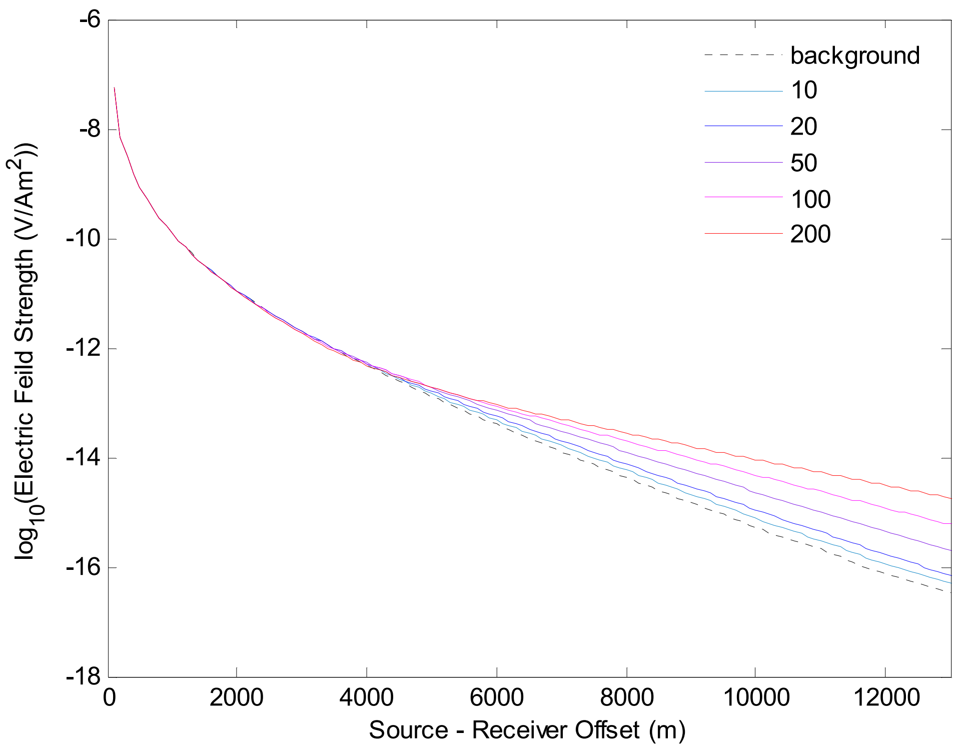

Figure 3.32 Response for the E_z component for the shallow water reservoir model shown in Figure 3.30; here the air-wave is not present and the response increases with increasing reservoir resistivity.

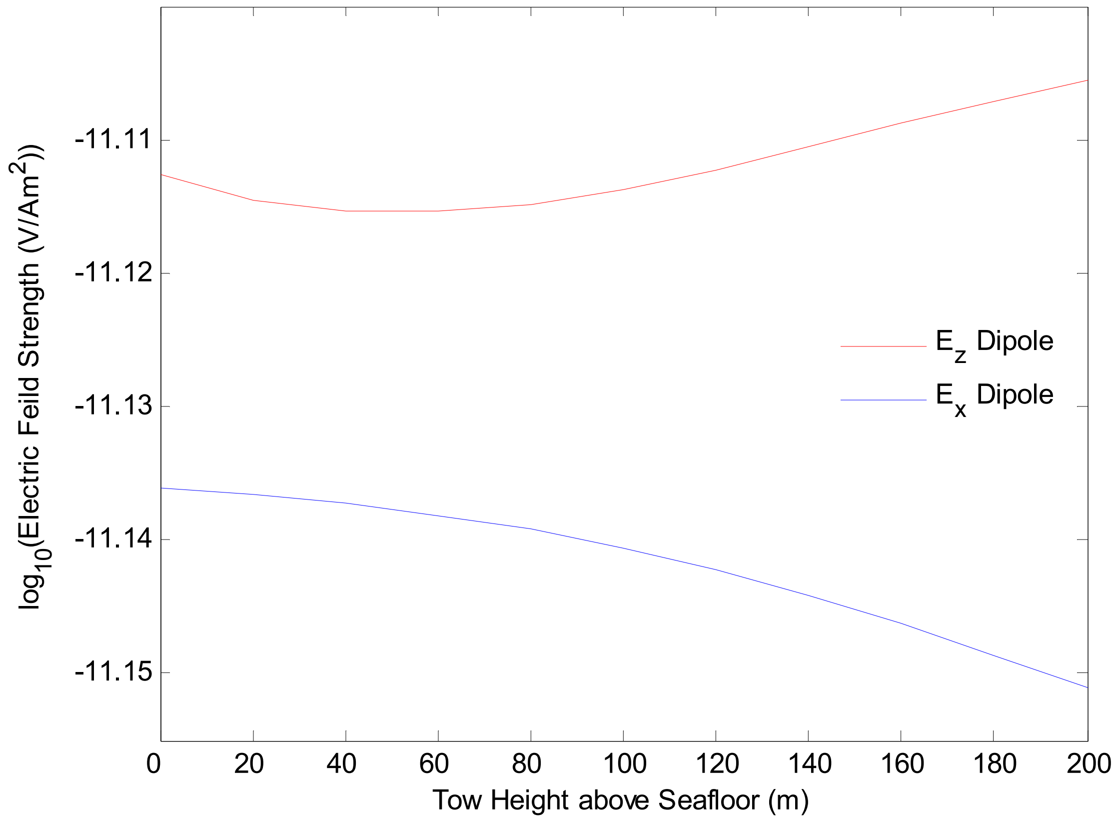

Figure 3.33 Electric field strength 2km from the source measured by horizontal and vertical electric dipoles versus the tow height of the transmitter above the seafloor. For the horizontal dipole the field strength decreases with increasing height due to more attenuation of the field within the conductive ocean. The same occurs for the vertical electric field up to around 40m above the seafloor, the field strength then increases as the field at the seafloor becomes more vertical as the transmitter is towed higher.

3.12 Response of a 3D Target

1D modelling helps to develop an intuitive feel for how controlled-source electromagnetic fields interact with a layered earth. 1D sensitivity analysis can provide good approximations to the frequencies and offsets required for a given target, but can overestimate the magnitude of anomalies (Hoversten et al., 2006). Modelling a layered earth over a halfspace gives a simplified representation of the response of the geo-electrical structure of the earth. However the structure of the earth is never simple. Modelling has been done to detect the presence of a resistive layer, assuming infinite lateral extent of that layer. In reality target hydrocarbons have a finite structure. Modelling the response of a 3D target embedded in a layered earth will provide more realistic results, allowing for diffusion of energy over the edge of the body.

The modelling code used here numerically evaluates the primary field (layering response) and the secondary field (scattering response due to the target) separately because the secondary field requires fine discretization. This allows us see the response of the just the body itself and how it contributes to the total field (combination of the primary field and secondary field). A 3D target has been modeled as shown in Figure 3.35 and the response of a receiver 2 km from the edge of the 3D body is shown in Figures 3.33 and 3.34. If both transmitter and receiver are above the body, the response closely follows that of a 1D layer. When the transmitter is far from the edge the response is closer to the background, when the transmitter approaches the edge there is a transition from the background response to a reservoir response. Figure 3.34 shows that the 3D reservoir response is the combination of the background layering response and the secondary field.

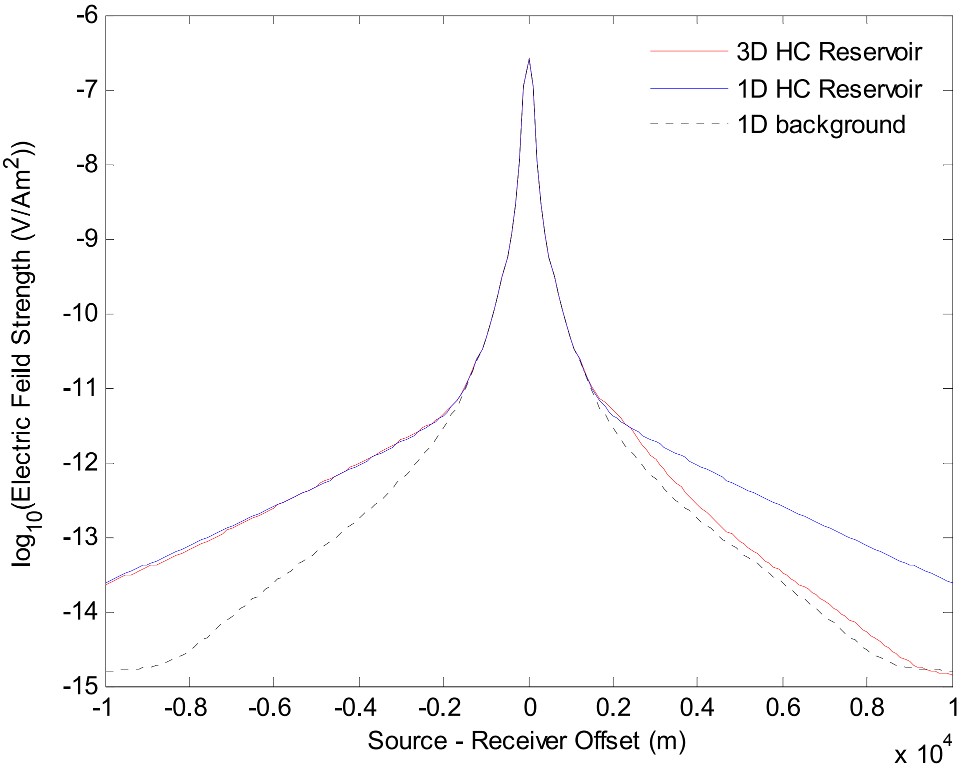

Figure 3.34 Inline electric field response of a reservoir modelled as a 3D body and a 1D layer.

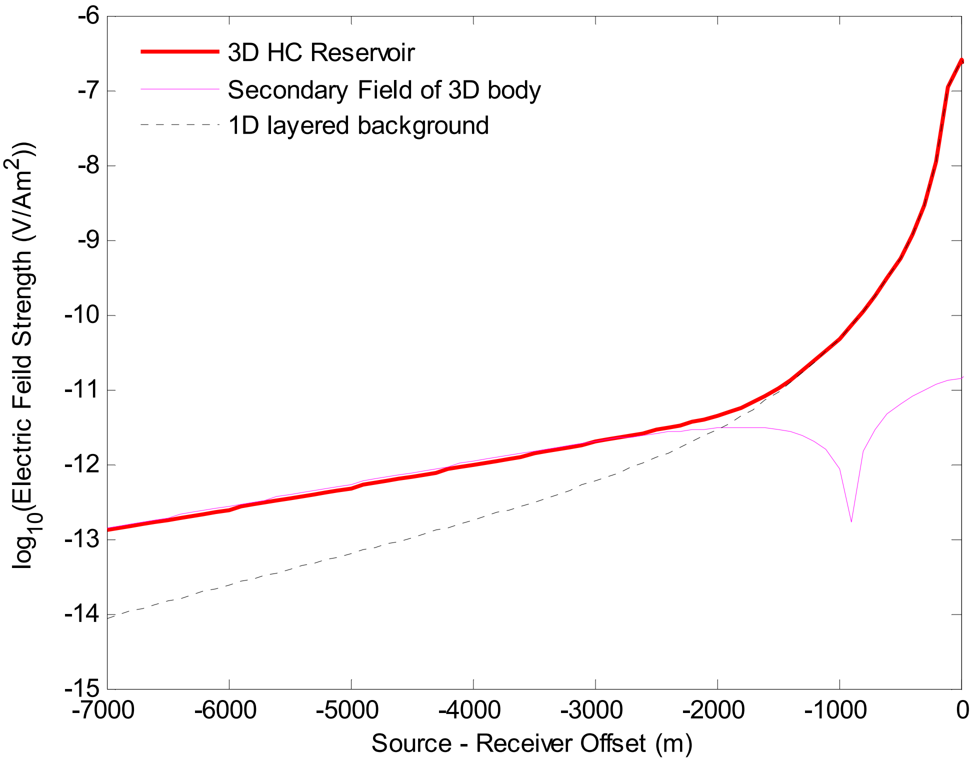

Figure 3.35 Inline electric field response of a 3D body showing layered response, secondary field and total field.

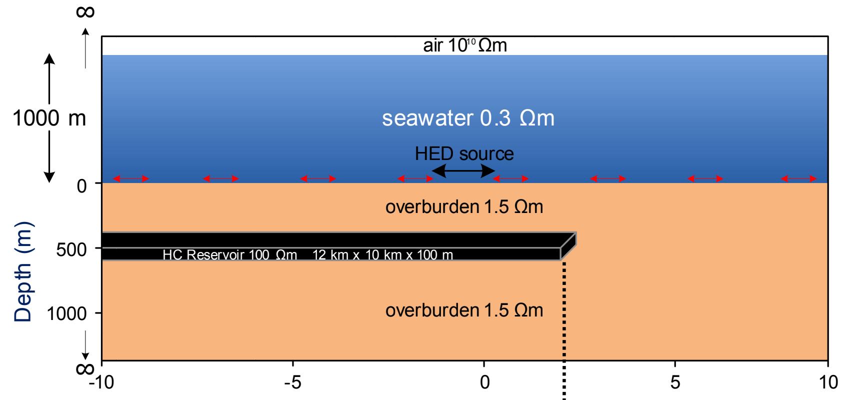

Figure 3.36 3D reservoir model with source 2 km from the edge of the reservoir.

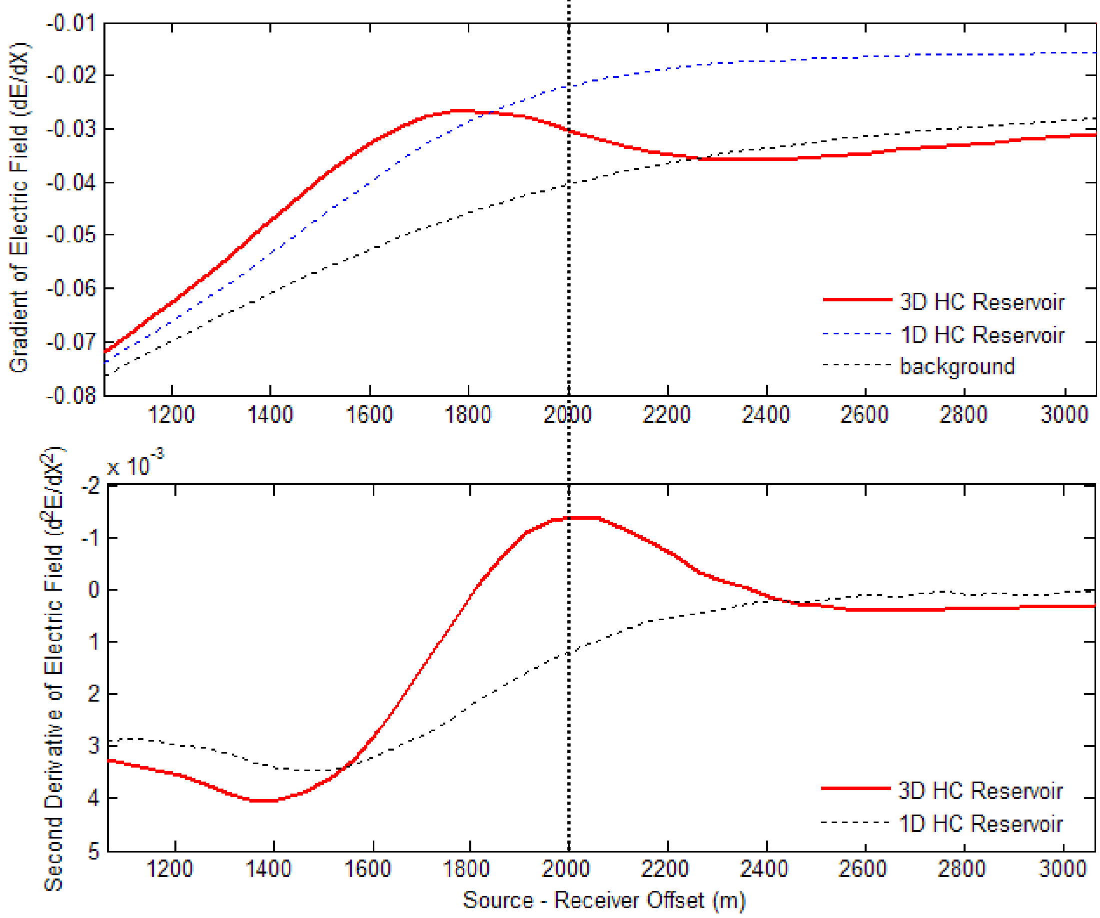

Figure 3.37 Gradient of the measured electric field with offset (above) and second derivative of the electric field with offset (below). Over the 3D reservoir the response closely follows the 1D reservoir response, the inflection point occurs at the edge and the response follows the background layering response off the reservoir. The maximum of the second derivative logically occurs at the edge of the body.

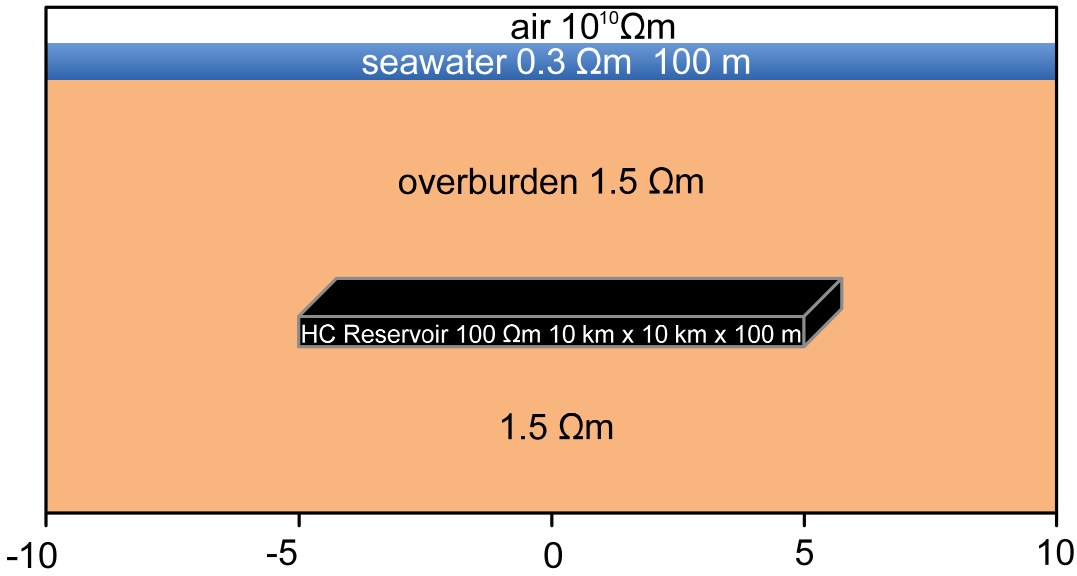

Figure 3.38 Simple 3D reservoir model.

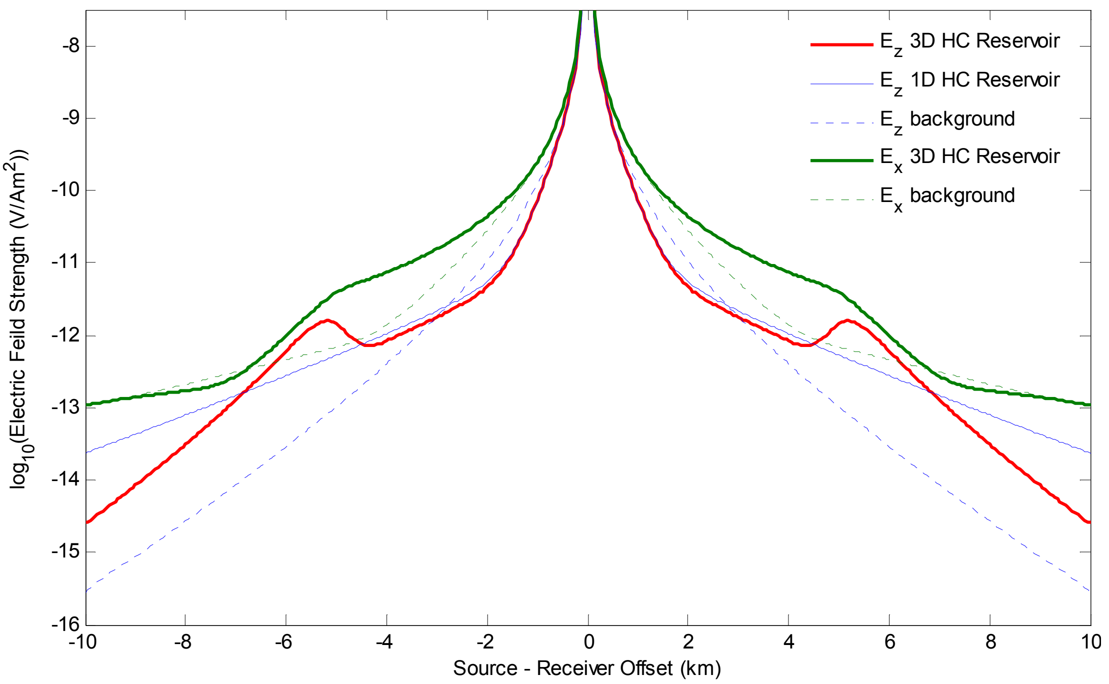

Figure 3.39 1D layer and 3D reservoir responses for the structure shown in Figure 3.38. The 1D response returns slightly higher amplitudes than the 3D response. The vertical electric field measurements illuminate the reservoir edges at offsets of ±5 km.

4 DEEP WATER BASINS OFFHORE WESTERN AUSTRALIA

The marine CSEM method has potential for widespread application in the Northwest Shelf (NWS) of Western Australia. This area is a proven world class hydrocarbon province with many areas that have been extensively surveyed with seismic methods and well-hole logging. CSEM exploration could be used for frontier exploration or used to scan for further prospects in the areas that are already developed. A feasibility study for the application of the marine CSEM method for two regions in the NWS area is given in this chapter; Scarborough Gas Field and Browse Basin.

4.1 Scarborough Gas Field, Central Exmouth Plateau

Scarborough Gas Field is located at the Central Exmouth Plateau, Northern Carnarvon Basin, as shown Figure 4.1. The extensive deep-water (800 - 3000 metres) Exmouth Plateau forms a bathymetric plateau outboard of the main depocentres. The Northern Carnarvon Basin is a large mainly offshore basin and is Australia’s premier hydrocarbon province (Geoscience Australia, 2007). The majority of wells have been drilled in deepwater, generally deeper than 500m which makes this basin for widespread application of the marine CSEM method.

The main depocentres contain up to 15km of sedimentary infill dominated by Triassic to early Cretaceous siliclastic deposits. Almost all the hydrocarbons resources are reserved within the Upper Triassic, Jurassic and Lower Cretaceous Sandstones beneath the regional Early Cretaceous seal (Geoscience Australia, 2007).

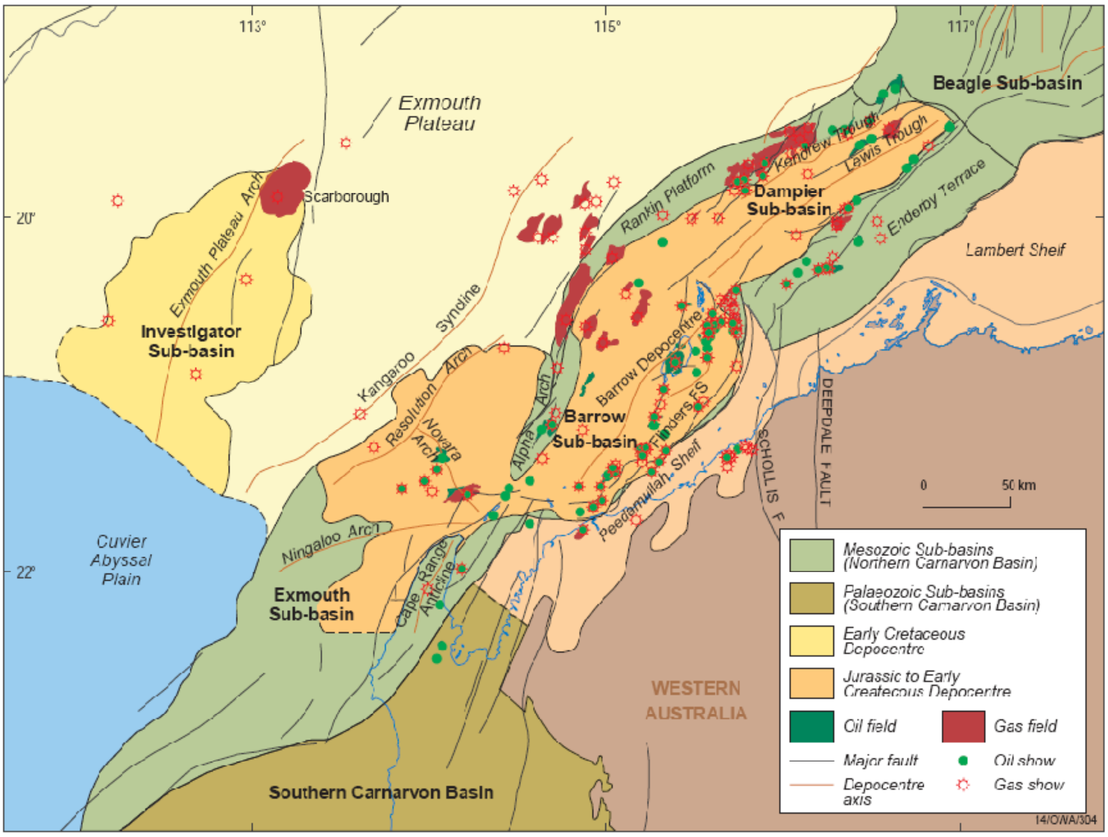

Figure 4.1 Regional geology of Northern Carnarvon Basin (Reproduced from Geoscience Australia, 2007).

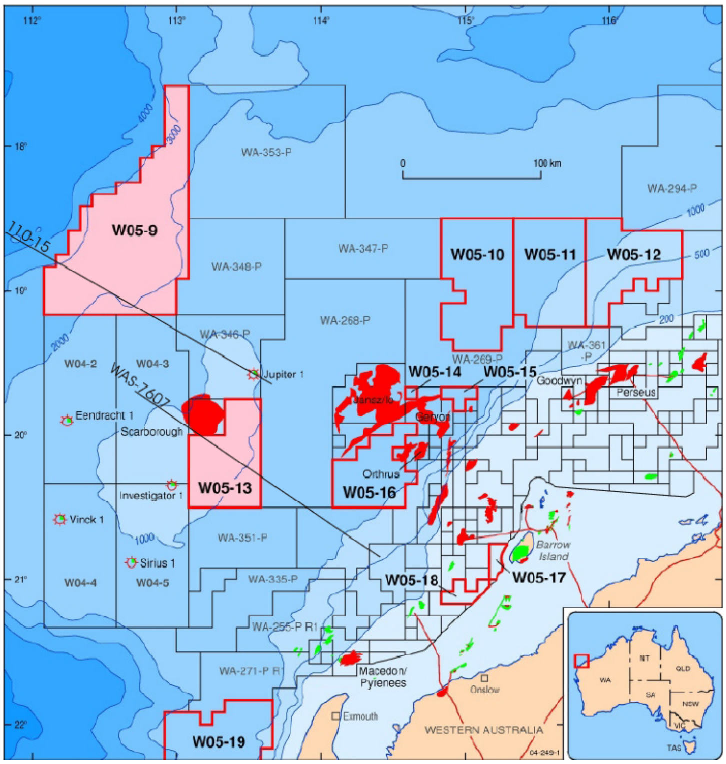

Figure 4.2 Location map of Scarborough Gas Field (red circle) at the 1000 m water depth contour. The field is approximately 400 km^2. The location of Seismic line WAS-7607 and well-hole Scarborough-2 are also shown (Reproduced from Geoscience Australia),

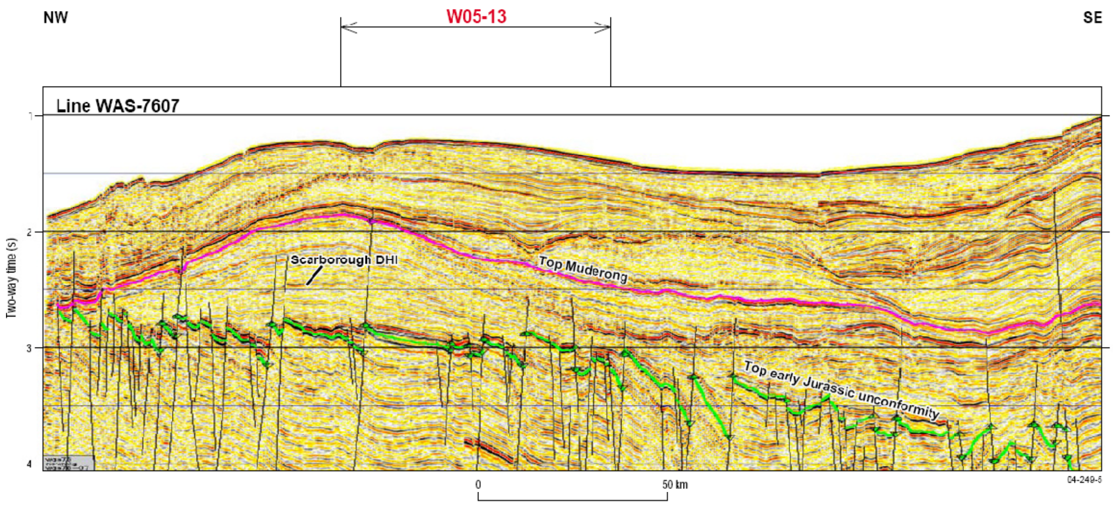

Figure 4.3 Interpreted seismic line WAS-7607 also showing the Scarborough DHI (Reproduced from Geoscience Australia).

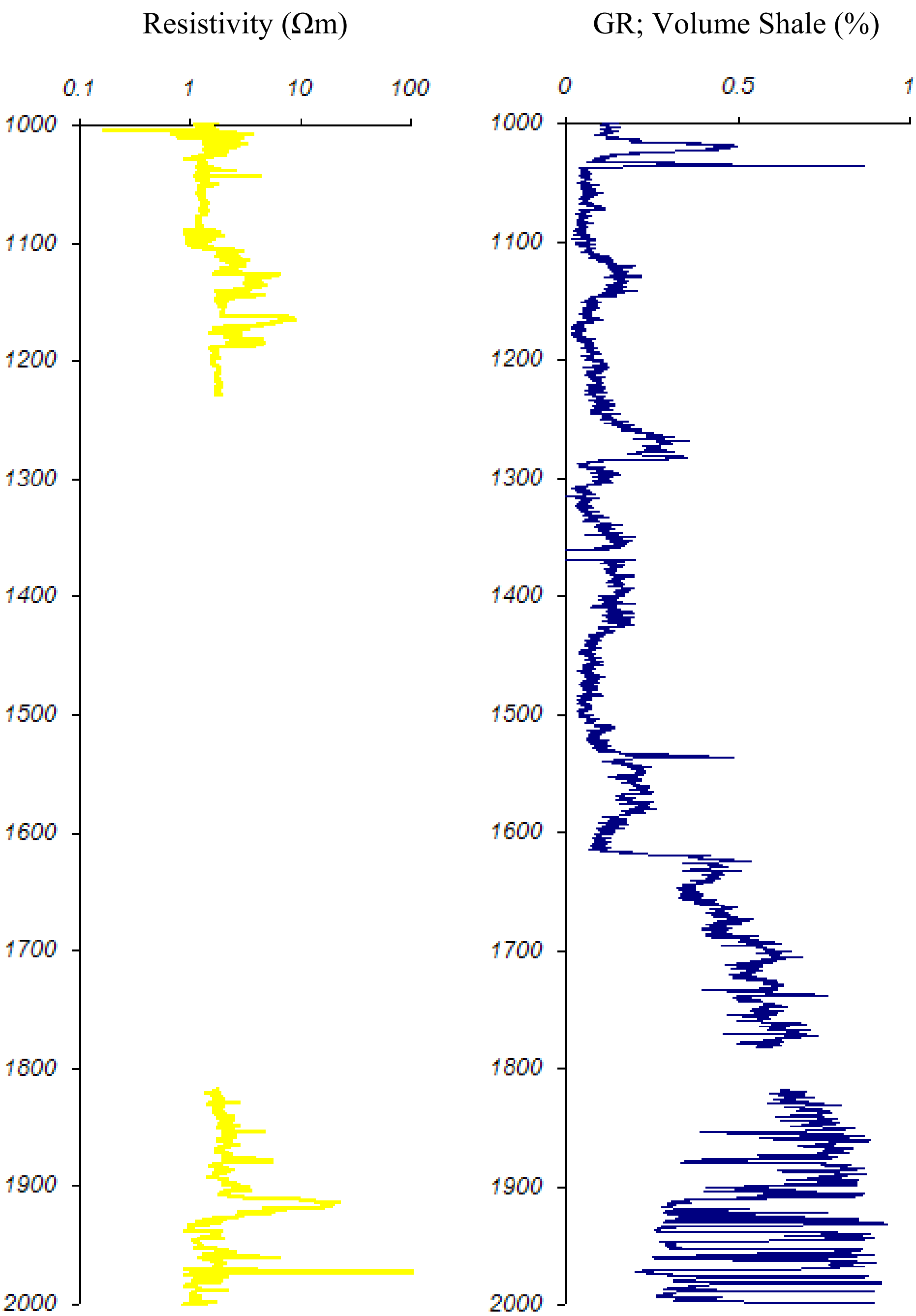

Figure 4.4 Scarborough-2 well; Deep LaterLog resistivity and volume of shale.

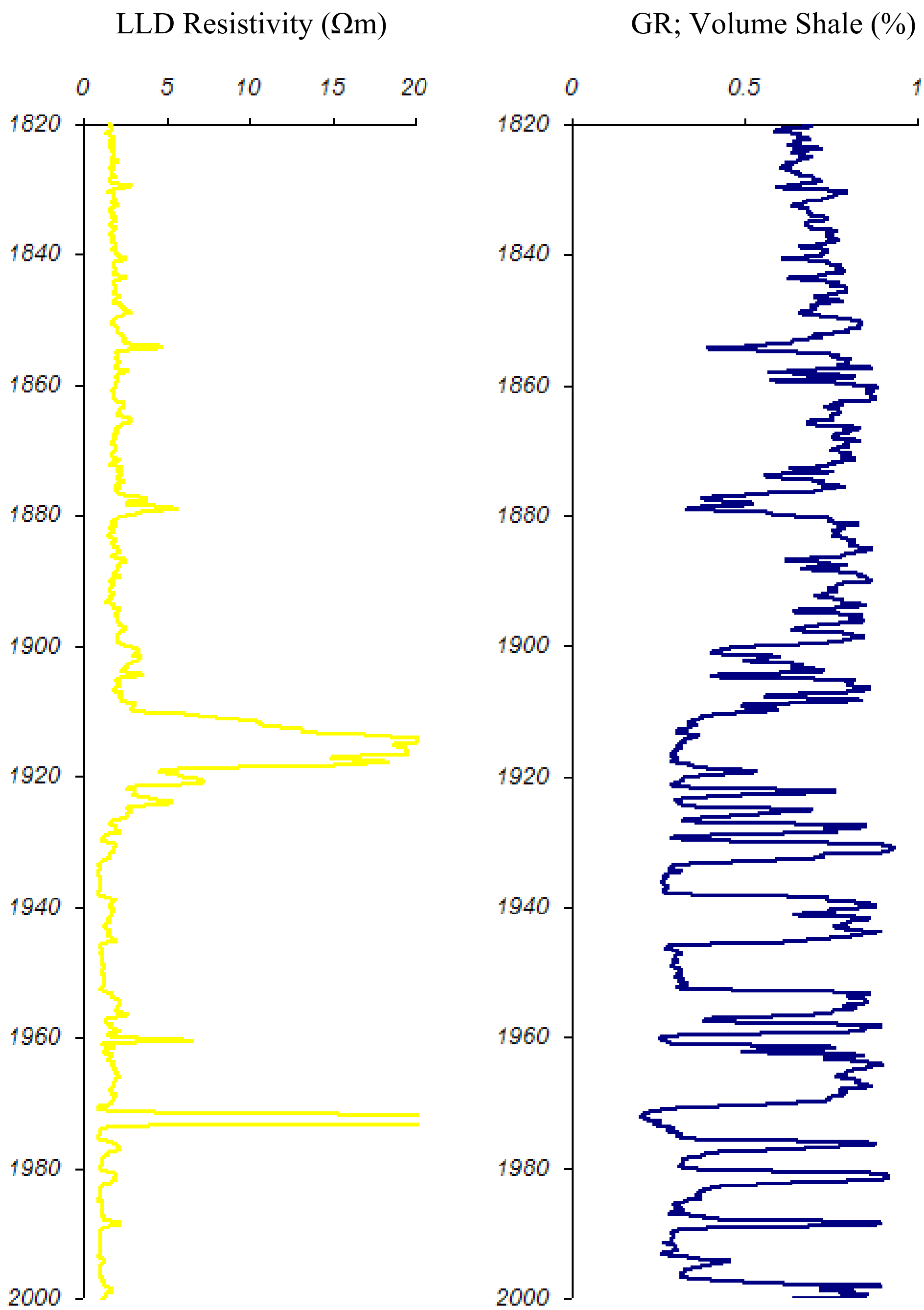

Figure 4.5 Reservoir interval interpreted between depths 1910-1930 m. Reservoir interval shows LLD reading of 20 Ωm, the true resistivity is likely to be closer to 30 Ωm. The reservoir is a clean sandstone as shown by the low volume of shale and is sealed by a shale horizon. Below the reservoir there is a well defined sand/shale sequence.

4.1.1 Geo-electrical model

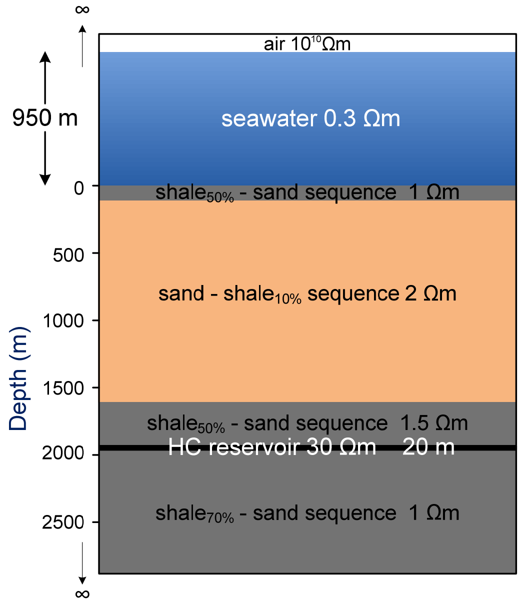

Figure 4.6 Geo-electrical model based on the Scarborough-2 well.

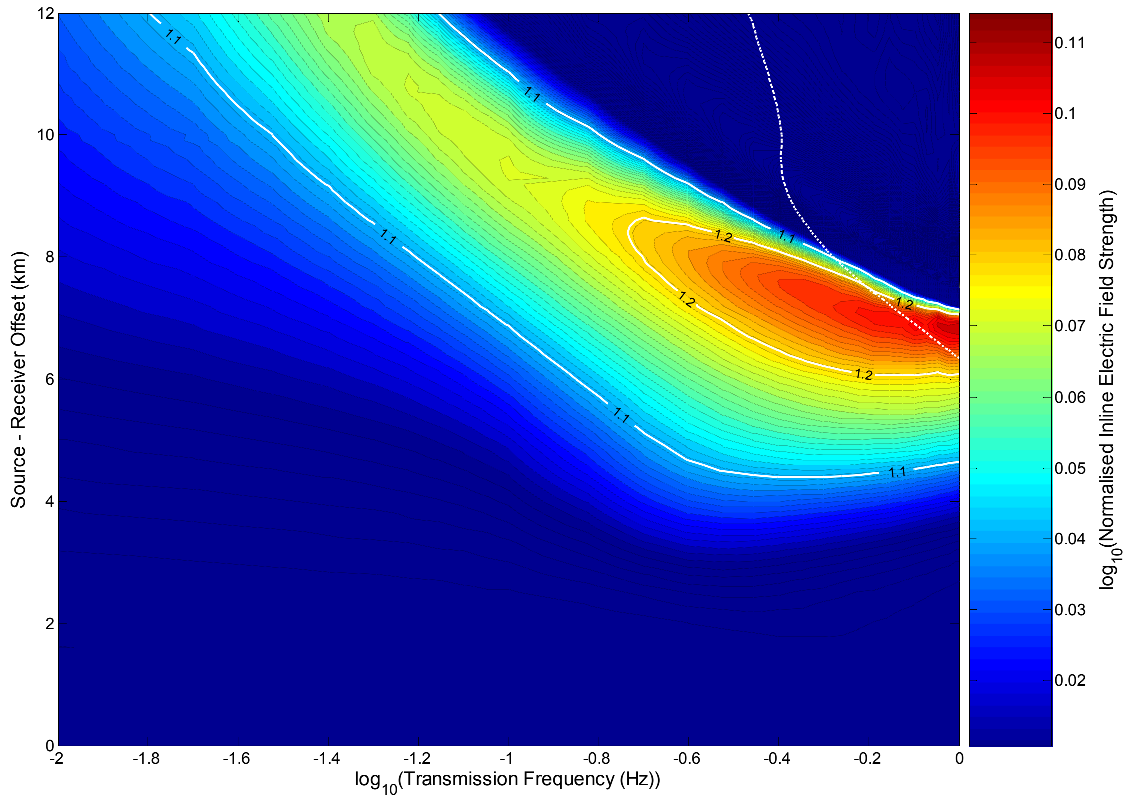

Figure 4.7 Contoured normalised inline electric field for 0.01 - 1.0 Hz transmission frequency. Solid contours indicate 110 % and 120 % anomaly due to the reservoir response normalised with the background response for the Scarborough model. Dotted line indicates the noise floor of the inline electric field for the reservoir model. The optimum fundamental frequency for this geo-electrical structure is indicated by the solid yellow line. This frequency is ~0.25 Hz (shown as $10^{\sim 0.6}$).

4.1.2 CSEM response

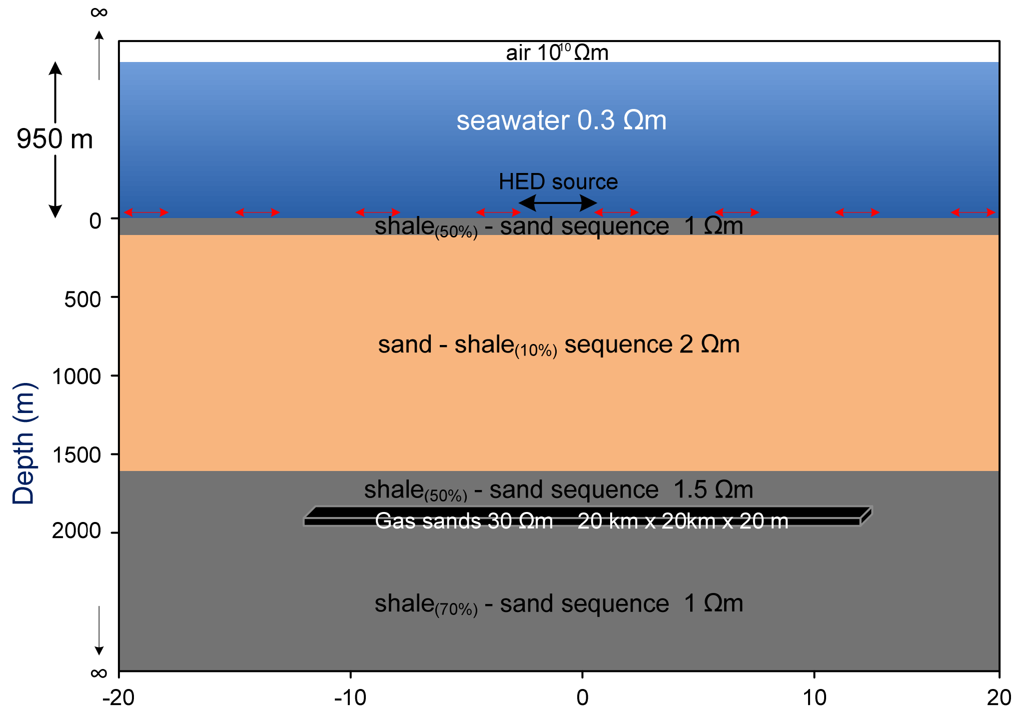

Figure 4.8 3D model of the Scarborough Gas Field; reservoir is modelled as a 20 km x 20km x 20 block.

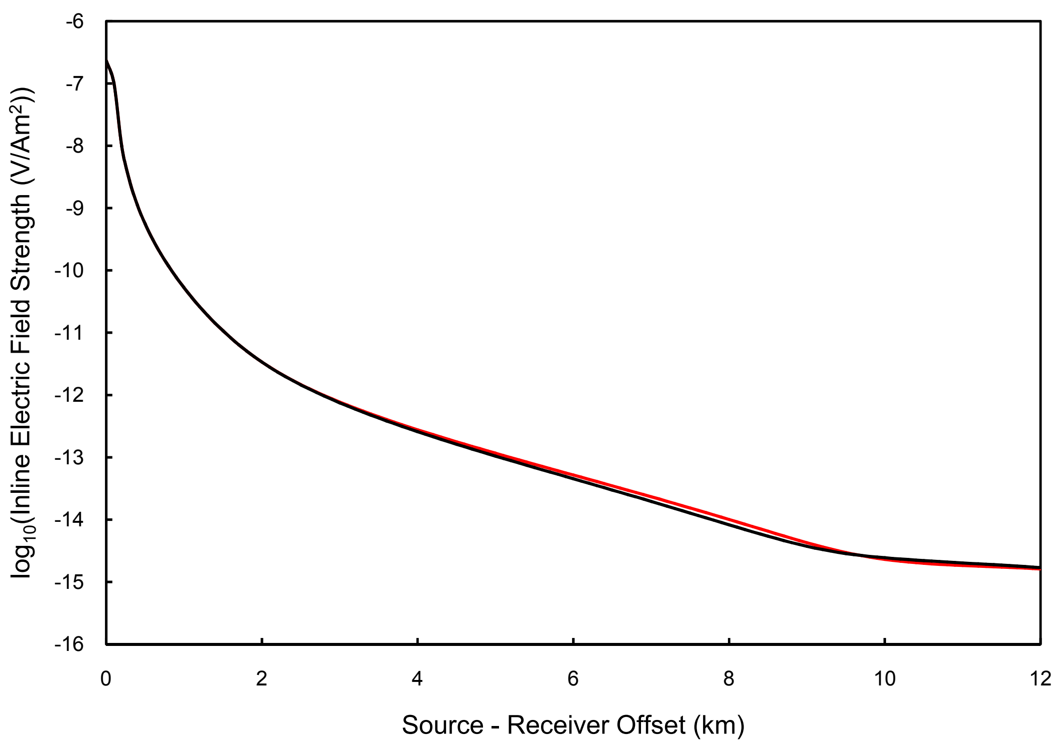

Figure 4.9 Expected response at 0.25 Hz. 3D reservoir response shown in red, background response shown in black.

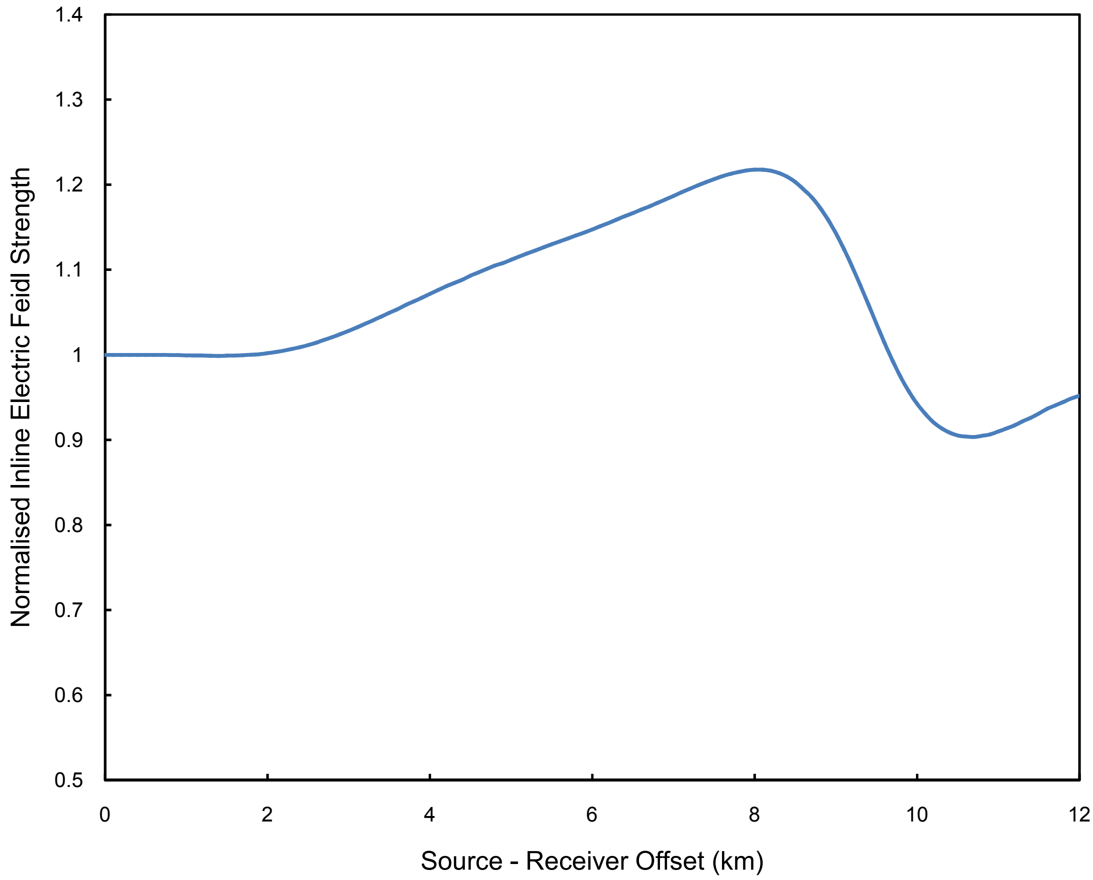

Figure 4.10 Normalised inline electric field strength for the results obtained at a transmission frequency of 0.25 Hz. The reservoir is detectable at offsets of ~5-9km with the maximum response (125 %) at an offset of ~8km.

4.1.3 Hydrocarbon detectability and survey parameters

Scarborough gas field is deep; however it is a laterally extensive deposit in a deep water setting. Forward modelling results indicate that this commercial scale deposit is detectable with current technology. Forward modelling results indicate an expected anomaly of 120% over this field as shown in Figure 4.10.

Based on the geo-electrical structure obtain from the Scarborough-2 well (Figures 4.4 and 4.5), the optimum fundamental frequency for a survey in this area would be 0.25Hz as illustrated in Figure 4.7. Offsets of ~ 5 to 9 km are required to detect this reservoir as shown in Figure 4.10.

4.2 Browse Basin, Offshore Northwest Western Australia

Browse Basin is a large offshore basin within the Northwest Shelf of Western Australia. The basin is a proven hydrocarbon province with major undeveloped gas fields in the outer and central basin and minor oil discoveries on the basins eastern margin (Figure 4.11). The depocentres contain in excess of 15 km sedimentary section and lie in 100 to 1500 m water depth. The outer Browse Basin underlies the deep-water Scott Plateau (1500- 4000 m water depth). The Early Cretaceous claystones provide a thick regional seal. Reservoir facies are best developed within the Middle-Early Jurassic section and submarine fans of Berriasian, Barremian, Campanian and Maastrichtian age (Geoscience Australia, 2007).

The regional basin structure is shown in Figure 4.12 with more detailed structure and geo-electrical data for North Scott Reef and Caswell/Walkley shown in Figures 4.13 and 4.15.

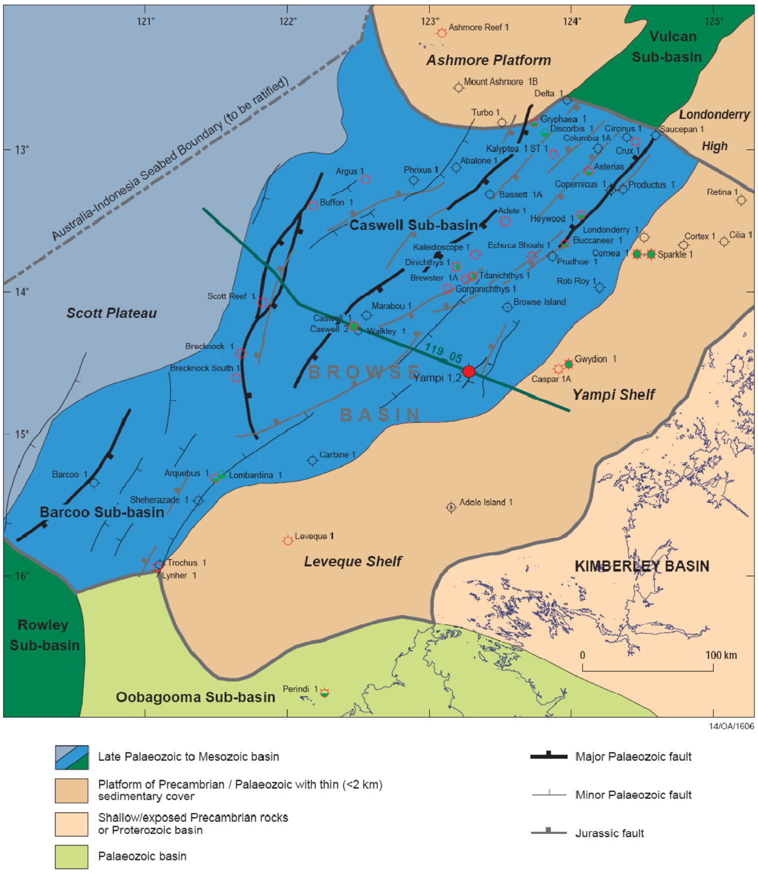

Figure 4.11 Location map of Browse Basin showing seismic line 119_05 and well locations of North Scott Reef-1, Caswell-1, Caswell-2, Walkley-1, Yampi-1 and Yampi-2 (Reproduced from Geoscience Australia, 2007).

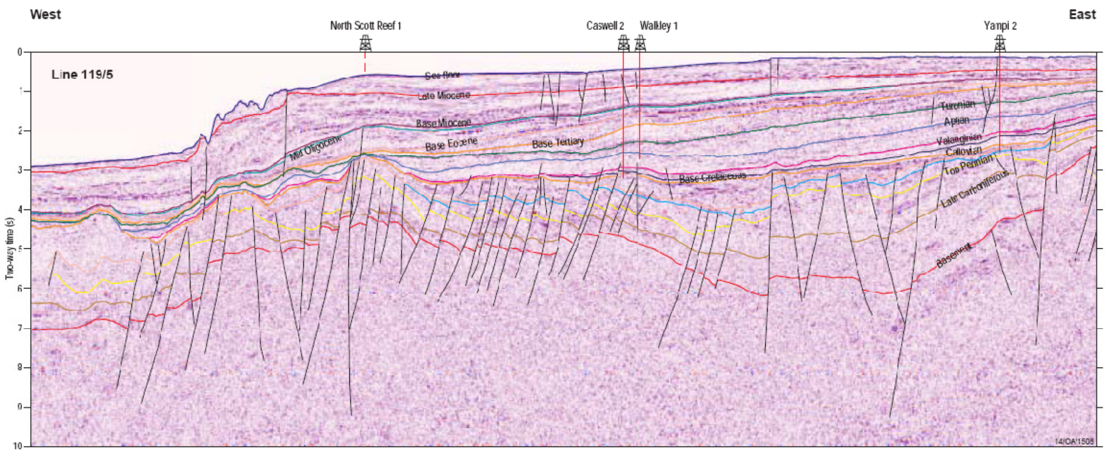

Figure 4.12 Interpreted Seismic line 119_05 (Reproduced from Geoscience Australia, 2007)

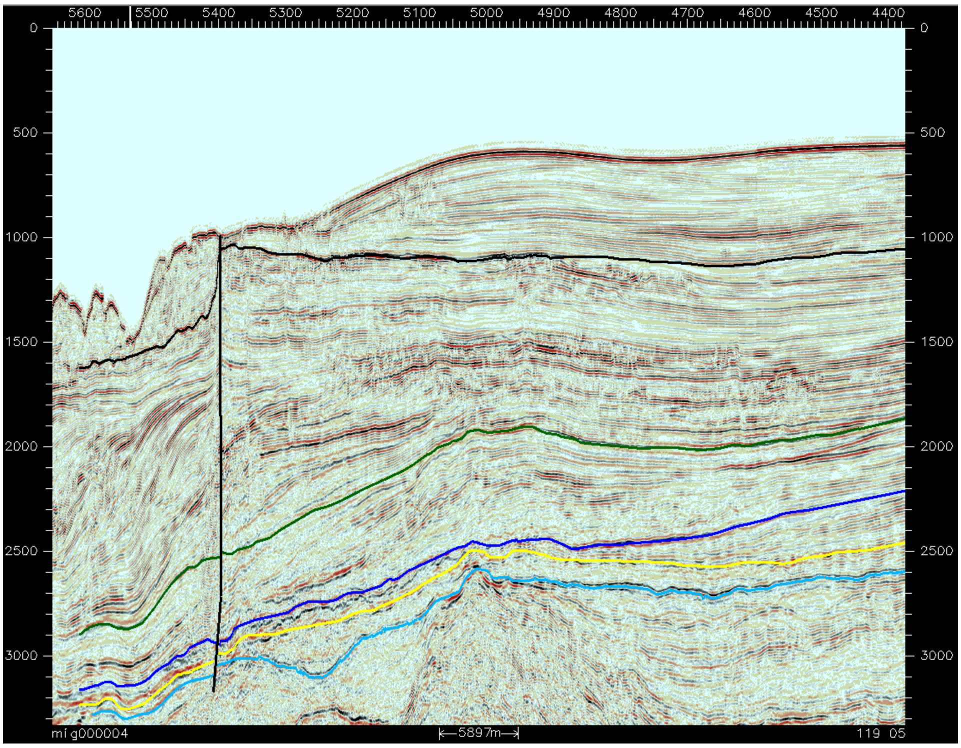

Figure 4.13 Interpreted seismic section at North Scott Reef well location.

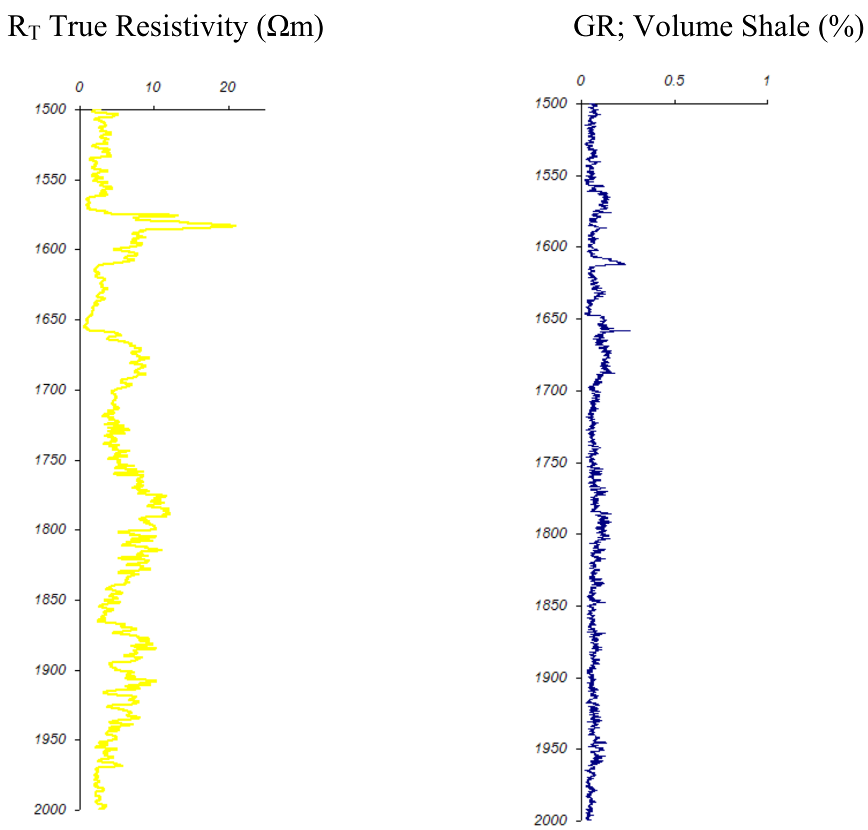

Figure 4.14 Reservoir interval interpreted between depths 1575-1625 m. Reservoir interval shows true resistivity of 20 Ωm.

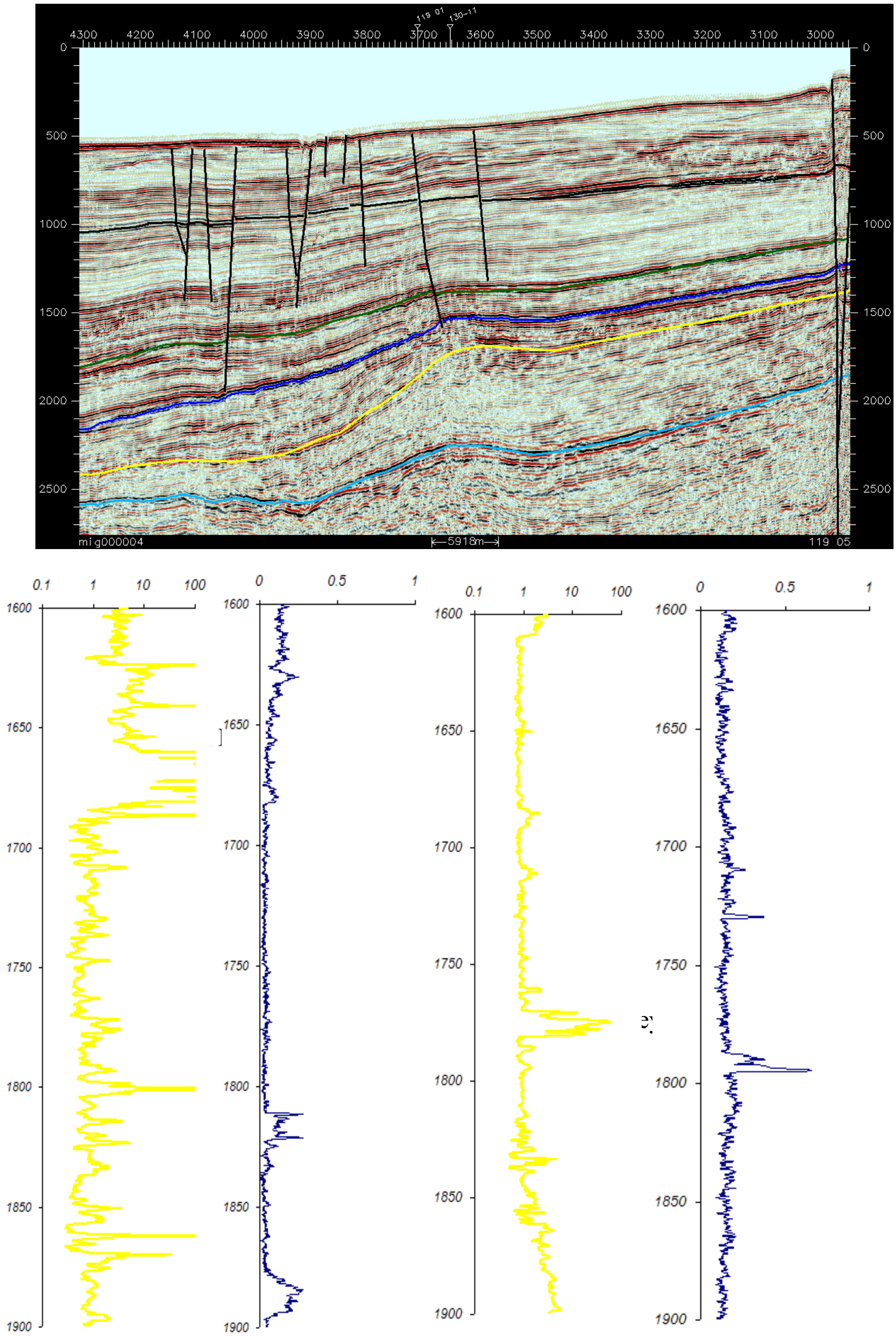

Figure 4.15 Interpreted seismic section at Caswell and Walkley well locations with reservoir interval. Well-hole logging data for Caswell and Walkley with interpreted reservoir intervals at a depth of ~1700 m below the seabed.

4.2.1 Water depth issue

The water depth is the main issue confronting CSEM exploration in Browse Basin. Reservoirs located at North Scott Reef, Walkley and Caswell are far enough offshore not to suffer from the water depth limitations and are considered to be detectable with current technology. However closer to the shore, at the Yampi well, the water is too shallow and moderately deep reservoirs in this area would not be detectable with the current technology

This is demonstrated in Figure 4.16 for a simple four layer model with a reservoir (transverse resistance of 2500 Ωm^2) at a depth of 2000 m. The minimum water depth for which the target reservoir is detectable against the background signal is ~500 m as indicated by the vertical yellow line. The range of source-receiver offsets over which the target is detectable, increases with increasing water depth. The marine CSEM method is feasible at North Scott Reef, Caswell and Walkley. On the Yampi Shelf the water is too shallow and as such the CSEM method is not a viable exploration tool along this shelf.

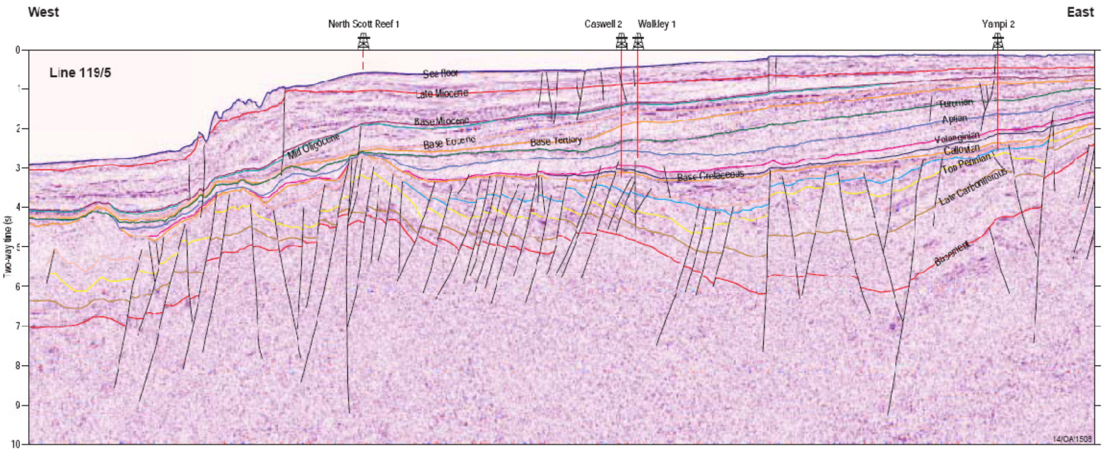

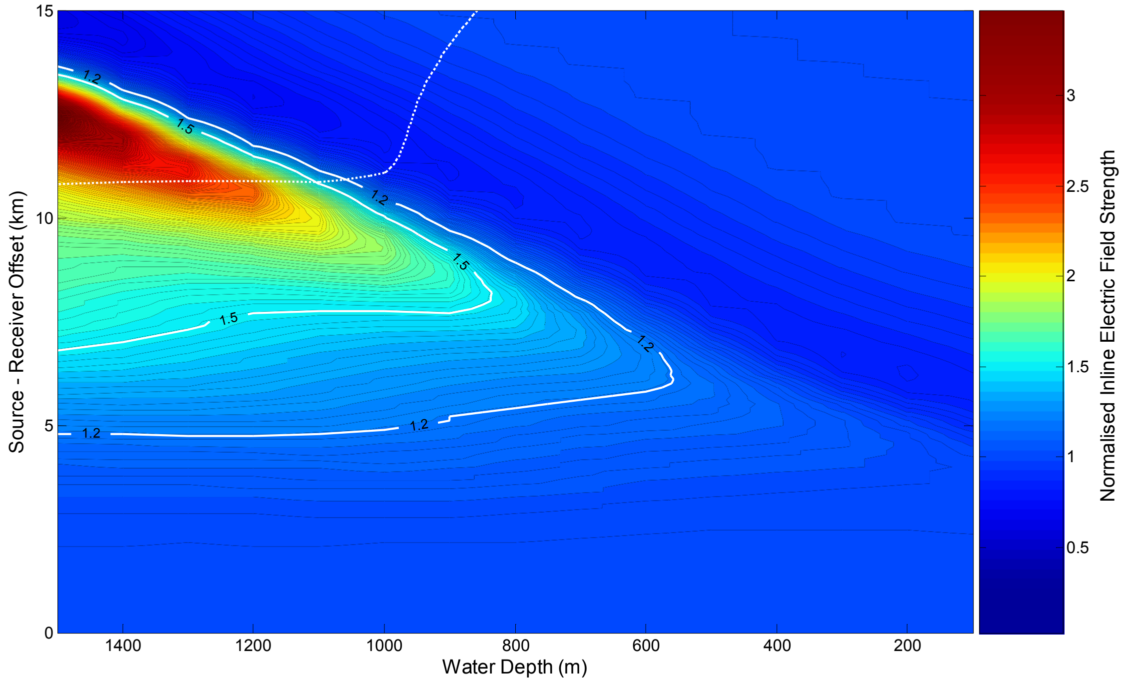

Figure 4.16 Contoured normalised inline electric field response for water depths 100 - 1500 m. Solid contours indicate 120 % and 150 % anomaly due to the reservoir response normalised with the background response for a simple four layer model with a reservoir (transverse resistance of 2500 Ωm^2) at a depth of 2000 m. The dotted line indicates the noise floor of the inline electric field for the reservoir model. The minimum water depth for which the target reservoir is detectable against the background signal is ~500 m as indicated by the vertical yellow line. The range of source-receiver offsets over which the target is detectable, increases with increasing water depth. The marine CSEM method is feasible at North Scott Reef, Caswell and Walkley. On the Yampi Shelf the water is too shallow.

5 CONCLUSIONS

The effects of the critical geological factors and survey parameters that must be considered in the design of a marine CSEM survey were investigated. These included water depth, bathymetry, target depth, saturation and thickness, host formation resistivity and the effect of shallow resistive formations. The survey parameters that were investigated were transmission frequency and harmonic content, required offsets and the components of the electromagnetic field that need to be measured. 1D sensitivity analysis provided good approximations to the frequencies and offsets required for a given target. The result of the modelling could then be used for optimal survey design to ensure the maximum response from the target reservoir.

For areas of the Northwest Shelf including Scarborough gas field and Browse Basin; 1D models were built from well-hole logging and seismic data. Scarborough gas field is deep; however it is a laterally extensive deposit in a deep water setting. Forward modelling results indicate that this commercial scale deposit is detectable. In Browse Basin the issue is water depth which is seen as the main problem with the CSEM method. Reservoirs located at North Scott Reef, Walkley and Caswell are far enough offshore not to suffer from the water depth limitations and are considered to be detectable with current technology. However closer to the shore, at the Yampi well, the water is too shallow and moderately deep reservoirs in this area would not be detectable with the current technology.

With the migration of hydrocarbon exploration into the deeper waters of the continental shelves the marine CSEM method has recently become an important exploration tool for the hydrocarbon industry. With current technology commercial scale reservoirs are detectable with this method in water deeper than 300m. The marine CSEM method works best in areas where the large scale resistivity of the background sediments is relatively uniform, with high reservoir resistivities, well defined field edges, and a smooth seafloor exist. The method does not work in areas where the reservoir is (a) deep relative to water depth (b) close to the crystalline basement, (c) below salt structures, or (d) in very shallow water. Vertical electric field sensors may provide the additional information required to move exploration into shallower water. In general, all components of the electromagnetic field should be acquired to move the marine CSEM method into areas currently considered unsuitable.

6 RECCOMENDATIONS

The results from this research suggest that CSEM is a viable exploration tool in deep water areas of the Northwest Shelf of Western Australia and thus should be used for frontier exploration in this region. An area of particular interest would be north of the Scarborough Gas Field. It is recommended that marine CSEM methods can be also used to scan for further prospects in well developed basins that have been extensively surveyed with seismic methods; providing quantification of both the structural geology and the geo-electrical properties of hydrocarbon plays in the area. This will allow drilling decisions to be made with the highest confidence.

It is strongly recommended that MT data should be collected during transmitter off-time during a CSEM survey. In most applications this will provide the best information on the background geo-electrical structure and can be obtained at a negligible logistical cost. This method will provide the most useful data for normalisation purposes. Conventional well-hole logging techniques are expensive and do not provide resistivity information at the scale required for CSEM methods.

Although it was not extensively investigated, the implementation of vertical electric field sensors is advised for the application of the marine CSEM method in shallow water settings. Further experimentation needs to be done to confirm the reciprocity of using a vertical electrical dipole transmitter with horizontal receivers to the same effect as using the conventional HED with vertical receivers. It is strongly recommended that we must aim to measure all components of the electromagnetic field so that we can obtain the most information about the sub-seafloor.

REFERENCES

Avdeeva, A., Commer, M., and Newman, G.A., 2007, Hydrocarbon reservoir detectability study for marine CSEM methods: time-domain versus frequency-domain: Presented at the SEG Annual Meeting, San Antonio.

Chave, A.D., Constable, S.C., and Edwards, R.N., 1991, Electromagnetic methods in applied geophysics: Volume 2, Applications, edited by Misac N. Nabighian Society of Exploration Geophysicists Tulsa, Oklahoma

Commer, M., and Newman, G.A., 2007, 3D CSEM modeling and inversion for hydrocarbon reservoir mapping: The bathymetry problem: Presented at the SEG Annual Meeting, San Antonio.

Constable, S., and Weiss, C.J., 2006, Mapping thin resistors and hydrocarbons with marine EM methods: Insights from 1D modeling: *GEOPHYSICS*, **71**, 43-51.

Constable, S.C., and Cox, C.S., 1996, Marine controlled source electromagnetic sounding 2. The PEGASUS experiment: *Journal of Geophysical Research*, **101**, 5519-5530.

Constable, S.C., Orange, A.S., Hoversten, G.M., and Morrison, H.F., 1998, Marine magnetotellurics for petroleum exploration part I: A sea-floor equipment system: *GEOPHYSICS*, **63**, 816-825.

Cox, C.S., 1981, On the electrical conductivity of the oceanic lithosphere: *Physical Earth Planetary International*, **25**, 196-201.

Eidesmo, T., Ellingsrud, S., MacGregor, L.M., Constable, S., Sinha, M.C., Johansen, S., Kong, F.N., and Westerdahl, H., 2002a, Sea Bed Logging (SBL), a new method for remote and direct identification of hydrocarbon filled layers in deepwater areas: *first break*, **23**, 144-152.

Eidesmo, T., Ellingsrud, S., MacGregor, L.M., Constable, S., Sinha, M.C., Johansen, S., Westerdahl, H., and Kong, F.N., 2002b, Remote detection of hydrocarbon filled layers using marine controlled source electromagnetic sounding: Presented at the EAGE 64th Conference & Exhibition, Florence, Italy.

Ellingsrud, S., Eidesmo, T., Johansen, S., Sinha, M.C., MacGregor, L.M., and Constable, S., 2002, Remote sensing of hydrocarbon layers by seabed logging (SBL): results from a cruise offshore Angola: *The Leading Edge*, **21**, 972-982

Electromagnetic Geoservices. Retrieved November 4th, 2007, from www.emgs.com

Flosadottir, A.H., and Constable, S., 1996, Marine controlled-source electromagnetic sounding: *Journal of Geophysical Research*, **101**, 5507-5517.

Geoscience Australia 2007. Retrieved May 25th, 2007, from http://www.ga.gov.au/oceans/og_RegPetGeol.jsp

Hesthammer, J., and Boulaenko, M., 2005, The offshore EM challenge: *first break*, **23**, 59-66.

Hohmann, G.W., 1975, Three-dimensional induced polarization and electromagnetic modeling: *GEOPHYSICS*, **40**, 309-324.

Hohmann, G.W., 1988, Electromagnetic methods in applied geophysics: Volume 1, Theory, edited by Misac N. Nabighian: Society of Exploration Geophysicists, Tulsa, Oklahoma.

Hoversten, M.G., Newman, G.A., Geier, N., and Flanagan, G., 2006, 3D modeling of a deepwater EM exploration survey: *GEOPHYSICS*, **71**, 239-248.

Johansen, S.E., Amundsen, H.E.F., Røsten, T., Ellingsrud, S., Eidesmo, T., and Bhuyian, A.H., 2005, Subsurface hydrocarbons detected by electromagnetic sounding: *first break*, **23**, 31-36.

Keys, K.W., 2003, Application of broadband marine magnetotelluric exploration to a 3D salt structure and a fast-spreading ridge: Ph.D. Thesis, University of California.

King, J., 2004, Using a finite 3D element code to analyze resistive structures with controlled-source electromagnetics in a marine environment: M.S. Thesis, Texas A&M University.

Li, Y., and Constable, S., 2007, 2D marine controlled-source electromagnetic modeling: Part 2 - The effect of bathymetry: *GEOPHYSICS*, **72**, 63-71.

MacGregor, L.M., 2006, *OHM short course; Section-1, Section-2*: Marine electromagnetic sounding for hydrocarbon applications, Perth 27 - 29 March.

MacGregor, L.M., Andreis, D., Tomlinson, J., and Barker, N., 2006, Controlled-source electromagnetic imaging on the Nuggets-1 reservoir: *The Leading Edge*, **25**, 984-992.

MacGregor, L.M., Sinha, M.C., and Constable, S., 2001, Electrical resistivity structure of the Valu Fa Ridge, Lau Basin, from marine controlled-source electromagnetic sounding: *GEOPHYSICS*, **146**, 217-236.

Mehta, K., Nabighian, M., Li, Y., and Oldenburg, D., 2005, Controlled source electromagnetic (CSEM) technique for detection and delineation of hydrocarbon reservoirs: an evaluation.

Nabighian, M.N., and Macnae, J.C., 2005, Electrical and EM methods, 1980-2005: *The Leading Edge*, **24**, 42-45.

OHM Surveys. Retrieved November 4th, 2007, from www.ohmsurveys.com

Sheriff, R.E., 1991, Encyclopedic dictionary of applied geophysics: Society of Exploration Geophysics, Tulsa, Oklahoma.

Spiess, F.N., Macdonald, K.C., Atwater, T., Ballard, R., Carranza, A., Cordoba, D., Cox, C., Garcia, V.M.D., Francheteau, J., Guerrero, J., Hawkings, J., Haymon, R., Hessler, R., T. Juteau, Kastner, M., Larson, R., Luyendyk, B., Macdougall, J.D., S. Miller, Normark, W., Orcutt, J., and Rangin, C., 1980, East Pacific Rise: Hot springs and geophysical experiments: *Science*, **207**, 1421-1433.

Tassos, S., and Phillips, S., 2007, Hydrocarbons in the context of a solid, quantified, growing and radiating earth: Presented at the AAPG Conference, Athens.

Wahrmund, L.A., Green, K.E., Pavlov, D., and Gregory, B.A., 2006, Rapid interpretation of CSEM reconnaissance data: Presented at the SEG Annual Meeting, New Orleans.

Wannamaker, P.E., Hohmann, G.W., and Sanfilipo, W.A., 1984, Electromagnetic modeling of three-dimensional bodies in layered earths using integral equations: *GEOPHYSICS*, **49**, 60-74.

Ward, S.H., and Hohmann, G.W., 1988, Electromagnetic methods in applied geophysics: Volume 1, Theory, edited by Misac N. Nabighian: Society of Exploration Geophysicists, Tulsa, Oklahoma.

Weimer, P., and Slant, R.M., 2004, Petroleum Systems of Deepwater Settings, Distinguished Instructor Series No. 7: Society of Exploration Geophysics, Tulsa, Oklahoma.

WesternGeco. Retrieved November 4th, 2007, from http://www.westerngeco.com/content/services/electromagnetic/index.asp?

Ziolkowski, A., Hall, G., Wright, D., Carson, R., Peppe, O., Tooth, D., Mackay, J., and Chorley, P., 2006, Shallow marine test of MTEM method: Presented at the SEG/New Orleans 2006 Annual Meeting.